EXPERIMENTELLE PHYSIK V
FAKULTÄT PHYSIK
TECHNISCHE UNIVERSITÄT DORTMUND

Unfolding of the atmospheric neutrino flux spectrum with the new program TRUEE and IceCube

Dissertation

zur Erlangung des akademischen Grades eines
Doktors der Naturwissenschaften
(Dr. rer. nat.)

vorgelegt von

Dipl.-Phys. Natalie Milke

Dortmund, Juli 2012

Contents

Abstract

High energy charged cosmic rays of unidentified origin arrive constantly at the Earth's atmosphere. This particles reach energies up to 10^{20} eV and are assumed to be accelerated by extragalactic sources. To track back the origin of cosmic rays the extragalactic high energy neutrinos have to be detected on Earth as their simultaneous production is predicted by theories.

The neutrinos produced in the Earth's atmosphere represent the main background for extragalactic neutrinos but at high energies their flux is expected to give way to the extragalactic flux. Therefore, the determination of the atmospheric neutrino flux spectrum can shed light on the contribution of extragalactic neutrinos to the measured flux spectrum.

IceCube is a cubic kilometer large neutrino telescope located at the geographic South Pole and is well suited for the detection of high energy neutrinos. The data used for this work was taken while the experiment was under construction and thus the measurement proceeded with the partially finished detector IceCube 59.

For the determination of the neutrino energy a sophisticated algorithm is needed to estimate the energy distribution from the measured observables. For this purpose, TRUEE, the new unfolding program is developed based on the proven unfolding program $\mathcal{RUN}$ (Blobel, 1984). The software provides a large set of extensions to enable a comfortable and user-friendly unfolding analysis.

In this work the new software TRUEE is introduced and applied on the IceCube 59 data to estimate the flux spectrum of the atmospheric neutrinos. The software provides reliable results and the energy range of the spectrum could be extended. The systematic uncertainties of the simulation have a large impact and have to be reduced to make conclusions about the neutrino flux origin.

Introduction

The evolution and structure of the universe and the natural laws of its internal entities have always attracted the mankind's interest. That promoted the development of the research fields of particle physics, astronomy and cosmology. While particle physics studies the nature at very small scales by investigating particle interactions, astronomy and cosmology deal with large scales and describe properties of celestial objects and evolution of the universe as a whole.

In the recent decades these disciplines could find a common ground in the astroparticle physics, which studies the particles coming from the galactic and extragalactic sources. The latter can be studied from the characteristics of different particle fluxes. Of special interest are the high energy astroparticles ($E > 10^{11}$ eV), which are assumed to be accelerated by very distant and giant sources. The structure and mechanisms of such high energy accelerators can be studied as well as the medium the particles travel through.

Significant contribution to the latest interesting results could be achieved by photon observations. Photons propagate without being deflected by magnetic fields and their spectra reveal the chemical and physical properties of the source. Giant extragalactic sources, such as Active Galactic Nuclei, have been identified as one kind of accelerators for γ-rays with energies $E > 10^{13}$ eV.

A more challenging task is to track the origin of the charged cosmic ray particles, which are mostly protons, electrons and heavier atomic nuclei. A large spectrum of cosmic ray particles has been measured on Earth and reaches very high energies, $E > 10^{20}$ eV. Due to the galactic magnetic fields the charged particles are deflected and their arrival directions are randomized. Only for the very high energy cosmic ray particles the deflections are expected to be negligible. However, such particles have not yet been measured with sufficient statistics.

Theories about the acceleration of the charged cosmic rays predict an accompanying neutrino flux. Neutrinos interact only weakly with a very small cross section. Therefore, they can escape from the source undistorted and travel long distances without being deflected. Thus, neutrinos are optimal candidates to find the acceleration sources of charged cosmic rays. The high energy neutrino astronomy is a very young branch of the astroparticle physics and a high amount of discoveries is expected in the coming decades. Not only the origin of charged cosmic rays but also the evidence of magnetic monopoles, topological defects and dark matter particles are subjects for studies with the new neutrino telescopes [Hel11].

In the neutrino spectrum, which has been explored until today, the measurement is dominated by the neutrinos coming from the cosmic ray showers induced in the atmosphere. These atmospheric neutrinos represent the background for extraterres-

trial neutrinos. Therefore, the knowledge of the atmospheric neutrino flux spectrum is an essential part of the neutrino astronomy. The energy distribution of the atmospheric neutrinos has a steeper slope than that of the predicted extragalactic neutrinos, coming e.g. from Active Galactic Nuclei. Hence, at very high energies the overall neutrino spectrum is assumed to be dominated by extragalactic flux with a corresponding flattening of the distribution. For this reason, the energy spectrum of all neutrinos arriving at Earth at very high energies provides information on a possible contribution of extragalactic neutrinos.

Due to the small cross sections the detection of neutrinos requires a large detector volume and a long observation time. In this way neutrino measurements can be collected with large statistics. The world's largest neutrino telescope, IceCube [A+11c], has been completed at the end of 2011 and is now in operation with its fully instrumented detector volume of one cubic kilometer, located in the glacial ice at the South Pole. The neutrinos are identified by the measurement of secondary particles, e.g. muons, that are produced by the weak interactions of neutrinos with matter and in turn emit photons, while traveling faster than the light in the detection medium.

Generally, ground-based astroparticle detectors suffer from finite resolution and limited, energy-dependent acceptance. Furthermore, the direct detection of astroparticles and their properties is often not possible. Instead, the secondary particles are detected and, from their measurement, the estimation of the primary energy has to be made. This is a so-called inverse problem. In reality, inverse problems usually feature unfavorable properties and have to be resolved with numerical approximations. Due to the finite resolution an observed variable cannot unambiguously be attributed to a primary particle energy. The limited acceptance implicates an incomplete measurement. Moreover, the production probability and the propagation of secondary particles have to be considered as well. To obtain the best possible estimation of primary particle energy an unfolding method has to be used. Unfolding is a technique to estimate the distribution of a variable that is not directly accessible by the detection method. It takes into account all imperfections of the measurement procedure and can provide a result with a precision that is compatible with the detector configuration and statistical accuracy. Consequently, a sophisticated and feasible unfolding software is an essential instrument in the astroparticle physics analyses.

The general software development has made large progress during the last decades by using increasingly flexible programming languages. In many research fields the object-oriented C++ programming language is widely used in many applications. Especially in the particle physics the C++-based ROOT [BR97] framework contains a high number of numerical methods and supplies advanced graphical tools. The goal is to provide a new unfolding software that is user friendly, easy to install and simply extendable. Considering these conditions a new unfolding software TRUEE [M+12] has been developed by using C++ and graphical tools of ROOT. The internal unfolding algorithm of TRUEE is based on the well tested $\mathcal{RUN}$ software [Blo84] that was developed in FORTRAN 77 thirty years ago. $\mathcal{RUN}$ has been proven to provide reliable results and realistic error estimation. Its ability to esti-

mate steeply falling distributions makes the algorithm optimal for the application in astroparticle physics.

The development of TRUEE and its application in the atmospheric neutrino analysis with IceCube is the objective of the present thesis. Since the IceCube telescope was build over several years, the measurement has been performed with the partially constructed detector. In the first chapter a general motivation on the atmospheric neutrino analysis is given. The second chapter is focused on the inverse problems and their solution with the TRUEE unfolding software. The advantages of the main algorithm are pointed out and the newly implemented software features are introduced. Chapter 3 covers the experimental part of the thesis. It starts with the explanation of the detection method, followed by the event reconstruction and the simulation, and proceeds with the individual steps of the analysis. Elaborated event selection techniques, which have been developed in Dortmund as well, are applied in the present analysis to deal with the very high background contamination of the measurement. The application of TRUEE on the data is described and the systematic uncertainties are estimated. The conclusions of the whole work and the outlook can be found in the last chapter. The technical details of the analysis development are left to the appendix.

1 Motivation within astroparticle physics

The main incitation of the current thesis is the contribution to the understanding the origin of the charged high energy astroparticles. It is well known, that giant cosmic particle accelerators, such as Active Galactic Nuclei (AGN) produce high energy γ-rays, which have been detected and studied by several experiments, see e.g. Ref. [A$^+$07a], [FS09], [Pun05]. In contrast, the origin of charged high energy cosmic particles could not be identified, yet. The deflection of particles with energies up to $E < Z \cdot 10^{17}$ eV by magnetic fields randomizes their arrival directions. Furthermore a suppression of the flux of proton dominated cosmic rays at high energies has been predicted, known as is the Greisen-Zatsepin-Kuzmin (GZK) cutoff [Gre66], [ZK66]. The protons with energies above $E > 6 \cdot 10^{19}$ eV interact with the cosmic microwave background and thus loose their energy.

To shed light on the origin of charged cosmic rays and ensure the measurement at higher energies, we need particles which are connected to the charged cosmic ray production and can pass long distances without loosing directional or energetic information. Neutrinos are such particles and neutrino astronomy is the new growing branch of astroparticle physics. An identification of high energy neutrinos from extragalactic sources could be the missing link between the γ-rays and charged cosmic ray particles as the origin would be considered as the same for both kinds.

The bigger part of neutrinos measurable with the modern high energy neutrino telescopes are atmospheric neutrinos. These are produced in the extensive air showers caused by interactions of cosmic rays with the atomic nuclei of the Earth's atmosphere. The atmospheric neutrinos represent major background for the extraterrestrial neutrinos. However, their dominance is decreasing at high energies due to the steeply falling energy spectrum. At very high energies a flattening of the spectrum is expected due to the contribution of flatter extragalactic spectrum. Therefore, the study of the full neutrino spectrum measurable on Earth is performed to confirm or reject the predicted flux model of extragalactic neutrinos. Additionally, conclusions about the cross sections of charmed meson production due to interaction of cosmic rays with the atmosphere can be made, as the related secondary neutrinos have a slightly flatter spectrum as well.

1.1 Charged cosmic ray particles

The charged cosmic rays are composed of electrons, protons and atomic nuclei with different compositions depending on the energy, as explained below. The particles arrive the Earth's atmosphere with energies up to 10^{20} eV as has been observed already in 1963 by the MIT Volcano ranch array [Lin63]. In Fig. 1.1 the cosmic ray energy spectrum is shown measured by different experiments. The observed differential cosmic ray flux is $\frac{dN}{dE} \propto E^{-\gamma}$, where the spectral index γ varies between 2.7 and 3.2 depending on the energy region. The features in the spectrum have to be noticed where the spectral index changes, because they indicate a change of the cosmic ray origin. Up to energies $E \approx 3 \cdot 10^{15}$ eV (the knee) the particles are expected to have galactic origin, e.g. from super nova remnants. At the knee the galactic contribution to the cosmic rays is assumed to decrease due to the Hillas condition [Hil84]

$$E_{max} = \beta \cdot Z \cdot B \cdot R, \tag{1.1}$$

which restricts the maximum acceleration energy E_{max} of a particle with charge Z by the relation between the magnetic field B and the radius R of the accelerating object. β is the characteristic velocity of the accelerating regions in terms of speed of light. Hence, the maximum acceleration energy of the primary cosmic ray particles from same sources is raising with the increasing particle charge. Therefore the flux from the galactic contributions does not drop down instantly at the knee but has a smooth decreasing distribution with a primary particle composition shifting toward heavier primaries at higher energies. This has been confirmed by the measurements of the composition of cosmic rays in the knee region [S+02], [A+05].

At the energies around $E \approx 3 \cdot 10^{18}$ eV the next feature, the ankle with subsequent flattening of the spectrum is observed. Here the contribution of the extragalactic sources is assumed to dominate. The galactic sources cannot produce such high energetic particles, which would escape from the galaxy at lower energies anyway, due to the large gyro-radius. The measurement of the primary composition around the ankle reveals a change from a steeper heavy nuclei spectrum to a flat proton-dominated one towards higher energies [B+93]. Considering Eq. 1.1 this is a strong indication for a transition from galactic to giant and powerful extragalactic sources for charged cosmic ray particles.

As predicted, the spectrum drops very abruptly at energies above $E \approx 4 \cdot 10^{19}$ eV. The trend to a flux suppression at high energies has already been visible in the Yakutsk observation [K+85]. The statistically significant measurement was provided by HiRes [A+08a] and confirmed by the results of the Pierre Auger Observatory [A+08b]. Further measurements are needed to clarify whether the suppression is caused by the predicted GZK cutoff or is due to the maximum acceleration energy of the most source. This problem can be solved by the measurement of ultra high energy cosmogenic neutrinos that are produced in the decay of mesons from the proton-γ interactions [BZ69].
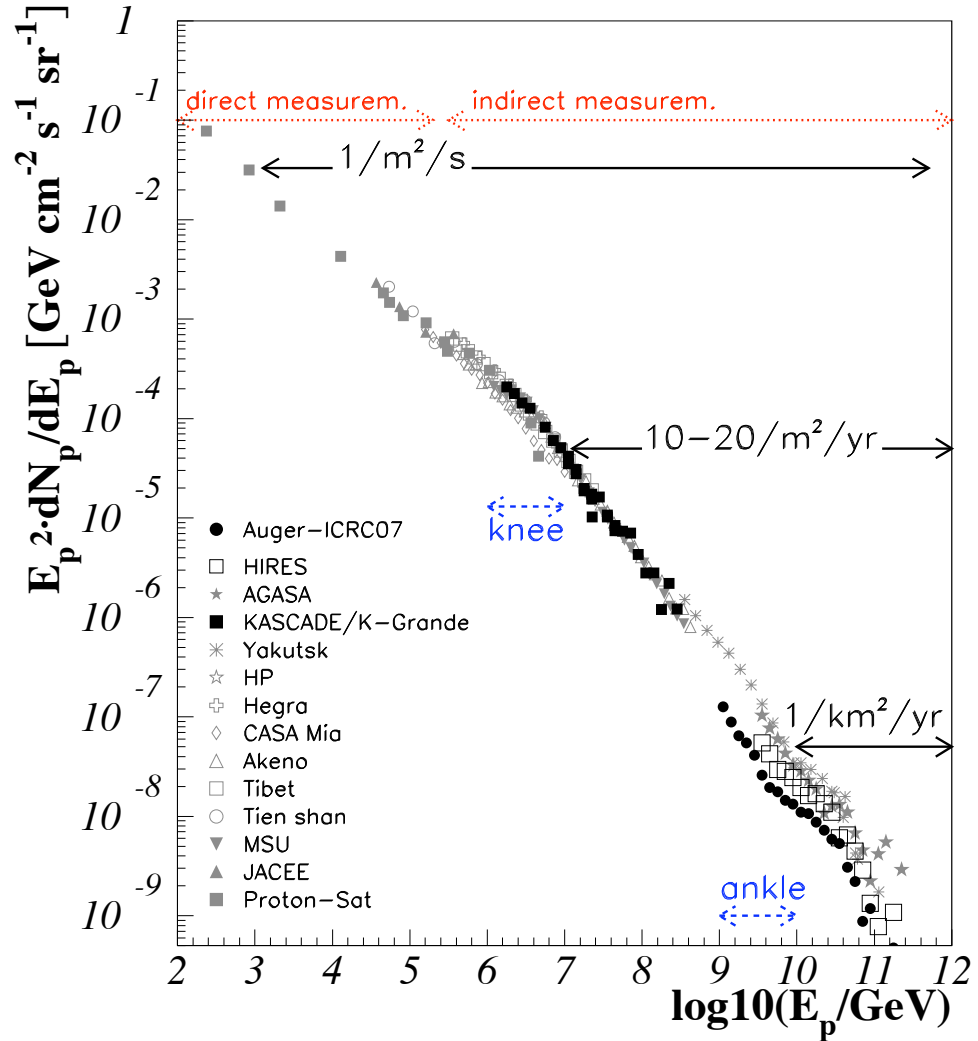
Figure 1.1: Differential flux of charged cosmic ray particles arriving on Earth and measured by different experiments. The flux is weighted by the square of energy to visualize the characteristic features. The structure around $E \approx 3 \cdot 10^{15}$ eV is called the knee. The particles with energies up to the knee have galactic origin and the spectral index is $\gamma = 2.7$. Above the knee the spectrum becomes steeper with $\gamma = 3.2$, where the contribution from the galactic sources such as supernova remnants is declining. The feature around $E \approx 3 \cdot 10^{18}$ eV is known as the ankle and signifies the probable transition from galactic to extragalactic sources for cosmic rays. Picture is taken from Ref. [Bec08] where full references to the results can be found.

1.2 Neutrino astronomy

The possible extragalactic sources for charged high energy cosmic rays are AGN and Gamma Ray Bursts (GRB). Assuming charged π-production in these sources

by hadronic interactions during the acceleration process, the component of high energetic neutrinos in the extragalactic cosmic rays is expected. Coming straight from the source without any deflection and interacting only weakly, extragalactic neutrinos are ideal candidates to perform a deep study of the accelerating objects.

The most favored model to describe the mechanism for particle acceleration in a galactic cosmic ray source is the first order Fermi acceleration [Fer49]. It suggests the acceleration of the charged particles due to magnetic deflection within propagating gas clouds with the additional influence of a shock region. The energy spectrum of the first order Fermi accelerated primary particles is expected to follow the flux $\frac{dN}{dE} \propto E^{-2}$. Due to the high density of matter and radiation around the accelerating object the charged particles undergo further interaction. Only neutrinos from charged π-decays produced in particle collisions retain the primary flux distribution. Therefore the search for extragalactic charged particle accelerators can be restricted to the search of neutrinos with the spectral index $\gamma = 2$.

1.3 Atmospheric neutrinos

The main component of the atmospheric neutrinos is represented by the conventional neutrinos, coming from the cosmic ray induced productions of the charged K and π mesons, due to interactions with atomic nuclei N in the atmosphere

$$p + N \rightarrow \pi^+ + \pi^- + K^+ + K^- + ... \tag{1.2}$$
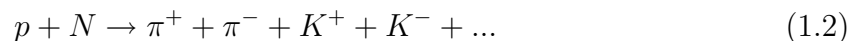
and their subsequent decay into leptons

$$\pi^+(K^+) \quad \rightarrow \quad \mu^+ + \nu_\mu \tag{1.3}$$
$$\pi^-(K^-) \quad \rightarrow \quad \mu^- + \overline{\nu}_\mu. \tag{1.4}$$

The neutrinos from the following μ-decay can be neglected in the current analysis because the atmospheric muons above a GeV begin to reach the ground. For the same reason the flux of conventional atmospheric electron neutrinos is suppressed to higher energies [Gai07]. In the following only the muon neutrinos (and antineutrinos) are considered.

Due to the relatively long lifetimes of few 10^{-8} s the K and π mesons undergo interactions in the atmosphere and thus, lose a part of their energy before decay. On account of this energy loss the resulting atmospheric neutrino flux has a spectral index $\gamma \approx 3.7$ and has therefore a steeper distribution, than the primary flux. Moreover, the conventional neutrino flux distribution depends on the zenith angle. Mesons, which travel through the atmosphere vertically, experience a larger density gradient, than the horizontally traveling mesons. Therefore, the interaction probability of vertically incoming mesons is high and leads to the energy loss and hence, decreasing of measured flux.

For higher astroparticle energies (> 100 TeV) the production of mesons ($D^\pm$, D^0, $\overline{D^0}$, $D_s^\pm$, Λ_c^+) containing charm quarks is possible [Gai03]. These massive and extremely short living mesons with lifetime shorter than 10^{-12} s decay promptly after

production without interacting with the atmosphere, as shown here exemplarily for two decay channels of D-Mesons:

$$D^0 \quad \rightarrow \quad K^- + \mu^+ + \nu_\mu \tag{1.5}$$

$$D^+ \quad \rightarrow \quad K^- + \pi^+ + \mu^+ + \nu_\mu. \tag{1.6}$$

Hence the energy distribution of the original cosmic rays is conserved in the resulting neutrino spectrum and no zenith dependency of the flux is assumed. Therefore, this so-called prompt neutrino flux follows the power law with the spectral index $\gamma \approx 2.7$. Due to the similar branching ratios the prompt electron and muon neutrino fluxes are expected to be roughly the same [B+89], [ERS08].
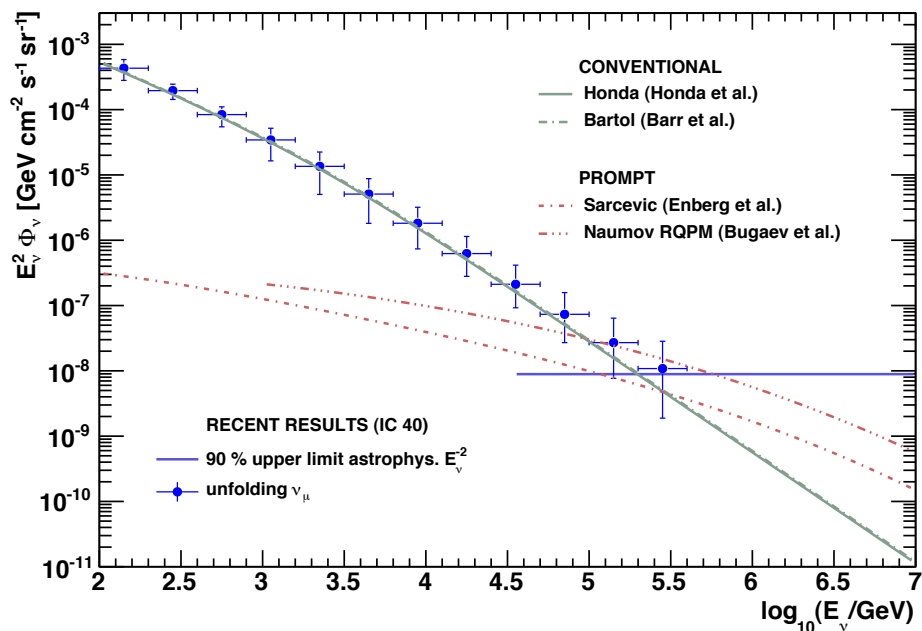
Figure 1.2: Atmospheric muon neutrino flux spectrum averaged over the Northern hemisphere and weighted by the square of neutrino energy. Shown are the theoretical models for the conventional flux of Honda [H+07] and Bartol [B+04]. Additionally the models of Sarcevic [ERS08]) and Naumov [B+89] for the expected prompt flux from charm meson decays are displayed. The most recent results from IC 40 analyses show the upper limit for the astrophysical E^{-2} flux [A+11a] and the atmospheric flux estimation from the unfolding analysis [A+11d].

Figure 1.2 shows the different theoretical predictions for conventional and prompt atmospheric muon neutrino fluxes. The presented fluxes are averages over the zenith region of the northern hemisphere, for a consistent demonstration throughout the thesis. For the analysis the models of Honda *et al.* (in the following referred to as Honda) and Enberg *et al.* (in the following referred to as Sarcevic) are used in

the simulation. Besides the theoretical predictions, the newest result of the atmospheric unfolding analysis and the search for isotropic astrophysical flux are given. The results have been obtained with the data from the half complete IceCube detector of 40 string configuration (IC 40) and demonstrate that the experiment is approaching the energy region of high interest, where the contribution from prompt and astrophysical flux is expected to have an non-negligible impact.

Further predictions on the possible distribution of the atmospheric neutrino flux under consideration of the primary cosmic ray flux variations and the influence of the cosmic ray knee can be found in the Ref. [FBTD12]. In the same Reference the contribution of pion decays is assumed to be negligible for high energies, since the main contribution for conventional neutrinos can be charged to the kaon decays.

In general the conventional and prompt neutrinos as well as extraterrestrial neutrinos are assumed to cause same signal pattern in the neutrino telescopes, thus an individual event cannot be classified as atmospheric or extraterrestrial, apart from the ultra high energy cascades, that are subject of other analyses [Joh11]. Therefore the atmospheric neutrinos represent the most significant background for the sought extragalactic signal.

A possibility to identify the extragalactic signal is to determine the whole incoming neutrino flux at high energies with a high precision. The expected spectral index of extragalactic neutrinos ($\gamma = 2$) is lower then the γ of the atmospheric neutrino flux. The flattening of the whole incoming neutrino flux at high energies would be an indication of the extragalactic component.

Thus the precise estimation of the neutrino energy flux for as high energies as possible is desired and is the subject of the present thesis.

2 Unfolding of distributions

The estimation of the atmospheric neutrino energy spectrum is a so-called inverse problem. The neutrinos themselves cannot be detected directly and thus a straight measurement of their initial energy is impractical. Only when neutrinos undergo weak interactions, it is possible to track their secondary leptons. From the signals, these leptons cause in the detector, conclusions about the neutrino energies can be made. Due to uncertainties and smearing effects in a measurement the handle of such inverse problems is not trivial.

The primary neutrino flux is folded with the neutrino cross sections, the detector response and the lepton range. This statistical problem requires application of sophisticated unfolding algorithms to obtain optimal solutions.

2.1 Theoretical description of the implemented unfolding algorithm

The general problem statement of an unfolding analysis is the determination of the distribution $f(x)$, while a direct measurement of x is not accessible. Instead, the measurement of y-values is made which are correlated with x. The goal is to obtain a best-possible estimation of the $f(x)$-distribution extracting information from the measured $g(y)$-distribution. This is an inverse problem. In a real measurement the transformation between x and y usually implies a limited acceptance and a finite resolution of the detector. Therefore a distinct allocation of a value x to a value y is not possible due to the smearing effect and loss of measurements (events). Thus, the migration probability between the measured values as well as the escape of events have to be taken into account.

In mathematics this relation between $f(x)$ and $g(y)$ is called folding or convolution[1] and can be described by the Fredholm integral equation [Fre03]

$$g(y) = \int_c^d A(y, x) f(x) dx + b(y), \tag{2.1}$$

where $g(y)$ is the distribution of the measured observable y that can be multidimensional. The integral kernel $A(y, x)$ is called response function and implicates all effects of a measurement imperfection. Usually this function is unknown and has to be determined by using Monte Carlo (MC) simulated sets of x and y values that comply theoretical models of the measurement process. c and d are the integral

---

[1]The term convolution is used only if the kernel fulfills the condition $A(y, x) = A(y - x)$

limits of the range where x is defined ($c \leq x \leq d$). $b(y)$ is the distribution of an optional background. The solving of the Eq. 2.1 is called unfolding or in the special case deconvolution.

A real measurement deals with discrete values and a parametrization of distributions is required. In the here presented algorithm the distribution $f(x)$ is parametrized by the superposition of the Basis-spline (B-spline) [dB01] functions $p_j(x)$ with the corresponding coefficients a_j

$$f(x) = \sum_{j=1}^{m} a_j p_j(x).$$

(2.2)

The B-spline functions consist of several polynomials of a low degree. In the following cubic B-splines are used, consisting of four polynomials of third degree (see Fig. 2.1). The equidistant points where the adjacent polynomials overlap are called knots. The resulting parametrization provides function values at equidistant knot locations, but due to the smooth B-spline interpolation between the values a continuous function can be accessed. An afterward fragmentation of the function into a histogram with lower number of intervals helps to reduce the correlation between the data points. An interpolation with B-spline functions does not tend to oscillations because of the low degree of the polynomials. With a given number of knots all B-spline functions
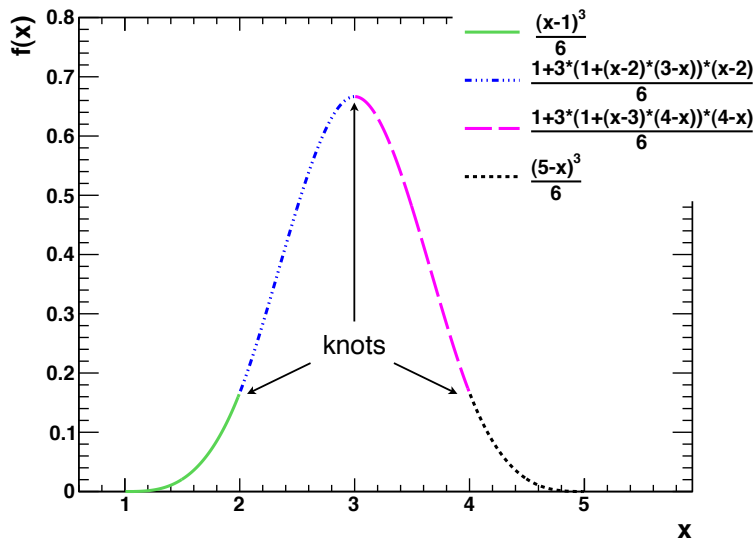
Figure 2.1: An example of a cubic B-spline function. The four polynomials of third degree overlap at the knots. Here the knot distances of 1 are chosen.

are defined and therefore only the coefficients a_j have to be determined. Thus the B-splines can be included into the response function by integration over the whole x-region

$$\int_{c}^{d} A(y,x) f(x) dx = \sum_{j=1}^{m} a_j \left[\int_{c}^{d} A(y,x) p_j(x) dx \right] = \sum_{j=1}^{m} a_j A_j(y).$$

(2.3)

The piecewise integration over y-intervals

$$A_{ij} = \int_{y_{i-1}}^{y_i} A_j(y) dy \qquad (2.4)$$

transforms the response function into a matrix with dimensions given by y-discretization (binning) and the number of knots. The same piecewise integration is made for the measured distribution $g(y)$ and the background distribution $b(y)$

$$g_i = \int_{y_{i-1}}^{y_i} g(y) dy,$$
$$b_i = \int_{y_{i-1}}^{y_i} b(y) dy,$$

to obtain discrete histograms with content g_i or b_i in the interval (bin) i. The Fredholm integral equation 2.1 becomes a matrix equation

$$\mathbf{g} = \mathbf{Aa} + \mathbf{b}. \qquad (2.5)$$

with vectors $\mathbf{g}$, $\mathbf{a}$ and $\mathbf{b}$ and the response matrix $\mathbf{A}$. To determine the sought distribution $f(x)$ the coefficients a_j need to be found.

The most straight forward method of solving the Eq. 2.5 is the inversion of the response matrix $\mathbf{A}$, if the matrix is non-singular. Because of the measurement distortion, especially the finite resolution, the response matrix is not diagonal and the off-diagonal elements become more important if the resolution gets worse. This is the so-called ill-posed[2] problem. The ill-posedness can be revealed when the matrix is diagonalized. After arranging the eigenvalues in decreasing order a difference of several orders of magnitude between the highest and the lowest eigenvalue can be observed. Correspondingly, a large condition number indicates ill-posedness [WZ91]. The number is calculated as the ratio between the highest and the lowest singular values [Smi58], which are square roots of eigenvalues. An inversion of a matrix with such properties leads to increasing of the small off-diagonal elements which now gain strong influence on the result. Consequently a little variation in the values g_i can cause large oscillations in the solution $f(x)$. Therefore ill-posed integral equations generally cannot be solved by simple matrix inversion. To suppress the oscillations in the unfolded distribution, regularization methods are used. In the present algorithm a specific kind of the Tikhonov regularization is implemented [Tik63].

In its generalized form the Tikhonov regularization method suggests the linear combination of the unfolded fit with an operator multiplied by a regularization parameter τ. The operator implies some a-priori assumptions about the solution. These can be e.g. the smoothness or monotony of the solution or the similarity of the unfolded function to a given trial function. Depending on the τ-value the

---

[2]At least one of Hadamard's conditions for a well-posed problem is not fulfilled. Those are the existence of a solution, the uniqueness of the solution and the stability against slight changes of initial conditions [Had02]

regularization term introduces a more or less bias into the solution towards an expectation, and is therefore called penalty term. The same approach of regularization has also been invented independently by Phillips [Phi62]. The Phillips-method has been upgraded by Twomey [Two63] and hence has been extended to the treatment of overdetermined systems, which imply a non-square response matrix.

In the treated case a smooth result is expected and therefore the smoothness of the result has to be included as a mathematical constraint into unfolding procedure. The smoothness is expressed by the curvature operator $\mathbf{C}$. Due to the cubic B-spline parametrization of $f(x)$, the curvature $r(\mathbf{a})$ takes a simple form of a matrix equation

$$r(\mathbf{a}) = \int \left(\frac{d^2 f(x)}{dx^2} \right)^2 dx = \mathbf{a}^T \mathbf{C} \mathbf{a}, \tag{2.6}$$

with $\mathbf{C}$ as a known, symmetric, positive-semidefinite curvature matrix. During the unfolding as described in the following this curvature term will be included in the final unfolding fit equation (Eq. 2.10) and will be minimized considering the fit.

The unfolding as it is processed in the current algorithm does not involve the matrix inversion. After determining the response matrix $\mathbf{A}$ using MC simulated event sample, a maximum likelihood fit of the equation

$$\mathbf{g}_{meas} \stackrel{!}{=} \mathbf{A} \mathbf{a} \tag{2.7}$$

is performed that has the coefficients a_i as free parameters. $\mathbf{g}_{meas}$ is now the real measured observable distribution. To simplify matters a negative log-likelihood function $S(\mathbf{a})$ is formed to be minimized:

$$S(\mathbf{a}) = \sum_i (g_i(\mathbf{a}) - g_{i,meas} \ln g_i(\mathbf{a})). \tag{2.8}$$

$g_{i,meas}$ is the number of measured events in an interval i including the possible background contribution in this region. The Poisson distribution in the bins is assumed with mean values g_i. A Taylor expansion of the negative log-likelihood function can be written as

$$S(\mathbf{a}) = S(\tilde{\mathbf{a}}) + (\mathbf{a} - \tilde{\mathbf{a}})^T \mathbf{h} + \frac{1}{2}(\mathbf{a} - \tilde{\mathbf{a}})^T \mathbf{H}(\mathbf{a} - \tilde{\mathbf{a}}), \tag{2.9}$$

with gradient $\mathbf{h}$, Hessian matrix $\mathbf{H}$ and $\tilde{\mathbf{a}}$ as a first assumption of coefficients, which is determined by an initial least square fit in the algorithm. The defined log-likelihood fit alone would lead to unrealistic fluctuating results for the mentioned reasons of an imperfect measurement, and therefore has to include the regularization term 2.6. The final fit function

$$R(\mathbf{a}) = S(\tilde{\mathbf{a}}) + (\mathbf{a} - \tilde{\mathbf{a}})^T \mathbf{h} + \frac{1}{2}(\mathbf{a} - \tilde{\mathbf{a}})^T \mathbf{H}(\mathbf{a} - \tilde{\mathbf{a}}) + \frac{1}{2}\tau \mathbf{a}^T \mathbf{C} \mathbf{a} \tag{2.10}$$

has to be minimized to obtain the estimation of the B-spline coefficients. At the same time a suitable value for the regularization parameter τ has to be found, to

get an optimal estimation of the result as a balance between oscillations and the smoothing effect of the regularization.

The here used method to define a value for τ implements the relation between τ and the effective number of degrees of freedom ndf

$$ndf = \sum_{j=1}^{m} \frac{1}{1 + \tau S_{jj}}.$$

(2.11)

S_{jj} are the eigenvalues of the diagonalized curvature matrix $\mathbf{C}$, arranged in increasing order. The summands in Eq. 2.11 can be considered as filter factors for the coefficients, which represent the measurement after internal matrix transformation. They are arranged in decreasing order. Hence, the filter factors of higher index j suppress the influence of insignificant coefficients. Consequently a variation of τ regulates the considered amount of information from the measurement and the number of degrees of freedom. In turn, the definition of number of degrees of freedom allows to specify the number of filter factors and thus the regularization strength.

To obtain Eq. 2.11, the Hesse and curvature matrices in Eq. 2.10 have to be diagonalized simultaneously. For this purpose a common transformation matrix can be found, that transforms the Hesse matrix into a unit matrix and diagonalizes the curvature matrix.

A lower limit of the parameter τ can be estimated by testing the statistical relevance of the eigenvalues of the response matrix. Applying Eq. 2.11, the number of degrees of freedom has to be chosen such that τ is above the suggested limit, in order to avoid the suppression of significant components in the solution. For more detailed information about the algorithm and mathematical descriptions see Ref. [BL98] and Ref. [Blo84]. Additionally to the unfolded result a full covariance matrix can be calculated following the error propagation. Therefore, a full information about the data point correlations can be obtained and used for testing theoretical models.

2.2 General remarks on unfolding

The solution of the inverse ill-posed problems is a challenging operation. The careful selection of observables and determination of binning of distributions and the regularization parameter is essential, to avoid a non-negligible bias of the result. In cases, when only the comparison of the result with the existent theoretical prediction is needed, it is indeed simpler to fold the theoretical model and afterwards make the comparison with the measurement, and thus avoid unfolding itself [Lyo11]. Nevertheless unfolding is a mighty tool and is always needed when results of different experiments have to be compared or when the distribution parameters have to be extracted after fitting the result by a function. Furthermore the storage of the response matrix or the necessary MC simulation is dispensable if the unfolding result is saved instead of the measured distributions. Thus, the comparisons with theories developed in the future are not impeded by lack of the response matrix.

Since the introduced unfolding method accounts for event migration between data points and estimates the uncertainties correctly, it gives more reliable results than for example the simple and still widely used bin-by-bin correction factors method. Also the dependence of the result on the MC assumption is in the latter very high. A detailed discussion on different approaches for solving inverse problems can be found e.g. in Ref. [Blo10].

2.3 Unfolding software TRUEE

TRUEE (**T**ime-dependent **R**egularized **U**nfolding for **E**conomics and **E**ngineering problems) [M$^+$12] is a software package for numerical solution of inverse problems (see Sec. 2). The basis for the algorithm is provided by the application $\mathcal{RUN}$ (**R**egularized **UN**folding) [Blo84]. The algorithm-internal mathematical operations for the solution of the ill-posed inverse problems are described in Sec. 2.1.

2.3.1 From $\mathcal{RUN}$ to TRUEE

The unfolding program $\mathcal{RUN}$ was developed in the early 1980's and was updated the last time in 1995 [Blo96]. Originally the algorithm has been developed and applied in the experiment CHARM, to determine the differential cross sections in the neutral current neutrino interactions [J$^+$81], [J$^+$83]. For the realization the programming language FORTRAN 77 was used. The graphical output is produced by making use of the Physics Analysis Workstation (PAW), an analysis tool of the FORTRAN 77 program library CERNLIB [CER93].

One of the main advantages of $\mathcal{RUN}$ is the event-wise input of all data. Accordingly the user can choose an individual binning for the response matrix. Furthermore additional cuts or weightings can be applied if necessary, without changing the data files. Moreover, based on event-wise input a verification of simulation and unfolding result could be developed (see Sec. 2.3.2). Up to three measured observables can be used for the unfolding at the same time and enhance the precision of the estimated function by extracting complementary information from the three observables. To achieve a physically meaningful result that is correct in shape and magnitude, an internal correction is performed by using the function of initially generated MC events. This function can be given by the user. Hence a correct reconstruction of the full distribution can be made even if the MC sample for the response matrix contains no events outside the measurement acceptance.

As described in the previous section the Tikhonov regularization is used assuming a smooth distribution of the unfolded function. This is a proper assumption for the astroparticle physics where in general the distributions do not show strong fluctuations or very narrow peaks. Above all the prior usage of $\mathcal{RUN}$ in astroparticle physics shows, that the algorithm is able to estimate a very steep distribution with function values covering several orders of magnitude and therefore provides a perfect basis for the here presented work [Goz08], [Cur08], [A$^+$10b].

The unfolding algorithm $\mathcal{RUN}$ has been tested and compared with different applications. It stood out with notably stable results and reliable uncertainties [A^{+}07b]. Today it is still used especially in the high-energy physics experiments.

Nowadays the programming language C++ is widely used in several research fields. Primarily for this reason the unfolding software TRUEE has been developed, starting in 2008 and is now being maintained and frequently upgraded. The software contains the C++ converted $\mathcal{RUN}$ algorithm and additional extensions to make the unfolding procedure more comfortable for the user. Furthermore, the extension of the algorithm to a two-dimensional unfolding is intended, for studying of e.g. time-dependent variations of estimated distributions. The results of the new and original algorithms are identical as shown in Fig. 2.2 using MC simulated toy function $f(x)$ of an arbitrary variable x.
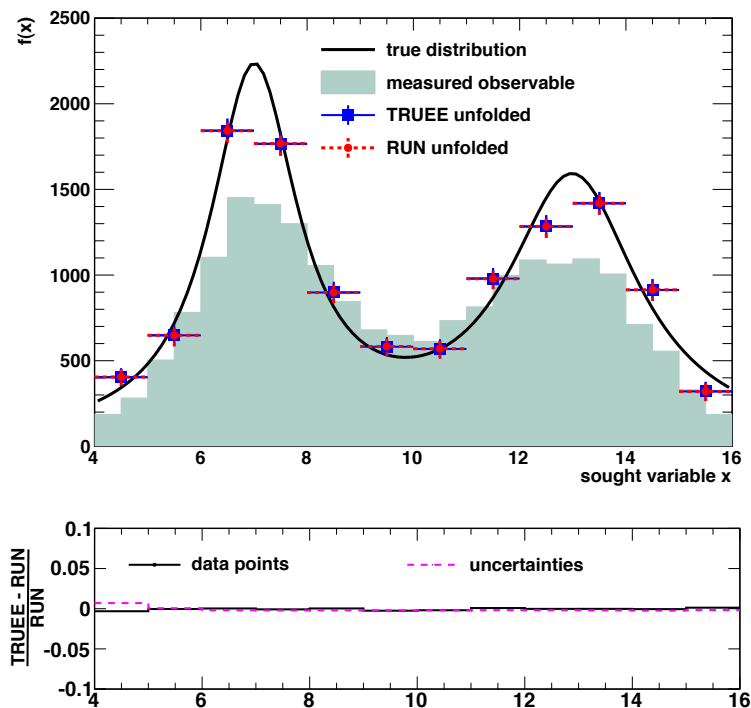

Figure 2.2: Comparison of the results of the original unfolding algorithm $\mathcal{RUN}$ (red/circles) and the new C++ version TRUEE (blue/squares). The solid black line is the true sought distribution. The shaded area represents the measured observable that is used for the unfolding. The relative difference between bin contents and uncertainties from both algorithms can be seen in the lower figure and show a good agreement between the unfolding results.

The new software allows an easy installation of the software package by using the build system CMake [MH03]. The comfortable creation of graphics benefits from the high variety of graphical tools in ROOT [BR97]. The new additional functions

such as test mode (see Sec. 2.3.3), make the choice of unfolding parameters and observables easier for the user. The most important functions are introduced in the following sections, while the complete information about the new extensions and the handling of the software can be found in the TRUEE manual, that is provided along with the source code [Tru12].

2.3.2 Adopted function

The original unfolding software $\mathcal{RUN}$ offers already some helpful tools that give the user the opportunity to check the performance of the unfolding procedure. They have been adopted in the new unfolding software and therefore are briefly introduced in the following.

Verification of the result and simulation

This method is executed after the unfolding and can be used to test the agreement between data and simulation and to check the unfolding result. The distributions of simulated and measured observables do not necessarily match in shape since the true distribution is not known. Therefore the unfolded and the MC distributions of the sought variable are different. After the unfolding the MC events are weighted such that the MC distribution of sought variable describes the unfolded function. In this case also the measured and simulated observable distributions have to match. This procedure is comparable to the first iteration of the forward-folding method [M+06].

For every observable a data and MC histogram value is produced and the corresponding χ^2 is calculated and can be viewed by the user. If one of the observables does not match, it is likely that this observable is not correctly simulated. If all observables show disagreement between data and MC then either the observables used for unfolding are not correctly simulated or there is a general data MC mismatch. To exclude the possibility of improper choice of unfolding parameters, prior unfolding tests on MC sample have to be carried out, as explained in Sec. 2.3.3. Nevertheless, various unfolding results with slightly changing parameters should be made also with measured data to test the stability of the result. The χ^2 of the presented verification method can be used for this testing purpose.

Test of the covariance matrix

An accurate estimation of a distribution requires a low correlation between the data points while the number of data points is as high as possible. This way the result comprises all important characteristics of a distribution with minimized bias and uncertainties. Because of the finite resolution of a measurement the final result will always have correlated bins, especially if the bin width is much smaller than the resolution. The negative correlations are dominant, if the regularization is low or in the extreme case non existent at all. The result fluctuates wildly and has unreasonably large uncertainties. With increasing regularization the positive correlations

become important and the characteristic features of distribution begin to vanish. It is the users challenge to keep balance between the correlation extrema. Therefore the subroutine to monitor the data point correlation by testing the covariance matrix has been developed. The correlation between data points is considered as negligible if the covariance matrix of the result is roughly diagonal. Accordingly, the test assumes a diagonal covariance matrix and checks generated statistical deviations from the result as explained in the following. A random Gaussian deviation $\tilde{f}(x_i)$ of the estimated bin content $f(x_i)$ in every bin i is generated $5\,000$ times. For every deviation the value z is calculated:

$$z = \sum_{i=1}^{n} \frac{(f(x_i) - \tilde{f}(x_i))^2}{\sigma_i^2}, \qquad (2.12)$$

where σ_i is the i'th diagonal element of the covariance matrix and n is the number of bins. The z^2 value is converted to a p-value which is then multiplied by 50. The resulting values are restricted to the range between 1 and 50 with interval width of 1, so that values outside this limits go into the outer bins. The distribution of the $5\,000$ p-values is visualized in a histogram. For statistically independent data points a flat uniform distribution of p-values is expected with mean bin content at 100. For a strongly correlated data points the p-value histogram shows a "sagging clothesline" behavior with very large outer bins (compare Fig. 2.3). Since there is always a slight correlation between the data points, the user has to decide when the distribution is flat enough and the covariance matrix can be assumed as diagonal. In
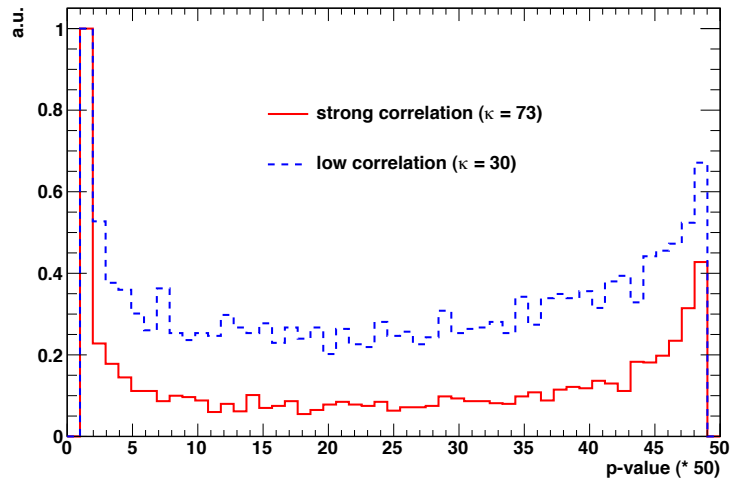

Figure 2.3: Comparison of p-value distribution for strong correlation among the data point (red) and the much flatter distribution for lower correlations (blue). The distributions maxima have been scaled to 1.

TRUEE the flatness is checked by calculating the deviation of the p-value histogram

bin contents from the value 100. The such constructed correlation value κ

$$\kappa = \sum_{i=1}^{50} \frac{(bin\ content_i - 100)^2}{50} \tag{2.13}$$

has to be minimal. Independent tests using known unfolded distributions showed that the correlation value should be $\kappa \leq 50$. This value range can be large, depending on the resolution and additional test is required as presented in Sec. 2.3.3. A further discussion on the data point correlation can be found in Ref. [Blo10].

2.3.3 New functions

The experience in working on inverse problems reveals, that some standard operations have to be carried out as preparation for the actual unfolding. As examples can be listed the selection of the suitable unfolding observables, which provide the highest amount of information about the sought distribution, as well as the selection of the optimal settings for the unfolded function, such as binning of the response matrix or the regularization parameter. Considering these requirements, additional functions have been implemented in TRUEE to make the unfolding analysis more comfortable and user-friendly. In the following the most important functions are introduced using an exemplary toy MC distribution $f(x)$.

Selection of Observables

The selection of suitable observables for the unfolding is crucial for estimating the result with high precision. An appropriate set of observables leads to result that is stable against moderate changing of regularization. The available event tuple file usually contains a large set of different observables. Since only three observables can be used for the unfolding fit at the same time, the user has to choose the best combination of maximum three observables to obtain a good estimation of the demanded distribution. The highest information content about the sought distribution is provided by observables, which have a strong correlation with the sought distribution. The correlation can be visualized in scatter plots with sought variable versus observable. Such scatter plots are created in TRUEE automatically for every input observable. Additionally the corresponding profile histograms are provided containing the mean value of the sought variable for every bin in the observable. A monotonically changing profile function over the whole range of the sought variable, together with small uncertainties, indicates a good correlation. The binning of the response matrix is equidistant, therefore a linear dependency between the observable and sought variable is optimal. In case of logarithmic dependency a transformed input of the observable or sought variable is possible.

The correlation between the chosen observables themselves should be as small as possible to avoid redundancy.
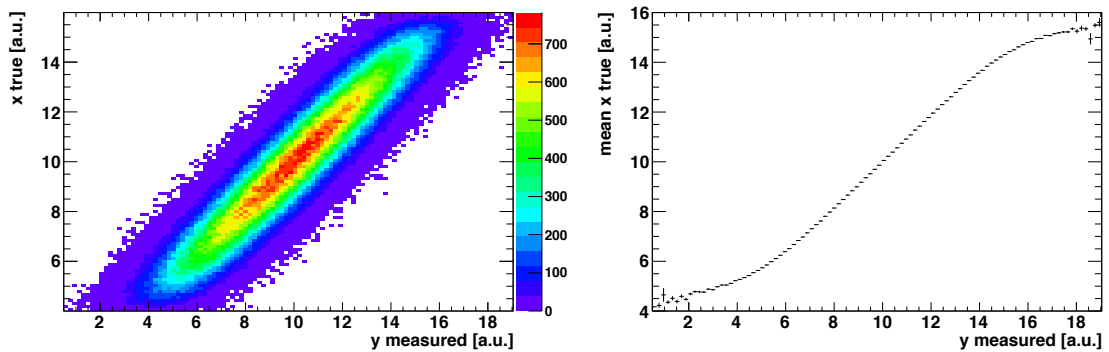
Figure 2.4: Scatter plot (left) and profile histogram (right) of the toy MC. The profile histogram is obtained calculating the mean value of the ordinate within every abscissa bin of the scatter plot. A monotonic distribution of the profile with small uncertainties over the whole x region shows a good correlation between the distributions at the axes.

Preparatory unfolding tests in the *test mode*

It is a common strategy to check the unfolding performance on a set of MC simulated data before analyzing the real measured data. To facilitate this procedure the *test mode* has been developed. While running TRUEE in *test mode* only the MC simulated sample is analyzed. A user-defined fraction of events is selected from this sample and is used as pseudo data sample for unfolding. The remaining MC events are used in the usual way to determine the response matrix and scale the result. The unfolded distribution is compared to the true distribution using the Kolmogorov-Smirnov test [CLR67] and the χ^2 calculation. This method allows to restrict the space of the possible parameter regions and can be helpful in finding the optimal observable combination, if the definite choice could not be made by the observation of the profile plots (Fig. 2.4).

Selection of parameter sets

Generally, the user of an unfolding software has to define different parameters. In the most cases these are bin numbers for the observable and the unfolded distribution and the influence of the regularization. In TRUEE the user has the possibility to define ranges of parameters. The unfolding result is provided for all parameter combinations. The in Sec. 2.3.2 introduced κ is calculated for every result and can be compared among those. For this purpose a two-dimensional histogram is produced with the parameters *number of degrees of freedom (ndf)* and the *number of knots (nknots)* at the axes. Every histogram is produced for a fixed number bins and has the κ-value as bin content (see Fig. 2.5). This parameter selection tool can be used in the *test mode* as well as in the standard unfolding.

An upgrade of such parameter space histogram has been developed for the *test*
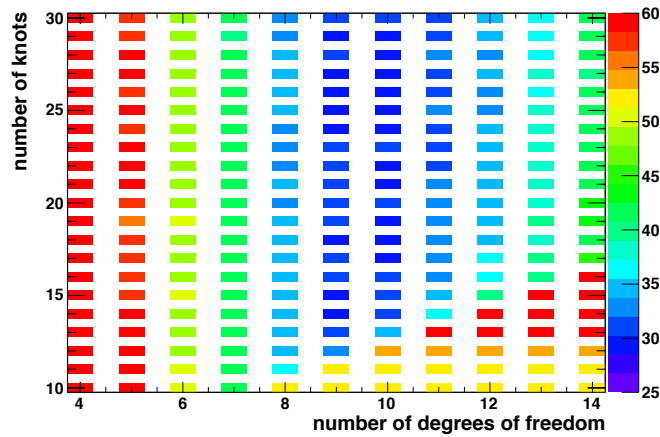
Figure 2.5: Figure for selection of results with optimal unfolding parameter sets. The results are produced for different parameter settings and the resulting quality values are compared. The color-coded data point correlation value κ is compared for different results with varying ndf and $nknots$ for a fixed binning of the result. The optimal results can be found in the region with low κ-value.
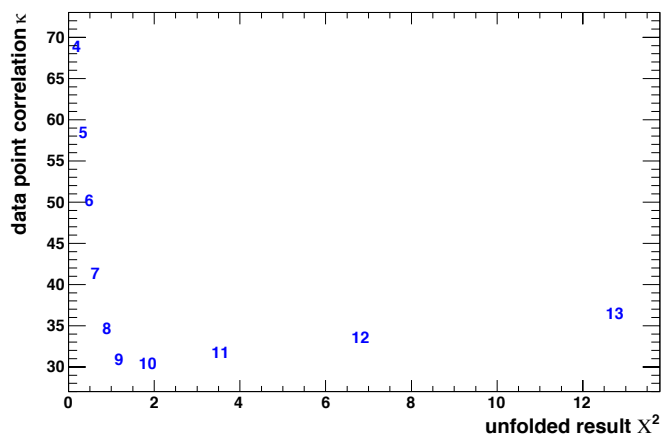

Figure 2.6: Figure of an upgraded parameter selection technique. The unfolding results are produced for different parameter settings and the resulting quality values are compared. The figure shows the value κ versus the χ^2 for different *test mode* results. Per default the results are numbered successively for different sets of parameters. For presentation reasons the results in this figure are labeled with ndf. The optimal results can be found in the kink with low axes values ($ndf = 8 - 10$). The displayed results include only the variation of ndf for simplicity.

mode. In the new histogram the κ-value is plotted versus the χ^2-value from the comparison of the unfolded and true distributions. Each result is indicated by a successive numbers in accordance to the parameter loops in the code. A list with result indices and corresponding parameter settings is produced as well. The distribution of the results in the graphics is expected to follow a curve similar to the one of the *L-curve* method [HL74]. Hence the best results can be found in the kink of the curve with the lowest κ and the lowest χ^2 (compare Fig. 2.6).

The advantage of curve histogram is that it is not restricted to a fixed dimension of parameters but can be extended easily for further parameters. Moreover the unsuitable parameter sets can be easily identified and excluded very quickly due to the large result distance from the kink.

Statistical stability check with the *pull mode*

After the selection of parameter sets and the observables the performance of the final unfolding configuration should be tested with a high number of different toy MC samples. For this purpose the *pull mode* have been implemented in TRUEE. Similar to the *test mode* only the MC sample is used and a pseudo data sample is chosen according to the expected measured data. The unfolding is executed with a fixed parameter set and the estimated and the true values are compared bin-wise. The extracted information of the residuals is stored in histograms. This procedure should be executed several hundred times and allows to make conclusions about the stability of the unfolding against statistical variations as described in the following. First the relative difference between true and unfolded $f(x_i)$ value for every bin i is created as

$$\frac{true_i - unfolded_i}{true_i}. \tag{2.14}$$

After few hundreds of *pull mode* runs the relative difference should follow gaussian distribution with the mean around zero. The deviation of the mean value from zero indicates a bias in this bin. The standard deviation of the distribution corresponds to the statistical uncertainty in the bin. Therefore the uncertainties of the unfolded function must not fall below this value.

Furthermore, the so-called pull distributions in separate histograms for each bin i are created (Fig. 2.7). The abscissa indicates the estimated uncertainty obtained from the unfolding in this bin. On the ordinate the difference over the uncertainty

$$\frac{true_i - unfolded_i}{uncertainty_i} \tag{2.15}$$

is shown. After few hundreds of runs an optimal pull distribution appears as a smooth cloud with the ordinate distribution between -1 and $+1$ with mean value at zero. A projection on the ordinate reveals a gaussian distribution. Any deviation from zero indicate a bias in the considered bin. The clouds standard deviation σ larger/smaller than the ± 1 interval means a general under-/overestimation of the uncertainties in the bin.
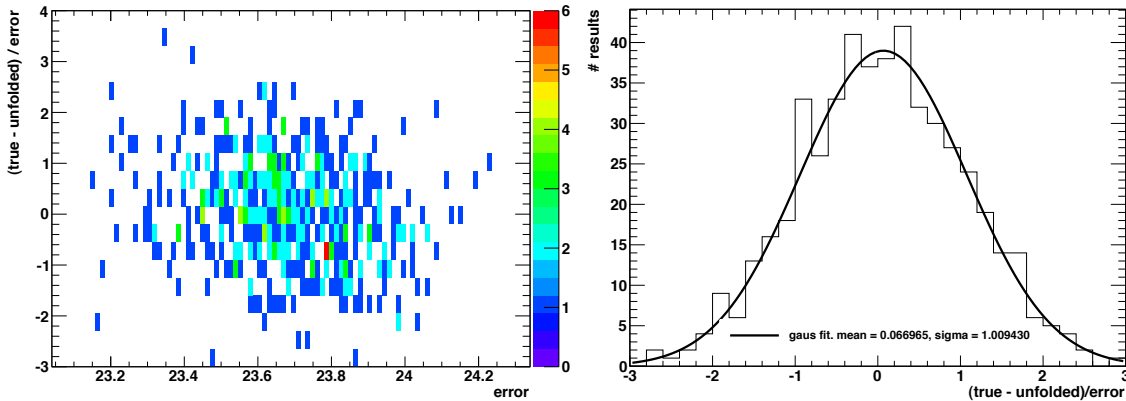
Figure 2.7: Example of a pull distribution for a random bin after 500 pseudo data
            unfolding runs (see text for explanation). The color-coded bin contents
            indicate the number of results. The left figure shows the projection of
            the pull distribution on the ordinate. A Gaussian fit is made with an
            estimated mean value and standard deviation σ.

2.3.4 Supplementary tests for unfolding with TRUEE

In this section some additional tests are made on behavior of the unfolded function
for different scenarios. The first part covers the investigation of the influence of the
assumption of the MC distribution used for the response matrix calculation on the
final result. The second part deals with unfolding of distributions with abrupt cut
off.

Impact of the model assumption in simulation

The true distribution of sought variable is not known, but generally an assump-
tion of its shape is made in the MC simulation, which is used for the determination
of the response matrix. Theoretically the distribution of the simulation should not
affect the unfolded distribution. But in a real measurement this is not the case
due to the finite binning and the therefrom resulting loss of distribution informa-
tion. Especially in the astroparticle physics, where distributions have a very steep
shape, the distribution of the MC simulation cannot be approximated as uniformly
distributed but assume a steeply falling shape. In the following the impact of the
MC assumption on the unfolding result is studied and an acceptable deviation range
between the spectral indices of MC and data distributions is found.

For the test four distributions have been simulated following a power law with
different slopes as shown in Fig. 2.8. The different distributions are used to determine
response matrices for the unfolding.

Two of the distributions with the steepest and the hardest slope have been taken
as pseudo data for unfolding. In Fig. 2.9 the steepest distribution is estimated
using four different response matrices, while in Fig. 2.10 the unfolding results of the
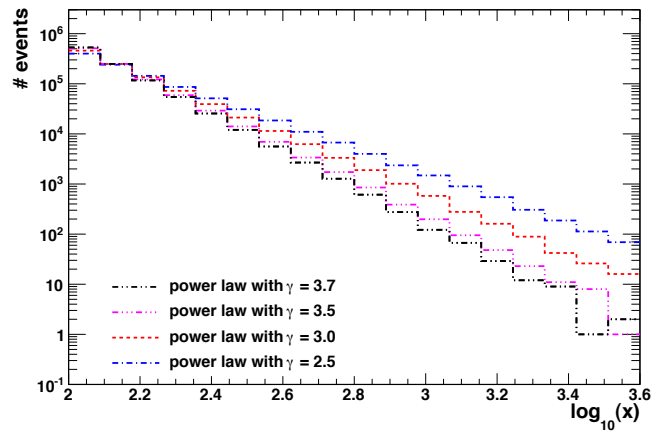
Figure 2.8: Toy MC simulated distributions following power law with different slopes. The statistics in the last two bins deviate according to the spectral index γ.

hardest distribution are shown. To compare the quality of the result the true sought distribution is shown as well.

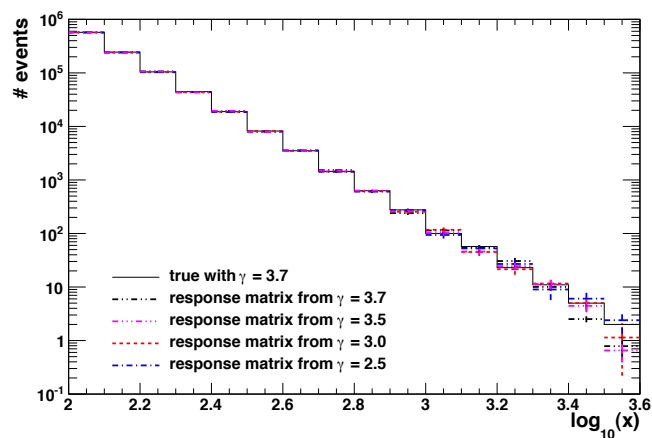
Figure 2.9: Unfolded toy MC distribution with the spectral index $\gamma = 3.7$, using four different response matrices determined from toy MC distributions with different slopes. The unfolded distribution is the same or steeper, than the MC for the response matrix. For comparison the true sought distribution is shown as a solid line.

In general the true distributions are reproduced very well at lower x-values. The steeper distribution is estimated well also with response matrix MC with highest slope deviation. The flatter distribution shows larger deviations in the last bins, while the estimated uncertainties are small. This can be explained by the strong
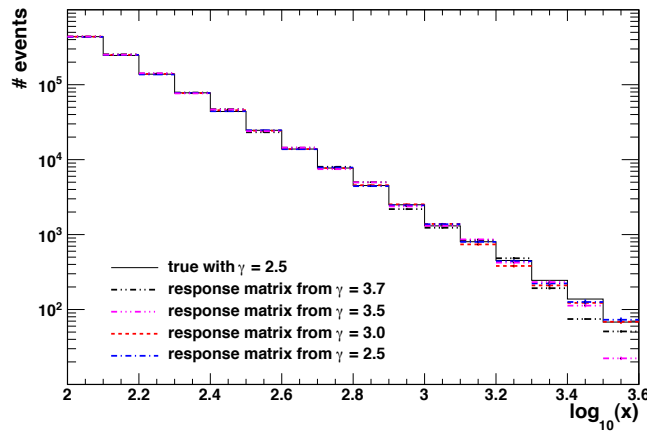
Figure 2.10: Unfolded toy MC distribution with the spectral index $\gamma = 2.5$, using
four different response matrices determined from toy MC distributions
with different slopes. The unfolded distribution is the same or flatter,
than the MC for the response matrix. For comparison the true sought
distribution is shown as a solid line.

variation in the event population of the last two bins according to the spectral
indices. Subsequently, the determination of the response matrix is not accurate
enough, when a steep distribution is used.

The conclusion of the test is that slope variations of $\gamma \approx 1.0$ between the MC
and the true sought distribution are acceptable, but the sufficient statistics have
to be ensured in the MC distribution. Therefore, a steeper MC distribution is not
recommendable. From comparison of Fig. 2.8, 2.9 and 2.10 can be deduced that
the response matrix is determined accurately, if the bin statistics count at least 10
events.

Unfolding of cut off distribution

Here the investigation on the behavior of the unfolded distribution is made, when
the true distribution has a hard cut off, for example due to the lack of events statistics
in a certain region of the sought variable. The unfolded distribution is a smooth
function, that is transformed to a binned histogram afterwards. The probability for
event migration causes a non-zero $f(x)$-values also outside the cut off.

The following test shows how an existent cut off appears in the unfolded result.
Figure 2.11 shows two distributions with abrupt break at $x = 3.2$ where the statistics
are higher and at $x = 3.3$ where the statistics are low.

In both distributions the first bin after the cut off estimates to have a non-zero
entry due to the finite resolution and hence event migration beyond the break. The
subsequent bin shows an estimated event number value compatible with zero in
both distributions. Therefore, in both examples the unfolded function behaves as
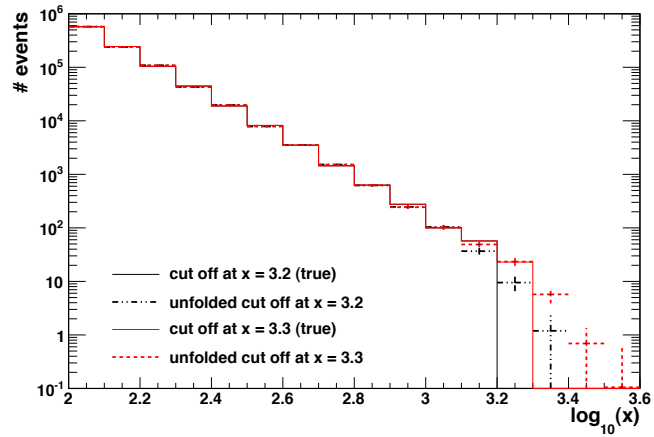
Figure 2.11: Unfolding results of two distributions with abrupt cut offs at different x-values. The solid lines show the true distributions. For both results the second bin after the break is compatible with zero, while the bin, following the cut off, still has a non-zero entry due to the finite resolution.

expected and the last bins, which are compatible with zero, can be neglected for the distribution estimation. Of course, the accuracy for determination of the cut off limit depends on the resolution and is thereby conditioned the bin size.

3 Determination of the atmospheric neutrino energy spectrum

The experimental accomplishment for the estimation of the neutrino energy spectrum requires a complex composition of detection, simulation and low and high level analysis chains. It begins with the measurement of the neutrino induced events using a large-volume detector setup. Subsequent general low level preselection procedures reduce the background contribution and amount of data. Further the high level analysis chain follows including optimized event selection techniques, energy spectrum estimation using unfolding program and the verification of the result as well as the study of the systematic uncertainties. The knowledge of the neutrino and background event behavior is essential to create authentic MC simulation which is used for the event selection and determination of the detector response.

Due to the so-called "blindness" policy [KR05] the full analysis is first developed on only 10 % of data (burn sample) to avoid any bias towards certain expectations. After approval by the collaboration the full data can be accessed and analyzed.

3.1 The IceCube neutrino observatory

The detection of neutrino induced events with a reasonable statistics requires a large detection medium volume. IceCube [A+04b], [A+11c] is the largest neutrino detector in operation and is well suited for this task. The main goals of this experiment is the search for extraterrestrial neutrinos from the Milky Way, extragalactic neutrinos from AGNs or GRBs and the cosmogenic neutrinos to clarify the question on the origin and energy range of galactic and extragalactic cosmic rays. Apart from this the search of exotic events such as magnetic monopoles or dark matter particles is performed with IceCube.

3.1.1 Experimental setup

IceCube is a cubic kilometer large neutrino telescope located at the geographic South Pole. Its detection principle is based on the measurement of the Cherenkov light, produced by charged particles in the glacial ice [Che34]. For this purpose 5 160 digital optical modules (DOMs) are arranged in the ice at the depths between 1 450 and 2 450 m. The DOMs are fixed on 86 vertical strings arranged in a triangular grid (see Fig. 3.1). Every DOM consists of a photomultiplier tube (PMT) [A+10a] with a diameter of 25 cm and programmable data acquisition board placed in a 35 cm
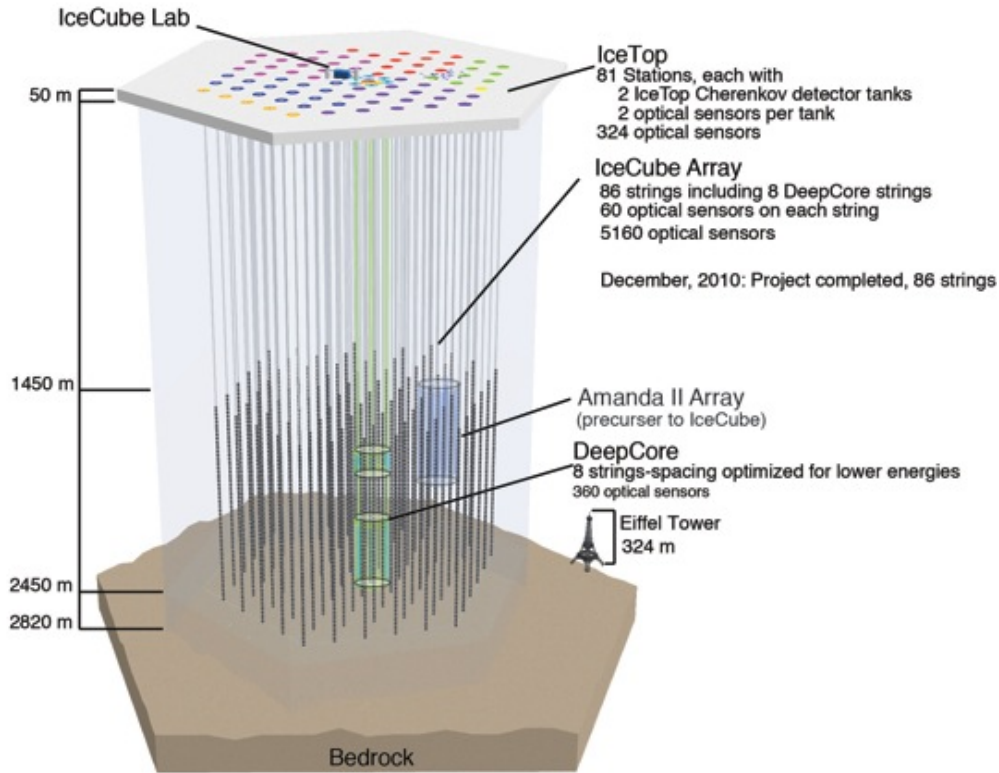
Figure 3.1: A schematic view of the complete IceCube detector. The color coding in the IceTop indicates the deployment seasons (see also Fig. 3.3). In the center of the IceCube array the DeepCore is highlighted consisting of 8 strings in its final configuration. AMANDA, the precursor of IceCube was in operation until the IceCube 59 string season. At the surface in the IceCube Lab the raw data is stored and processed. The large size of IceCube is compared to the height of Eiffel Tower. Figure is taken from Ref. [Ice12].

pressure sphere, as shown in Fig. 3.2. The photocathode of the PMT is sensitive to the photons with 300 nm - 650 nm. Single Cherenkov photon arriving at a DOM and producing a photoelectron is called hit. The acquisition system records the amplitude and time information of the PMT caused by the Cherenkov photons and sends them to the surface in a digitalized form. For a detailed description of the DOM electronics and the full data acquisition system see Ref. [The08]. To reduce the noise only signals are recorded, that ensure a hard local coincidence (HLC). The HLC is given, if two nearest or next-to-nearest DOMs show a hit within a time window of $1\,\mu$s. This can be measured because the DOMs are able to communicate

with their nearest neighbor DOMs on a string. Since May 2009 also the soft local coincidence (SLC) mode is available that additionally to the coincident hits allows to record limited information from separated DOMs. This makes the signal pattern of the event more fine-grained. On the surface the computers of the IceCube laboratory build physical events from the signals of individual DOMs if some necessary trigger criteria are fulfilled [Kle09].
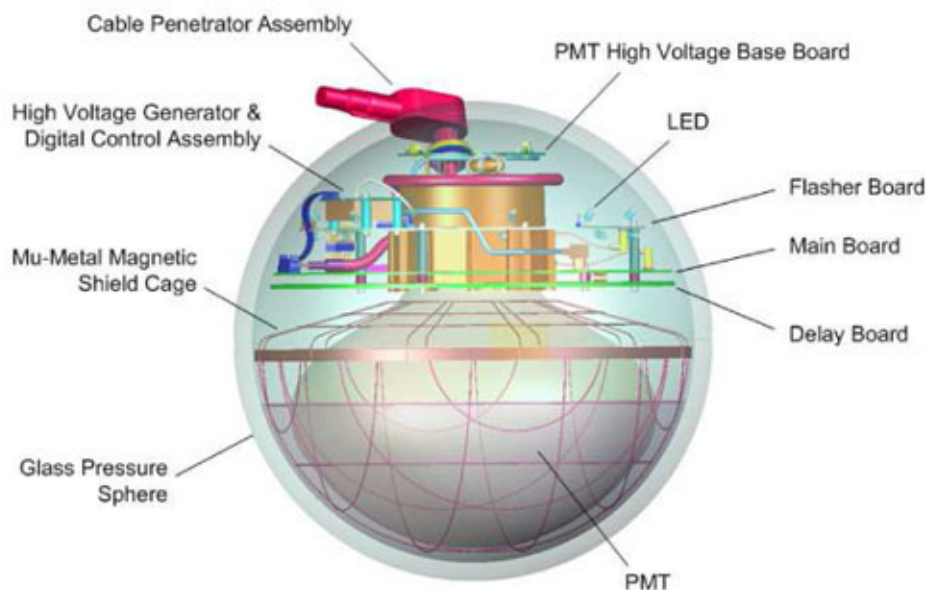

Figure 3.2: The schematic view of a Digital Optical Module containing a PMT, corresponding electronics and the acquisition board. The installed LEDs are used for calibration and study of ice properties [A+11e]. The mu-metal magnetic shield cage is used to decrease the influence of the Earth's magnetic field. Figure is taken from Ref. [Ice12].

Around the center in the bottom part of the IceCube detector a compact arrangement of strings is located, equipped with DOMs containing high quantum efficiency PMTs. This DeepCore array together with the outer IceCube strings as veto is capable to decrease the threshold for low energy events and improve the signal to background ratio for the low energy analysis such as the dark matter search [A+12b]. Additionally, a two-dimensional array of DOMs covers the surface above the IceCube setup and represents the air shower array IceTop [Kis11]. The surface DOMs are arranged in double tanks containing two DOMs each above each of the IceCube strings. IceTop is developed to investigate the cosmic ray composition and to reduce the amount of background events caused by the atmospheric muons.

The deployment of strings and IceTop tanks was carried out during the antarctic summer seasons starting in the year 2005 and being finished at the end of 2010. Nevertheless, the partially constructed detector has been continuously in operation

and data has been taken and analyzed with the different continuously developing string configurations. Figure 3.3 illustrates the chronological development of the detector. The data analyzed in this thesis has been taken during the season from the 20th May 2009 to the 30th May 2010 with the 59 string configuration (IC 59) including one DeepCore string.
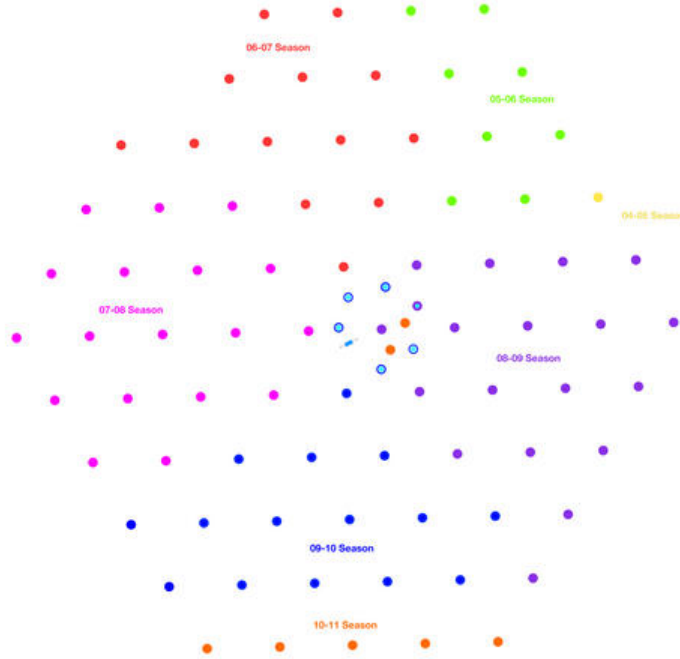
Figure 3.3: The top view of the IceCube array. The color code visualizes the seasonal development of the detector. The IC 59 configuration was achieved in the season 09 - 10 (blue). Figure is taken from Ref. [Ice12].

3.1.2 Neutrino detection method

Neutrinos undergo only weak interactions and therefore cannot be observed directly. If a neutrino of the considered energy range interacts in the vicinity or within the detector volume the secondary charged lepton induces Cherenkov light in the ice that can be detected by the PMTs. From the hit time difference and amount of charge in the involved DOMs the information about neutrino energy and arriving direction can be extracted. According to the flavor of the neutrino the secondary particle is an electron, muon or tau lepton. Only the muons produce a track-like signature and give sufficient directional information. Thus, only muon-neutrinos are considered in this analysis. The electron- and tau-neutrino interactions lead to cascade-like events and are the subject of other analyses [A+12a], [A+11b].

The energy loss of muons in the ice per distance X is described by the formula [A$^+$08c]

$$\frac{dE}{dX} = -a(E) - b(E)E. \tag{3.1}$$

The parameter $a(E) \approx 0.24 \, \text{GeV/m}$ is the continuous energy loss through ionization and $b(E) \approx 3.3 \cdot 10^{-4} m^{-1}$ is the stochastic radiative energy loss caused by bremsstrahlung, pair production and photonuclear scattering. Both parameters slightly depend on the energy. For energies $E \approx 10^3 \, \text{GeV}$ and higher, the stochastic energy losses become important. They appear in form of relativistic showers which emit Cherenkov light as well. Thus, the produced amount of light becomes proportional to the muon energy. About $75\,\%$ of the primary neutrino energy is transferred to the secondary muon [BCK02].

The median angular resolution of IceCube for muon energies $E > 10^4 \, \text{GeV}$ is about $1°$ as has been demonstrated by the moon shadow analysis of the cosmic ray induced muons [Chi11]. The mean angle between the primary neutrino and the secondary muon is $\theta \approx 1°/\sqrt{E_\nu/TeV}$, thus the directional information of the primary neutrino is conserved within the angular resolution range of the detector. This fact is important in this analysis for the application of zenith cuts.

3.1.3 Event reconstruction

A muon event in IceCube usually appears as a track and can be described by a set of parameters, such as direction, location of an arbitrary point along the track in the detector or the time at this point. To determine these track parameters different event reconstruction methods are applied in IceCube data. The fast first guess algorithms make a rough quality estimate of the track and provide initial hypothesis (seed) to the more advanced iterative algorithms for more precise estimation of the parameters.

Line fit

The *line fit* [Ste90] is a fast and simple first guess reconstruction algorithm that enables a quick decision about the quality of a lepton track. It works with simplified assumptions about Cherenkov light propagation and ignores the detector geometry. The light is assumed to travel with a velocity $\mathbf{v}$ along a single line through the ice. The positions $\mathbf{r}_i$ of the hit DOMs are connected by a line

$$\mathbf{r}_i \approx \mathbf{r} + \mathbf{v} \cdot t_i, \tag{3.2}$$

with hit time t_i of hit i. A χ^2 minimization over all hits with respect to the free parameters $\mathbf{r}$ and $\mathbf{v}$ is performed analytically. The obtained parameter include vertex point and the direction and hence a zenith angle of the track. The result is used as seed for the iterative likelihood algorithms [A$^+$04a].

Likelihood algorithms

The more sophisticated muon track reconstruction algorithms are based on the iterative maximization of likelihood functions [A$^+$04a]. The most important likelihood functions consider the time residuals $t_{res,i}$ between the expected and the actual arrival time of a direct non-scattered photon i. The simplest function works with the probabilities p_1 for the arrival times of single photons at the location of the hit DOMs (Single PhotoElectron = SPE)

$$L_{time} = \prod_{i=1}^{N_{hits}} p_1(t_{res,i}|\mathbf{a} = d_i, \eta_i, ...), \tag{3.3}$$

where the free variables $\mathbf{a}$ are track parameters. The probability function p_1 is deduced from the simulation of photon propagation through the ice (Sec. 3.1.4). In IC 59 eight iterations of the SPE fit are executed. Very often more than one photons hit the photocathode within a very short time window (few 100 ns), generating only one pulse due to the limited time resolution. This can be considered with the multi-photo-electron (MPE) probability function. The MPE likelihood fit uses the arrival time distribution of the first hits accounting for all measured N photons per DOM. Since the first photon is usually less scattered than the following $N - 1$ photons its determined arrival time distribution becomes narrow. This increases the track reconstruction accuracy. The MPE fit uses the resulting parameter of the SPE likelihood function as seed to find the global extremum.

Center of gravity

The so-called *inertia tensor algorithm* treats the pulse amplitude in a DOM with position $\mathbf{r}_i$ as a virtual mass a_i [A$^+$04a]. Hence, for each event a tensor of inertia $\mathbf{I}$ can be constructed using the virtual mass distribution. The origin of the tensor is the center of gravity (COG)

$$COG \equiv \sum_{i=1}^{N_{ch}} (a_i)^w \cdot \mathbf{r}_i, \tag{3.4}$$

with N_{ch} the number of DOMs with non-zero virtual mass and $w \geq 0$ the arbitrary amplitude weight. The position of COG in the detector is described by the X, Y and Z directions. Z is the vertical axis and corresponds to the depth of the detector with origin in the middle of the in-ice setup. In the following the abbreviation $COGZ$ is used to indicate the COG in the depths of the detector.

Quality parameters

The measurement provides different variables obtained from direct measurement such as number of DOMs (*NCh* for number of channels) or from different reconstruction algorithms such as *MPEFit_Zenith*. In the latter case the name of obtained quantity is attached to the fit name at the end. For this analysis important quantities and their titles, as they used in the data files, are described in the following.

- *NCh* provides the number of all DOMs involved in an event track.

- *NStrings* is the number of all strings involved in an event track.

- *NHits* is the number of all hits in all DOMs including the early and the late hits.

- Number of direct hits (*NDir*) indicates the amount of non-scattered direct photon hits, that arrive within a certain time window compared to the expected hit time. There are different time windows, indicated by the letters *A, B, ... E*, that correspond to increasing time residuals. Therefore the variable *NDirA* contains less hits than *NDirE*, which contains all hits from *NDirA* and additional latter arriving hits.

- The length of direct hits (*LDir*) is calculated by projecting direct hits along the reconstructed track and taking the distance between the outermost DOMs and is given in meters. The time window of direct hits is assigned in the title with the corresponding letter e.g. *LDirC* for t_{res} between -15 ns $+75$ ns [A$^+$04a].

- *NEarly* and *NLate* are the numbers of hits measured before or after the direct hits respectively.

- *Zenith* and *Azimuth* are the direction angles of the track in the detector system. The events with *Zenith* $\Theta = 0°$ are called down-going and come from the southern hemisphere while $\Theta = 180°$ stands for up-going events coming from the direction of the Earth core. The $\Theta = 90°$ indicates horizontal events.

- *LFVel* is the lepton velocity estimated by the *line fit*. Tracks from muon events have a velocity comparable with the speed of light. Cascade-like events have a low velocity [A$^+$04a].

- Smoothness of the muon track *SmoothAll* is a topological parameter, that describes the evenness of the light emission and hit distribution along the track. The parameter varies between -1 and 1, with the most homogeneous track at *SmoothAll* $= 0$ [A$^+$04a].

- The average energy loss per unit propagation length *dEdX* is a variable, that is estimated by the PhotoRec algorithm [GBH08]. *dEdX* is an energy estimator, which has been used in the previous atmospheric neutrino analysis for the unfolding of the energy spectrum [A$^+$11d]. The *dEdX* is given in arbitrary units.

- Additional energy estimator, commonly used, is the muon track energy from the reconstruction algorithm *MuE*. The energy is determined from estimated number of photons emitted per unit track length, but in opposite to *dEdX* bulk ice without dust layers is assumed. *MuE* energy is defined in units of GeV.

- *QTot* is the total charge deposit in all DOMs. Apart from minor corrections *QTot* is a directly measured quantity. The unit corresponds to the charge of one photoelectron (PE).

- *logl*, *rlogl* and *Plogl* are related variables that are derived from the likelihood maximization. *logl* is the logarithmic likelihood of the corresponding fit algorithm. *rlogl* is called reduced *logl* and is calculated by dividing the *logl* by the value (*NCh* - 5). Similarly the *Plogl* is calculated by dividing the *logl* by the value (*NCh* - 2.5). The "P" stands for the first name of the inventor P. Berghaus of the variable. *Plogl* is a strong event classification variable and is constructed for the event selection (see Sec. 3.2.2).

- *status* provides information whether the corresponding likelihood fit succeeded or failed.

- *pbf_err* and *pbf_sigma* are parameters that estimate the pointing precision of the maximum likelihood reconstructed track. They are obtained from the *paraboloid fit*, which constructs a confidence ellipse by fitting a paraboloid to the likelihood space near the best fit minimum [Neu06]. The uncertainty refers either to the ellipse axes or to the ellipse projection on the detector geometry system.

- *nmini* is the number of minimization calls in the algorithm.

More information on the quality parameters can be found in Ref. [A+04a] and [A+02].

3.1.4 Simulation

To identify and collect the neutrino-induced events in the IceCube data a parallel analysis with MC simulated data has to be performed. Furthermore the final MC sample obtained after event selection is used to determine the detector response function for the unfolding. In the MC simulation all physical effects have to be considered with an accurate approach to keep systematic uncertainties low and provide an authentic scenario of the particle propagation and measurement.

The MC simulation consists of two kinds of datasets: neutrino data and atmospheric muon data. The simulation of neutrino events corresponds to the the true demanded neutrino events that have to be identified. In the event classification techniques these are called signal events. The atmospheric muons coming from the air showers in the atmosphere are simulated to identify them as background in the data and distinguish from the sought signal events. The simulation is handled within the collective software framework IceSim [O+12].

Neutrino simulation chain

The simulation of neutrinos begins with the neutrino generation at the surface of the Earth with the neutrino generator software based on ANIS (All Neutrino Interaction Simulation) [GK04]. The neutrinos are generated isotropically and propagate through the Earth and ice towards the IceCube detector. Thereby the energy loss due to neutral current interactions is taken into account in the simulation by ANIS as well as absorption and regeneration due to charged current interactions. The non-absorbed neutrinos are forced to undergo an interaction within or close to the detector volume. This procedure is necessary to save memory and simulation time. The real interaction probabilities are included in a specific event weight, called *OneWeight*. It considers all relevant factors such as generated spectral index or generation volume and can be used to weight the simulation to match a certain model. The initial spectral distribution of the generated neutrino data sets used here is proportional to E^{-2} to ensure high statistic in the energy region of atmospheric neutrinos. The energy spectrum covers the range between $10\,\text{GeV}$ and $10^9\,\text{GeV}$. As the output of the neutrino generator the information of the primary particle and the secondary particle after the first neutrino interaction is stored. After a charged current interaction a muon is produced and propagates through the detection volume. The propagation of muons in the rock and glacial ice is simulated with the MMC (Muon Monte Carlo) software [CR04]. There the muon energy loss according to the Eq. 3.1 is implemented and the number of the Cherenkov photons produced by muons and secondary particles is calculated. The propagation of the photons through the ice is managed with the Photonics software package [L$^+$07] considering scattering and absorption of photons in the ice. The time distributions and flux of photons are recorded averaged over cells throughout the approximated detector volume grid. To complete the imitation of a real measurement, the detector response has to be simulated. The hit construction is made by using the photon propagation output while considering the propagation probability from the pressure sphere of the DOM to the PMT cathode. The simulated electronics response and the fulfilled conditions of trigger logic complete a simulated MC event.

Atmospheric muon simulation

Atmospheric muons coming from the cosmic ray induced air showers represent the dominant background for the neutrino events. The primary cosmic ray energy spectrum and the air shower propagation is simulated with the CORSIKA (COsmic Ray SImulation for KAscade) software [H$^+$98]. For the composition and spectrum the poly-gonato[1] model is chosen [Hoe03]. The poly-gonato model assumes a cosmic ray composition of all stable nucleons ($Z_{max} = 92$) and their successive cut offs with increasing energies. The hadronic interaction model SIBYLL is applied [A$^+$09]. The muon and photon propagation in the ice is handled the same way as for neutrinos. The zenith angle for atmospheric muons is restricted to the southern hemisphere

---

[1]Greek: "many knees"

and thus has a zenith region of $0° - 90°$, since muons from below the horizon are absorbed by the Earth. A CORSIKA data set is simulated for a certain time scale and therefore the distribution has to be scaled to the requested live time.

Ice model

For an accurate description of the muon energy loss and the photon propagation in the ice the optical properties of the ice have to be examined. Therefore the absorption and scattering coefficients have been measured over the depths between $1\,100\,\mathrm{m}$ and $2\,350\,\mathrm{m}$ using in-situ light sources in IceCube's precursor AMANDA [A$^+$06].

The glacial ice developed during a long period of time and is not homogeneous due to varying climatic conditions. A frequent dust accumulation became enclaved in the depths of the ice in form of horizontal layers. The measurement revealed particularly high concentration of dust at the depths of around 2050 m. Further little dust layers are identified in the upper part of the ice. Below the main dust layer the scattering and absorption of the ice for light (400 nm) is at a minimum and shows low variations. From the measurement a model (AHA - Additionally Heterogeneous Absorption model) could be created to describe the ice properties and is applied in simulation.

The more recent measurements with the IceCube's LEDs as light sources have been made to study the ice properties over the whole depth of the detector [Chi09]. The model introduced in Ref. [A$^+$06] has been fitted by a new method to measured in-situ light data. The hence obtained parameters could be used to develop a new ice model called SPICE (South Pole ICE).
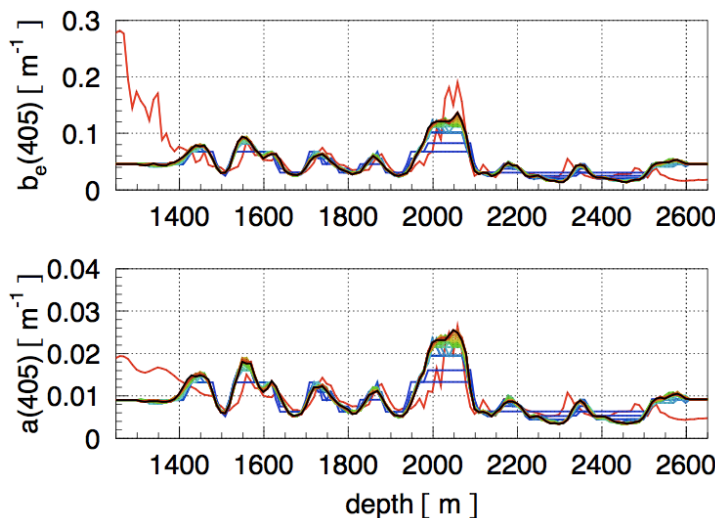

Figure 3.4: Depth-dependent absorption (a) and scattering coefficient (b) at the 405 nm for the AHA (red) and SPICE (black) models. The dust layer at 2050 m is clearly visible.

Figure 3.4 shows the absorption and scattering coefficients depending on the depth for the SPICE and AHA models. The simulation applied in the presented work implements the SPICE model. Moreover, an newer SPICE model SPICE Mie [A$^+$11e] has been developed and is used in the analysis for systematical checks.

3.2 Neutrino sample

The most relevant background for neutrino induced events in the IceCube detector is represented by the atmospheric muons originating from cosmic ray air showers. Due to insufficient knowledge about the atmospheric muon spectrum the background cannot be considered in TRUEE during unfolding but has to be suppressed. Therefore, to estimate the neutrino energy spectrum with high precision a sample of neutrino events is required with a possibly low contamination by the background events.

The atmospheric muon tracks within the detector show the same signal pattern as the neutrino-induced muon tracks. Bundles of multiple atmospheric muons can fake a high energy event of a single neutrino-induced muon. To distinguish the interesting neutrino-induced events from the atmospheric muon events and thus to obtain a sufficiently large neutrino sample with high purity, a chain of event selection techniques has been developed using MC simulation and has been applied on data. The purity of the data increases after every data selection step from low level up to the highest level (neutrino level).

3.2.1 Low level neutrino event selection

The recording of events which satisfy the trigger condition is done with very high frequency. To a large extend the data at trigger level consists of down-going atmospheric muons. The ratio of neutrino-induced events to the measured background muons is roughly $1 : 500\,000$ [HK10]. All events are stored on tape and transported to the Northern hemisphere every year. A faster data transfer is made via satellite. For this purpose the large amount of data is reduced locally at the South Pole by a Processing and Filtering system. The filters reject poorly reconstructed events using simple conditions, such as minimum number of DOMs or zenith restrictions from first-guess algorithms (muon filter). After filtering, the obtained *level 1* data is transmitted to the Northern hemisphere via Satellite. The data movement is managed by the South Pole Archival and Data Exchange (SPADE) system [Mac05]. The processing of data to the purity *level 2* is performed with more memory consuming techniques using sophisticated algorithms such as introduced in Sec. 3.1.3.

From *level 2* the event selection becomes more characteristic with respect to the analysis goal. As the basis for the high level event selection in this thesis the *level 3* sample for the point source analysis is used. The event selection has been developed and applied on data by Mike Baker. The background suppression is made by a series of straight cuts aiming a concentration of high quality muon tracks in the remaining

data [Bak11]. The estimated purity is roughly 0.2 %.

3.2.2 High level neutrino event selection

The final event selection chain consists of preselective straight cuts and a multivariate classification method. It has been developed in Dortmund by Tim Ruhe and is aligned for an atmospheric neutrino analysis, ensuring high statistics over the whole accessible energy region and a smooth zenith angle distribution [RMS11],[RM11]. The application starts from the *level 3* data sample mentioned above.

Straight cuts

Since neutrinos with energies up to 1 PeV can pass through the Earth while the atmospheric muons get absorbed, the Earth can be used as a filter. Taking into account only neutrinos from the Northern hemisphere, by applying a zenith cut at the horizon, reduces the background significantly. Additionally, the cut on the velocity of the track is performed to reduce the cascade-like events.
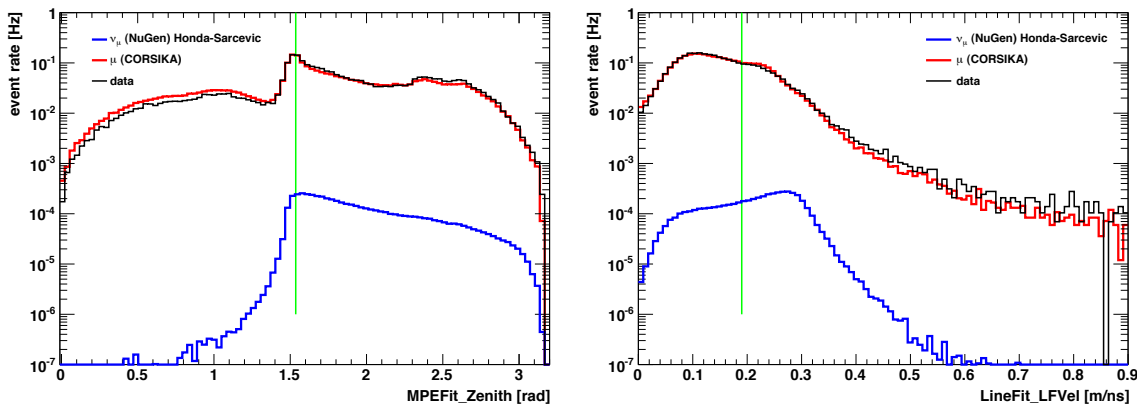

Figure 3.5: Event rate distributions of precut variables for MC and data. The green lines indicate the cut locations. The cut for zenith angle (left) is made at $> 88°$, the velocity cut (right) at > 0.19 meter per nanosecond.

variable	cut value
zenith (MPE)	$> 88°$
velocity (*line fit*)	$> 0.19\,\text{m/ns}$

Table 3.1: Preselection cuts applied on *level 3* data to significantly reduce the background.

The MC and data distributions of both observables used for the precuts are shown in Fig. 3.5. The optimal cut values of zenith and velocity have been determined by comparing the data and MC simulation in the space of the two variables.

The precuts are summarized in Tab. 3.1. Due to a better performance the zenith cut is made slightly above the horizon. Nevertheless at the final neutrino level no events remain with zenith $\theta > 90°$.

Random Forest

The obtained sample has now an increased purity level (*level 4*) but still contains a high amount of mis-reconstructed background events caused especially by multiple atmospheric muons, which coincidently trigger the detector. Tree-based algorithms, such as Boosted Decision Trees (BDT) [DC95] have already been successfully used for event classification in analyses within the IceCube collaboration. The algorithms are efficient and stable against minor variations in the data set. For the current analysis the Weka-Random Forest [Bre01],[H⁺09] is applied using the Java-based framework RapidMiner [F⁺02]. Its advantage is the high robustness against over-training. A Random Forest consists of a defined set of decision trees. Every tree provides a Boolian value whether the even is classified as signal or background. The output of the Random Forest for an event is called *signalness* and is the average value over all decision tree results. Since *signalness* is a pseudo-real value between 0 and 1 a cut can be set at the *signalness* value with best ratio of signal over background. The applied model for event classification has to be determined by training with MC simulations. The determination of an appropriate set of 27 observables (attributes) for the event classification with Random Forest out of a large set of more than 2 000 event attributes has been developed in Dortmund [Wor11]. The attributes are mostly geometrical track parameters and the likelihood values determined with different fit functions, as well as directly measured observables, such as number of strings. Three of the attributes are constructed from other observables, as they are not existent in the data set (see Tab. 3.2).

attribute	formula
Plogl	MPEFit_logl / (NCh - 2.5)
Δ *zenith*	|MPEFit_Zenith - LineFit_Zenith|
Δ *logl*	SPEFit8Bayesian_logl - SPEFit8_logl

Table 3.2: Additional attributes constructed from observables provided by the data files.

The attributes applied in Random Forest are shown in Fig 3.6 - 3.9 including the zenith distribution in Fig. 3.5 (left). The comparison of MC simulation and measured data is presented at *level 4*.
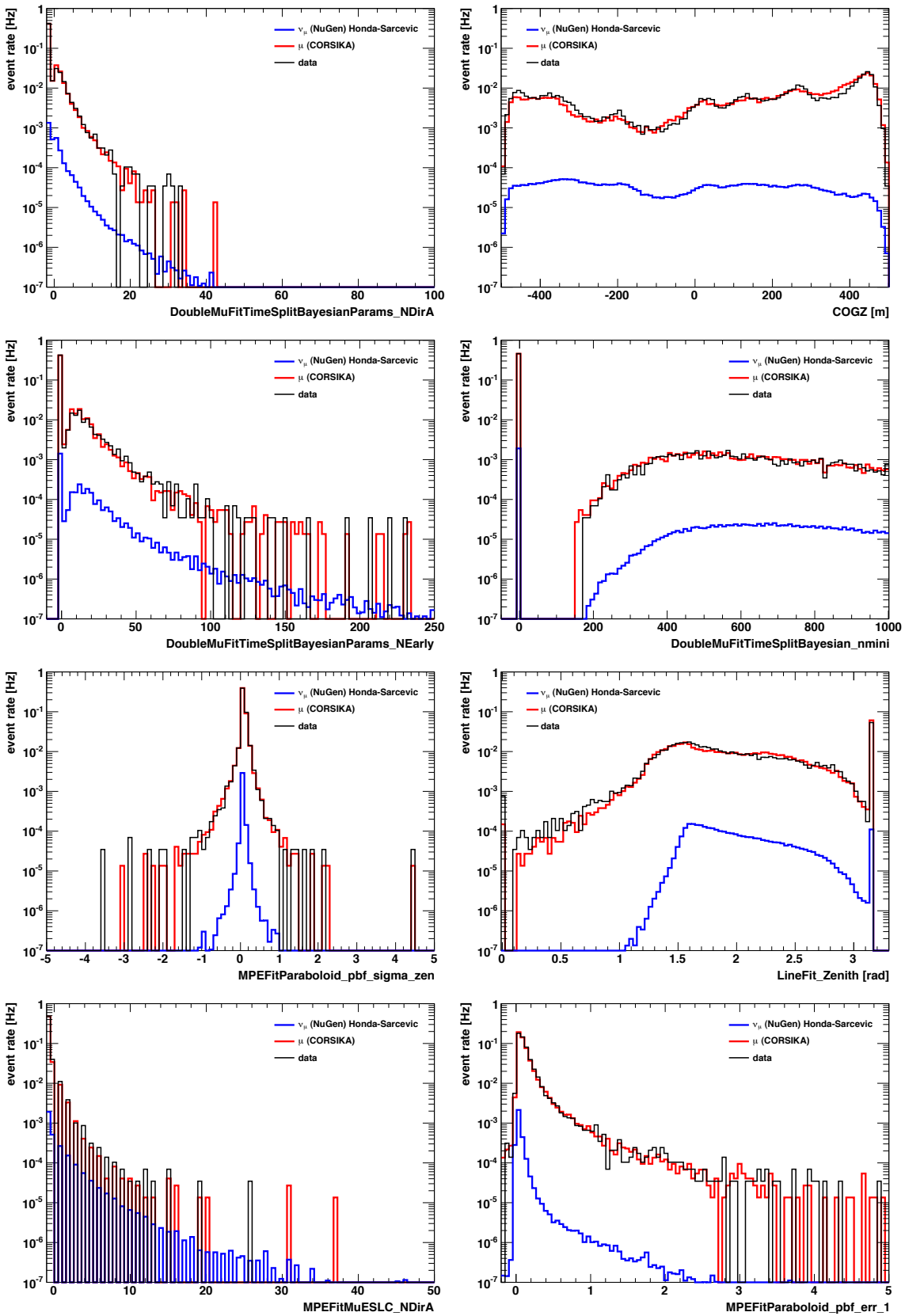
Figure 3.6: Simulation and data comparison of a set of attributes used for the event classification with Random Forest after precuts to the purity *level 4*. The entries represent event rate in Hertz.
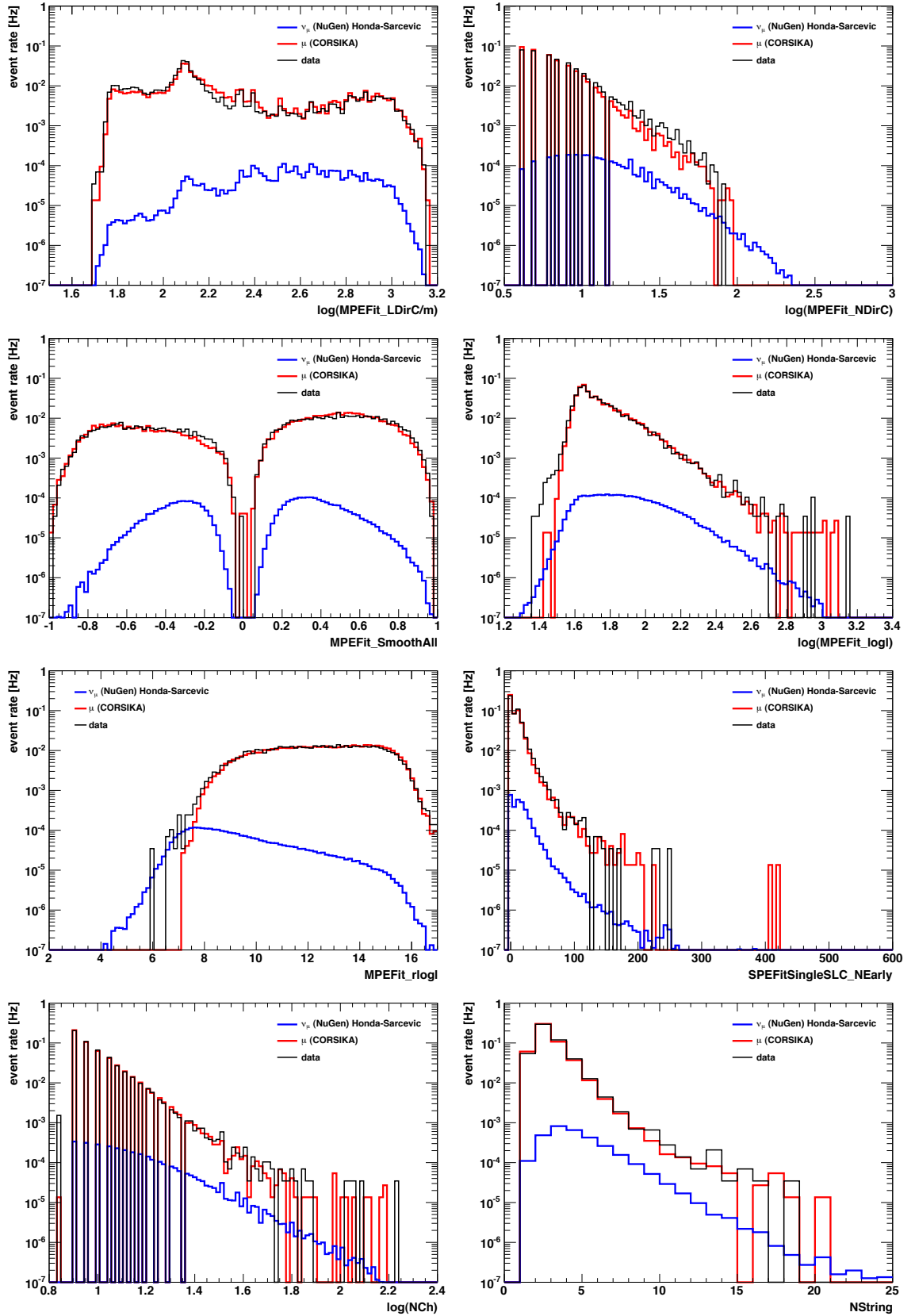
Figure 3.7: Simulation and data comparison of a set of attributes used for the event classification with Random Forest after precuts to the purity *level 4*. The entries represent event rate in Hertz.
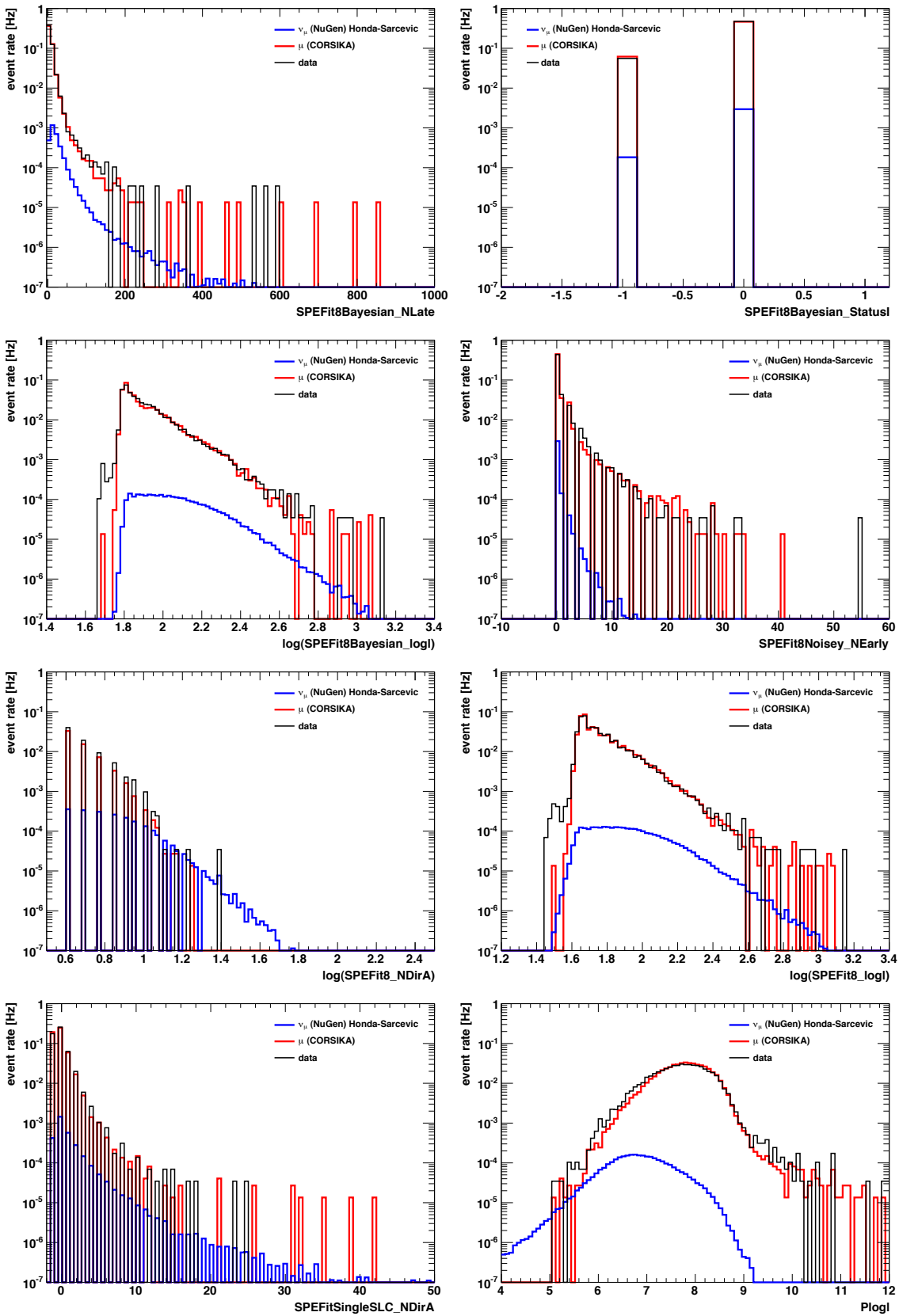
Figure 3.8: Simulation and data comparison of a set of attributes used for the event classification with Random Forest after precuts to the purity *level 4*. The entries represent event rate in Hertz.
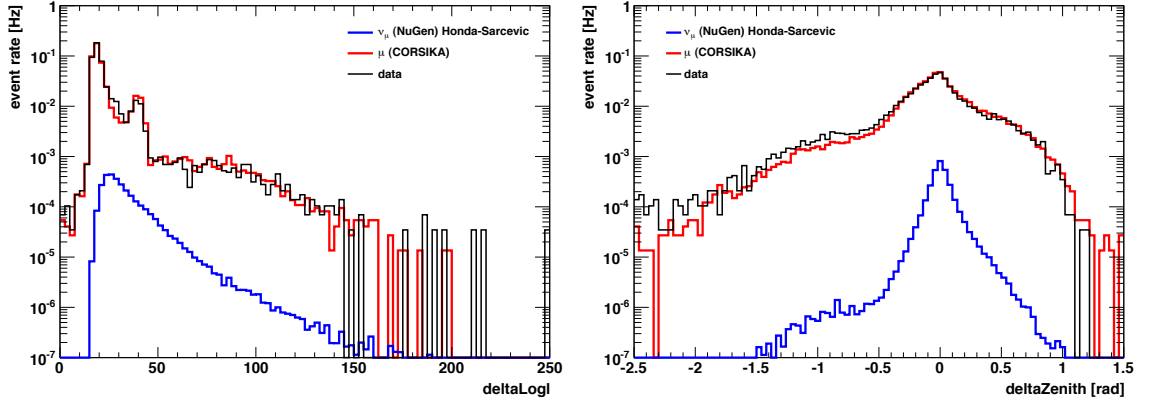
Figure 3.9: Simulation and data comparison of a set of attributes used for the event classification with Random Forest after precuts to the purity *level 4*. The entries represent event rate in Hertz.

The internal alignment of the Random Forest is set as follows. From the signal and background samples 28 000 events each are taken to train the classification model with 500 trees. Only the events with signalness of 1.0 are selected as signal events and chosen to form the final neutrino sample. The distribution of the Random Forest output for the burn sample and the full year data sample is shown in Fig. 3.10. For
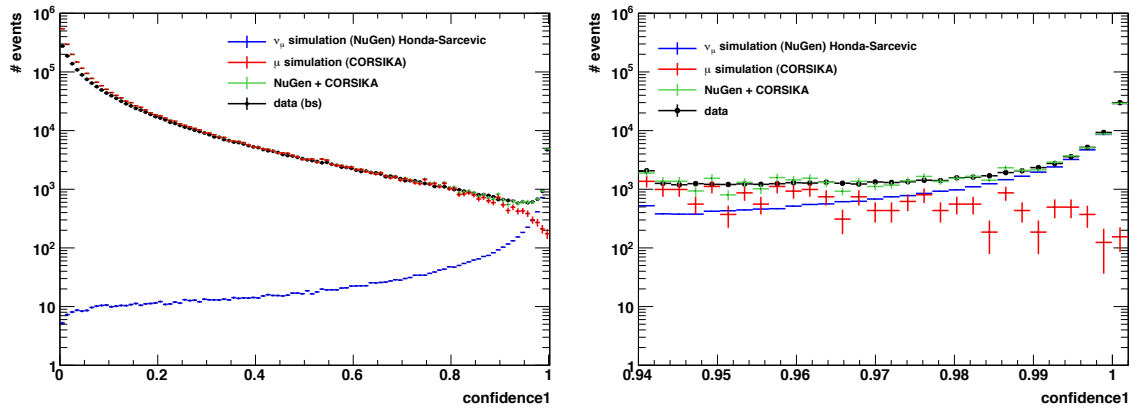

Figure 3.10: *Signalness* as the Random Forest output classifies the events as signal at *signalness* = 1 or as background at *signalness* = 0. The left histogram shows the full *signalness* distribution for the burn sample data (10 % of full year). The right plot is a zoom into the high *signalness* region for the full IC 59 data. The overestimation of simulation at low *signalness* values is caused by the uncertainty in the primary cosmic ray spectrum and thus by the varying amount of mis-reconstructed low energy background muons, which dominate in this region. For the analysis the *signalness* cut at 1 is made. The sum of neutrino and muon simulation describes well measured data in this region.

the background estimation in the measured data sample a 5-fold cross-validation is performed. For this purpose 35 000 simulated neutrino and background events are used as input for the Random Forest. From these a sample of 7 000 events is chosen to test the model application while the remaining 28 000 events are used in the usual way for the training. The verification has been executed five times with statistically independent samples and the average of the remaining misclassified background events was determined. The cross-validation predicts 50 ± 110 background events in the final sample. This defines a purity of around 99.4 % in the final data sample.

The development of the neutrino event selection at the different purity levels is summarized in the Tab. 3.3. The simulated number of neutrinos remaining at

one year IC 59 data	level 3	level 4	neutrino level
number of events	100 861 000	17 538 400	29 890
estimated purity [%]	0.2	0.5	99.4

Table 3.3: Development of the IC 59 neutrino sample and its purity over different levels after successive application of series of cuts and Random Forest method.

the final level is 28 975, if models of Honda and Sarcevic are used for weighting and 30 880 for Bartol and Sarcevic. In the following the Honda-Sarcevic model is used as standard weighting model. The slightly lower amount of estimated number of events compared to the real data is caused by the uncertainty in the neutrino flux model, which is $\sigma_{theor.} \approx 15$ % [B^{+}06]. The true number of remaining simulated neutrino events is 227 088 and ensures enough statistics for a proper determination of the response matrix for the unfolding. The obtained amount of background events is 155, scaled to the full year live time. This value is within the predicted uncertainties, and therefore the contribution from background is neglected in the following study.

3.2.3 Data-simulation comparison

After the event selection the simulated neutrino sample has to describe the measured data with a high precision. The comparison of simulated and measured distribution of the variables used for further analysis and for different energy estimators is shown in the following. The simulated neutrino events are weighted according to different atmospheric neutrino models for comparison. Honda-Sarcevic includes the contribution of conventional and prompt neutrinos while Bartol weights consider only conventional neutrinos. The agreement between data and MC is checked by the relative difference plots shown directly below the observable distributions. Furthermore, the χ^2 and the Hellinger Distance [CY00] is calculated for the Honda-Sarcevic model and shown in the histogram canvas. Hellinger Distance (HD) is a test value for matching between two distribution shapes and their possible shift

against each other. The HD is defined in the interval $[0,1]$ where zero stands for maximal agreement and 1 means a missing overlap between distributions.
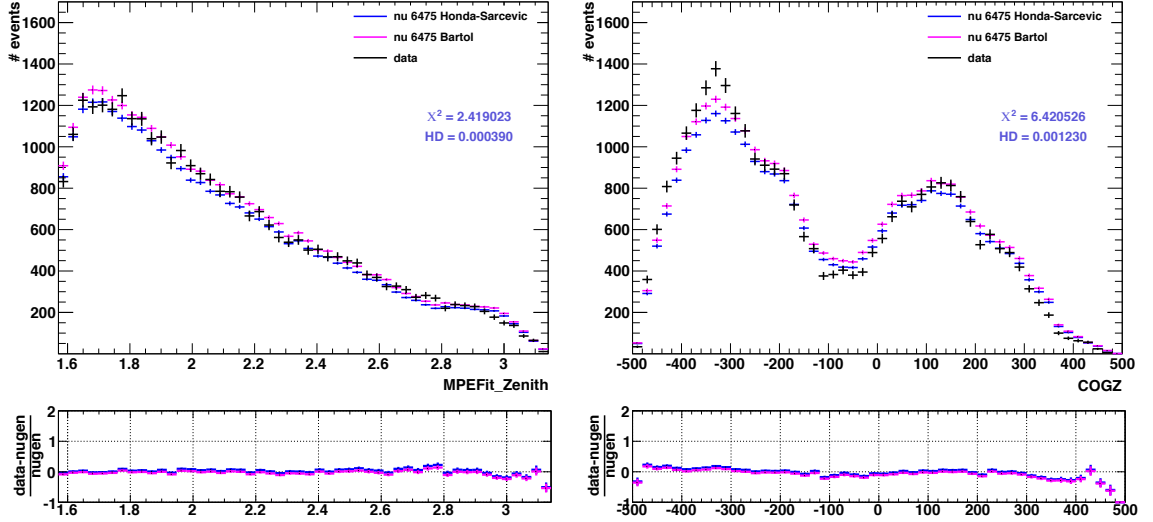

Figure 3.11: Comparison MC and data distributions at the final neutrino level for the depth variable COGZ in metern and the zenith angle θ in radiant. Two different models for the atmospheric flux are used for the MC neutrinos. The histograms with the corresponding relative distances of the MC and data values are placed below each distribution respectively and have the same abscissa scale. Additionally the χ^2 and the Hellinger Distance (HD) for the Honda-Sarcevic model w.r.t. the measured data is shown in the figure.

The energy estimators have to show a good agreement between data and MC simulation. Among the directly measured observables in Fig. 3.12 the *NCh* shows best agreement according to the quantity values. But in the systematics checks based on the burn sample *NCh* showed strongly divergent behavior in the upper and lower part of the detector (see Appendix A). Therefore the *QTot* is considered as one of the directly measured observables for the unfolding (see Sec. 3.3.1). From the reconstructed observables in Fig. 3.13 the *LDirC* and *NDirC* have been chosen since they work with the direct non-scattered hits and are therefore less sensitive to the variation in optical ice properties. The data - MC agreement of *dEdX* and *MuE_Energy* is not optimal.

Figure 3.12: Comparison of energy correlated observable distributions of MC and data at the final neutrino level. The shown observables are directly measured without using a reconstruction algorithm. The histograms with the corresponding relative distances of the MC and data values are placed below each distribution respectively and have the same abscissa scale. χ^2 and the Hellinger Distance (HD) for the Honda-Sarcevic model w.r.t. the measured data is shown in the figure.
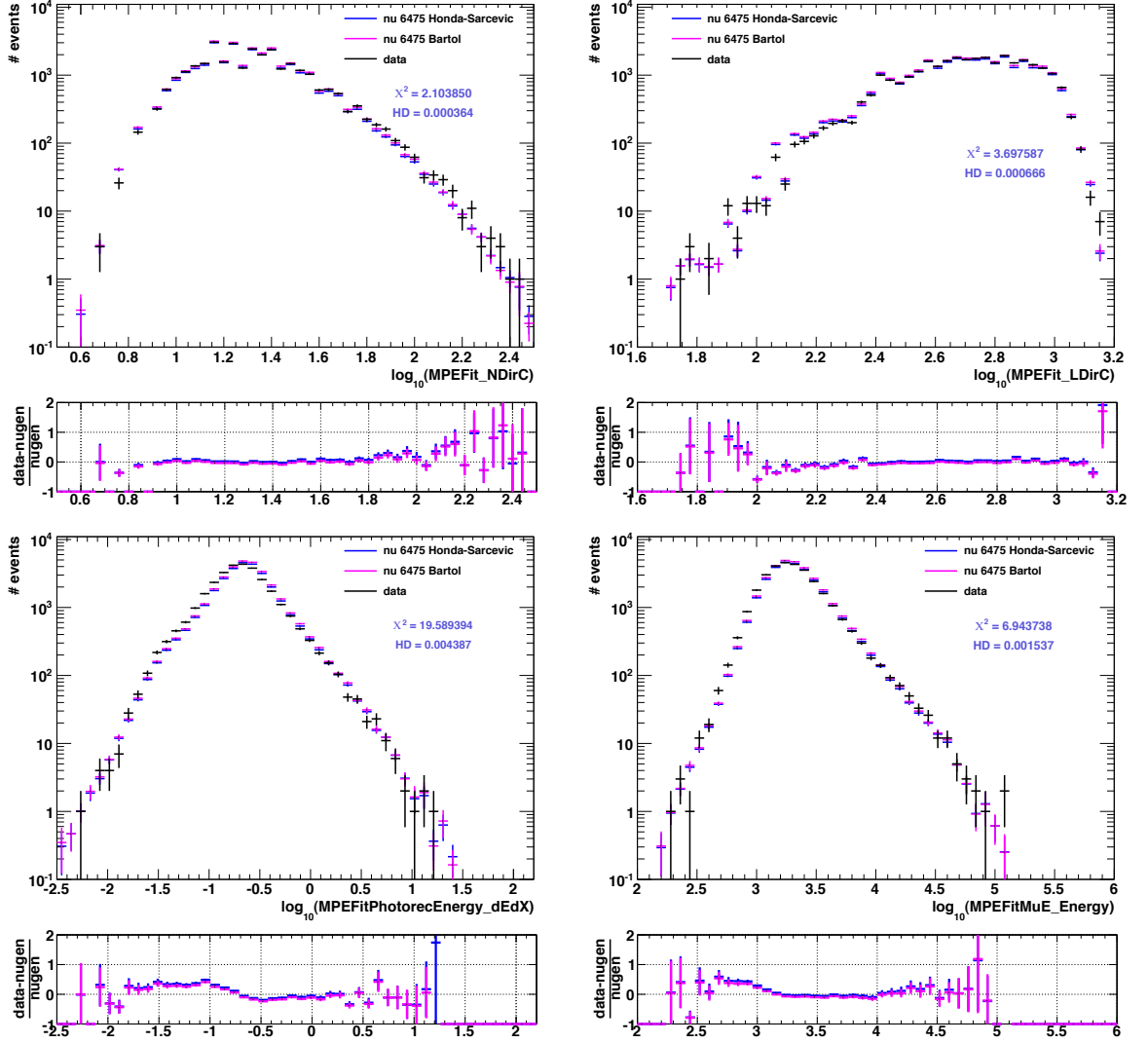
Figure 3.13: Comparison of the muon energy estimators obtained from MPE fit at the final neutrino level. The number and track lengths considering the direct hits are shown in the upper plots. The lower plots show constructed variables that have been developed to estimate the muon energy. The histograms with the corresponding relative distances of the MC and data values are placed below each distribution respectively and have the same abscissa scale. χ^2 and the Hellinger Distance (HD) for the Honda-Sarcevic model w.r.t. the measured data is shown in the figure.

3.3 Unfolding analysis with TRUEE

The final neutrino sample obtained from the one year measurement with IC 59 is described well by the MC simulation, as demonstrated in the Sec. 3.2. This is an important condition to ensure that the physical effects, such as particle propagation and detector response have been understood well and are incorporated in the MC simulation by an accurate approach. Hence, a reliable response matrix can be determined for the estimation of the true neutrino flux. In the following the unfolding analysis with the software TRUEE is presented.

3.3.1 Choice of energy-dependent observables

The unfolding analysis with TRUEE typically starts with the selection of the best observable combination. The automatically produced correlation and profile histograms (Sec. 2.3.3) of the different energy-dependent observables are examined and the energy dependency is checked. The profile plots reveal the overall energy dependency of all presented observables.

Before a final decision is made, the combination of the different observables for the unfolding have to be checked using the *test mode* (Sec. 2.3.3). Here also the optimal binning of the observables is determined. In Fig. 3.14 - 3.15 the correlation and profile plots of observables are shown, which are considered as candidates in the unfolding analysis.

Preparative systematics tests with the burn sample showed that the observable combination summarized in Tab. 3.4 leads to the best and most stable results especially against depths variation in the detector (see Appendix A). The maximal bin

observable	number of bins
MPEFit_NDirC	20
QTot	20
MPEFit_LDirC	10

Table 3.4: Observables and their binning as it is used in the final unfolding.

width is estimated by determination of resolution with simulated mono-energetic events (see Appendix A).
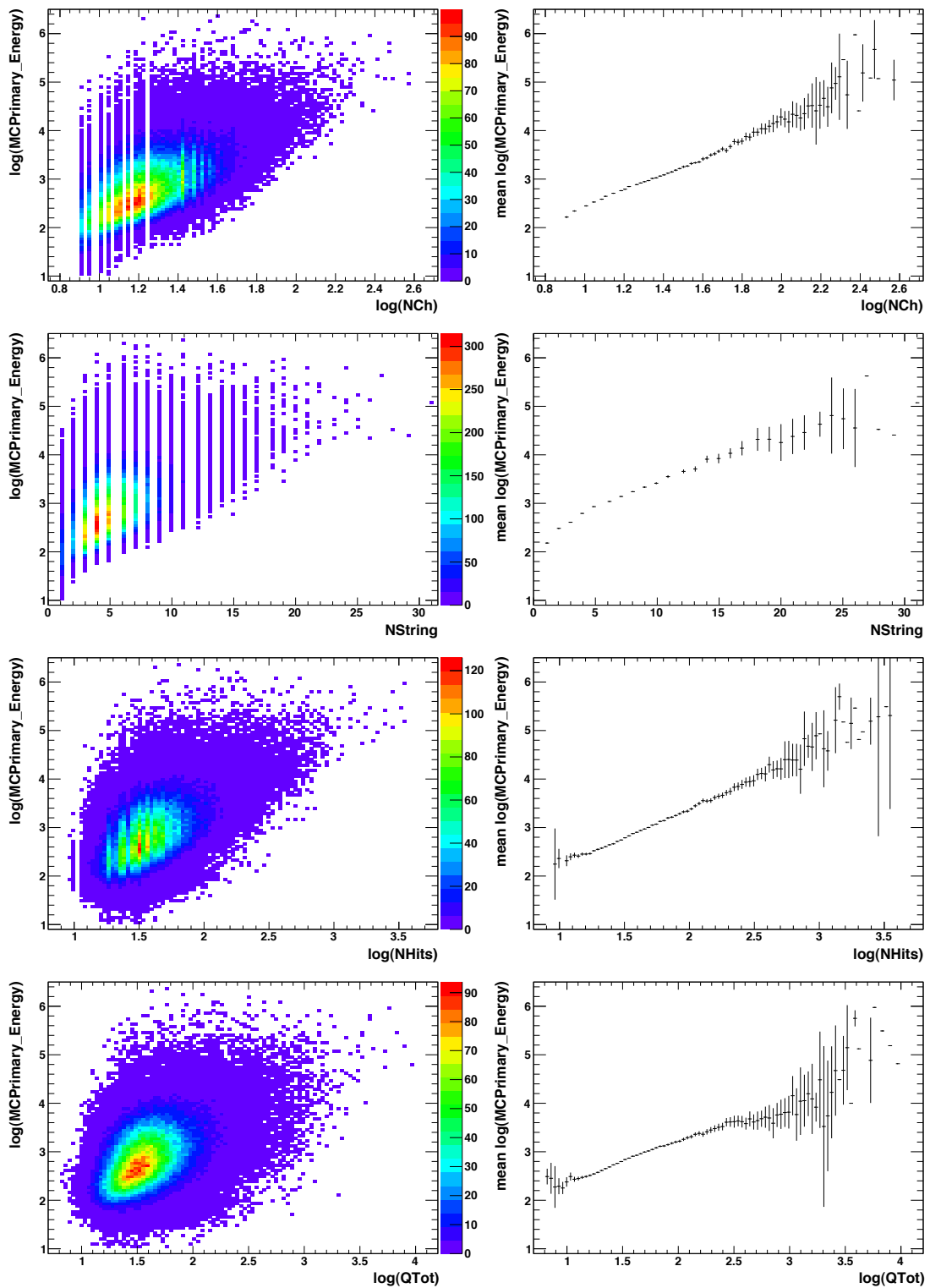
Figure 3.14: Scatter plots (left) and the corresponding profile histograms (right) of different energy-dependent directly measured observables.
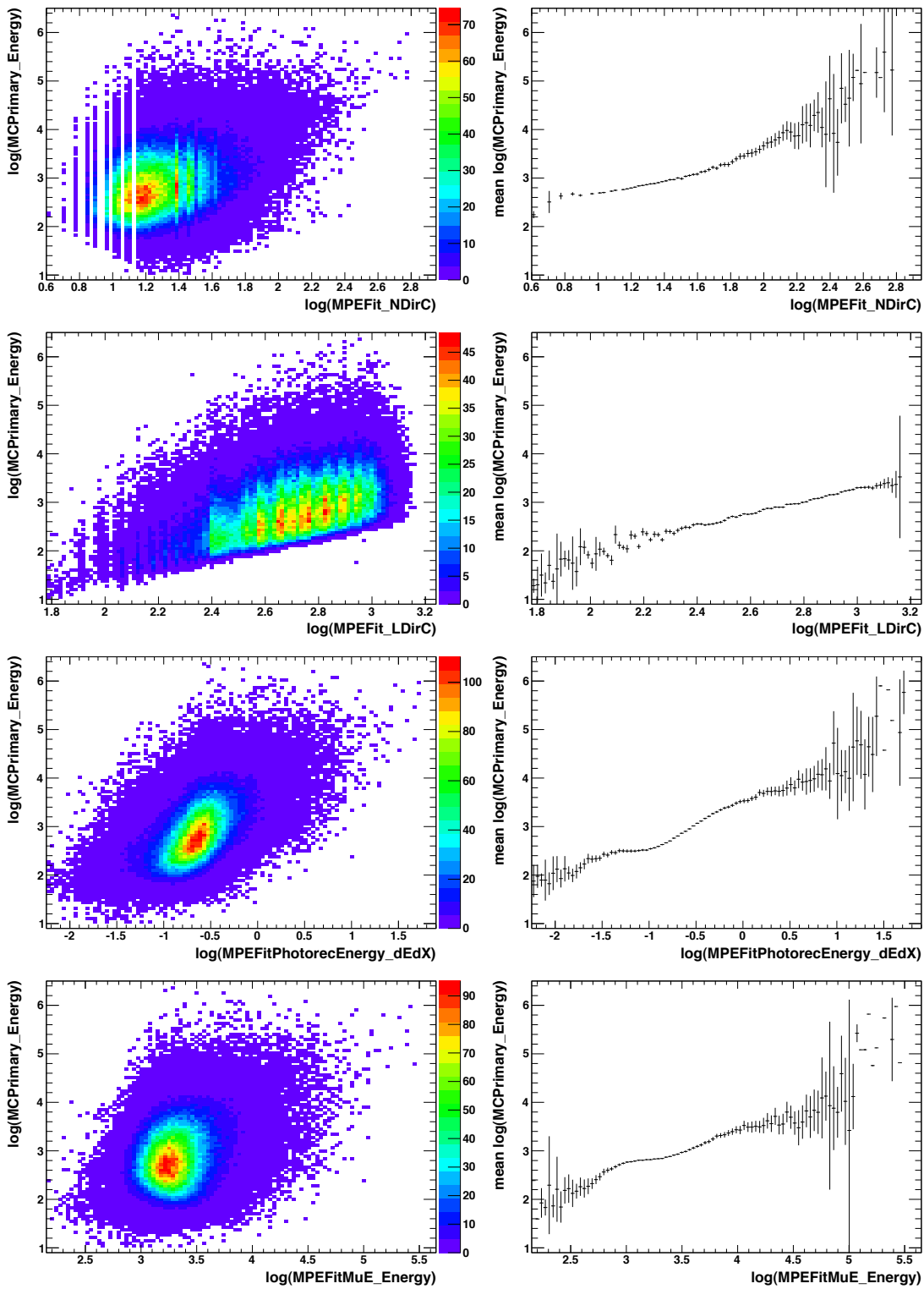
Figure 3.15: Scatter plots (left) and the corresponding profile histograms (right) of different energy-dependent observables reconstructed from the MPE fit and additional algorithms.

3.3.2 Test mode results

In the *test mode* different observable combinations are checked as well as the parameter sets for the unfolding. The pseudo data sample is chosen to correspond to the one year IC 59 measurement of the expected atmospheric neutrino flux following the Honda-Sarcevic model. The resulting distribution is a differential flux as it is seen by the detector at the neutrino level. Figure 3.16 shows the *test mode* results compared to the true distribution for different *ndf*. The additional histogram with relative difference shows a good agreement between the distributions.
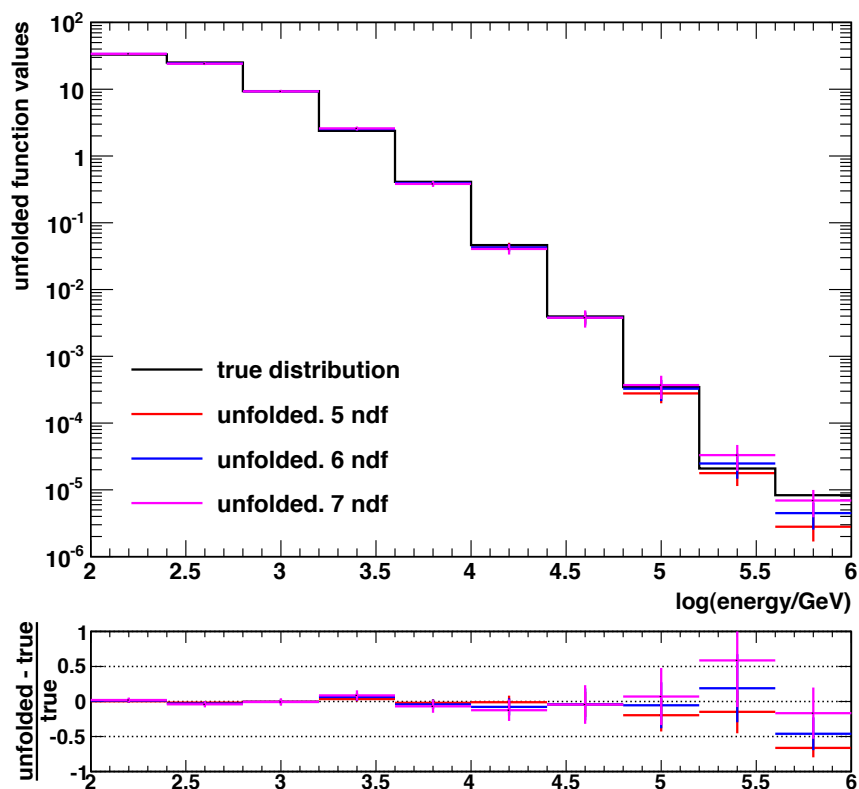

Figure 3.16: *Test mode* result of the MC pseudo-data sample with the final unfolding settings and varying numbers of degrees of freedom. The true distribution is shown as well. No acceptance correction is applied. The relative difference between the unfolded and true values is demonstrated in the lower histogram.

Parameter selection is carried out by executing unfolding in *test mode* for large parameter ranges and the successive observing of the parameter selection plot κ vs. χ^2 (Sec. 2.3.3). The unfolding settings have to be chosen such that the result is stable against minor variations of parameters, as is shown in Fig. 3.16. The correct choice of observables is crucial to ensure stability in the results. The setting of parameters for the unfolded function is summarized in Tab. 3.5.
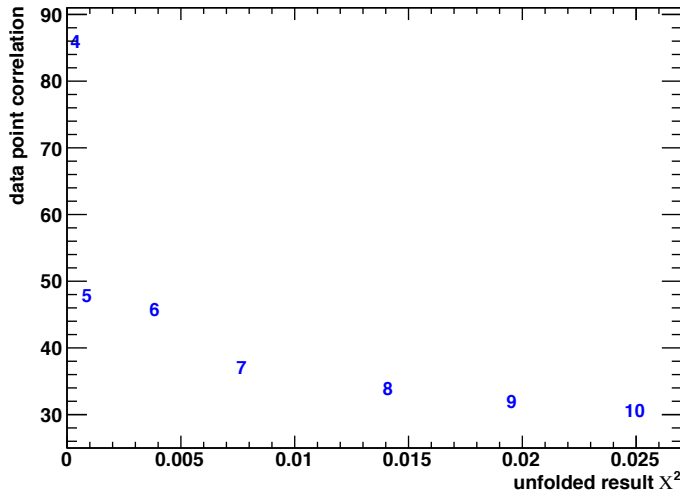
Figure 3.17: The parameter selection plot for different *ndf* (blue numbers). The three results with *ndf* in the kink are shown in the Fig. 3.16. The variation of the number of bins and *nknots* is not shown in this figure due to clearness of display.

parameter name	value
ndf	6
nknots	19
number of bins	10
size of bins $\Delta\, log_{10}(E_{\nu_\mu}/GeV)$	0.4 (equidistant)
energy range $log_{10}(E_{\nu_\mu}/GeV)$	2.0; 6.0

Table 3.5: Parameters for the estimated function as used in the final unfolding. The different available options are inactivated, if not listed in the table.

3.3.3 Pull mode results

The stability of the result against statistical variation is checked by performing unfolding tests in the pull mode. The same fraction of MC events is used as for the *test mode* to imitate the real data sample. The unfolding of 500 pseudo-data samples is executed for the test. The resulting projection plots are shown in Fig. 3.18. The mean values do not show any significant bias and the standard deviation is $\sigma \approx 1$ range. For the last two bins it is not reasonable to make the pull distributions, because the lack of statistics forbids the Gaussian approach. Furthermore, the last bins of the true distribution in some cases contain no entries, and that additionally distorts the pull distribution.
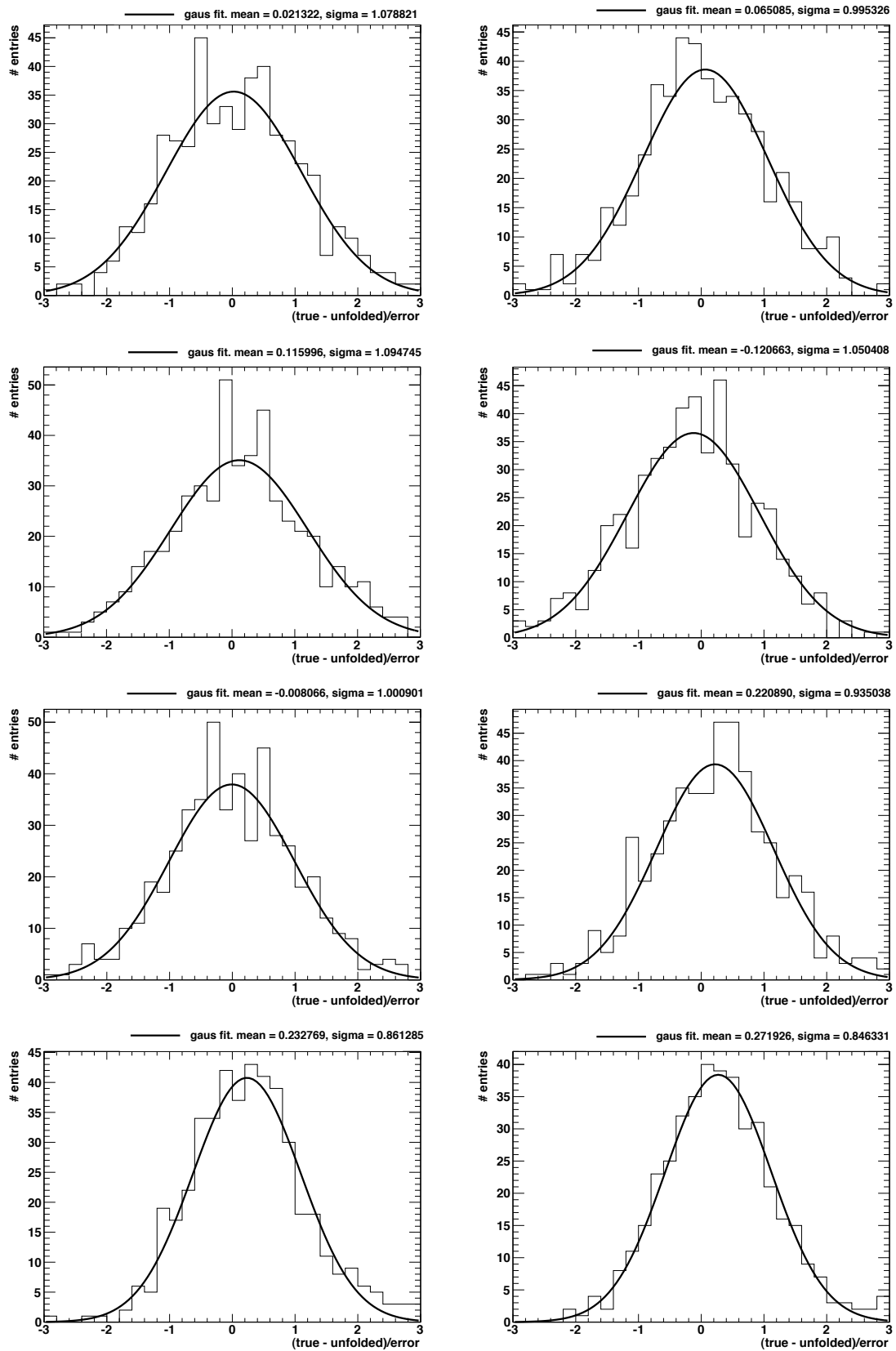
Figure 3.18: Pull distribution, projected on the ordinate for each bin. The number of unfolded pseudo-data samples is 500. Pull distributions for the last two bins are not possible, because the Gaussian approach fails at the low statistics.

3.3.4 Unfolded atmospheric neutrino flux spectrum

The performed study of the unfolding with MC simulation ensures that the optimal observables are chosen and various values of usable parameters are restricted to low ranges, showing stable behavior against minor variations of parameter configuration. Now the unfolding of measured data can be performed using the determined parameter settings.

The unfolded neutrino event distribution for the IC 59 sample is shown in Fig. 3.19. The data sample used for the unfolding as well as the MC sample for the response function include only events after the event selection. Therefore, the unfolding result provides the distribution of neutrino event, which could be seen by the detector and passed all event selection steps only. For the correct accounting for limited acceptance, interaction probabilities and event loss due to cuts, the generated function of MC neutrinos has to be defined in TRUEE.
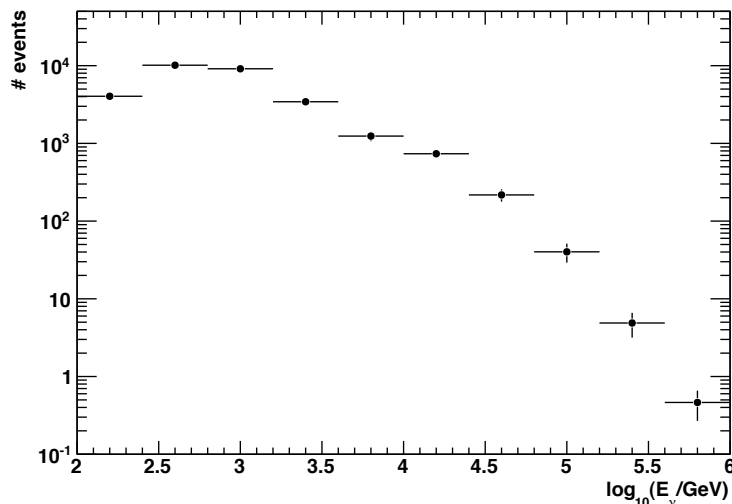

Figure 3.19: Unfolded energy-dependent neutrino event distribution. The uncertainties include only statistical fluctuations, provided by TRUEE. To get the full neutrino flux, the event loss due to small neutrino cross sections and limited detector acceptance has to be considered in the individual effective area.

The generated function is proportional to E^{-2}, but includes only events which are forced to interact in the detector volume. Hence, for the correct reconstruction of the spectrum the function has to consider the interaction probabilities in *OneWeight*. In IceCube analyses the common procedure to scale the unfolded event distribution to the initial neutrino flux is to determine the flux at the detector and divide it by the effective area.

The effective area is the hypothetical area $A_{eff}(E, \theta, \phi)$ of the idealized detector with 100% detection efficiency. It considers the physical effects such as absorption by the Earth and cross sections. The effective area is individual for every analysis
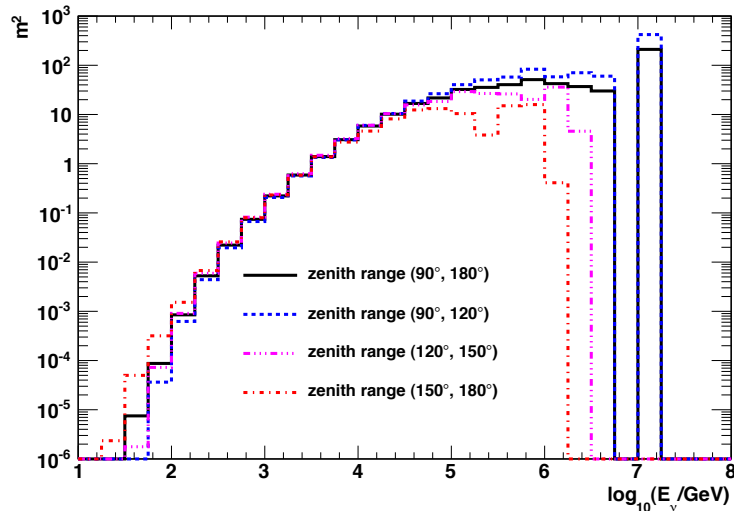
Figure 3.20: Energy-dependent effective area for the full neutrino sample averaged over the Northern hemisphere (black/solid). Additionally the areas for different zenith angle regions are shown for comparison. The most up-going high energy neutrinos are absorbed by the Earth.

and depends on the event selection and detector configuration. The effective area $A^\nu_{eff}(E_\nu, \theta, \phi)$ for the here used muon neutrino events is determined using MC sample and therein provided event-wise *OneWeight*, mentioned in Sec. 3.1.4. A detailed description on calculation of effective area can be found in Ref. [Kel08]. As can be seen in Fig. 3.20 the obtained effective area is averaged over energy bins and the considered solid angle of primary particles.

The calculation of the flux $\Phi(E_\nu, \theta, \phi)$ is performed according to the formula

$$N_{events} = \int dE_\nu \, d\Omega \, dt \, \Phi(E_\nu, \theta, \phi) \, A^\nu_{eff}(E_\nu, \theta, \phi). \tag{3.5}$$

If treating the distributions as binned histograms, the N_{events} can be considered as the unfolded number of events in a bin with interval size dE_ν. $d\Omega$ is the solid angle and is set to 2π to obtain flux averaged over the Northern hemisphere. dt can be set to the live time of the sample, here roughly 347 days. The effective area $A^\nu_{eff}(E_\nu, \theta, \phi)$ is an average over the solid angle and energy bins as shown in Fig. 3.20. After application of the effective are the unfolded distribution is converted to the binned flux averaged over the zenith angle of the Northern hemisphere. In Fig. 3.21 the result of 10 % data is shown as well as the full year data. The systematic uncertainties are not included, yet.
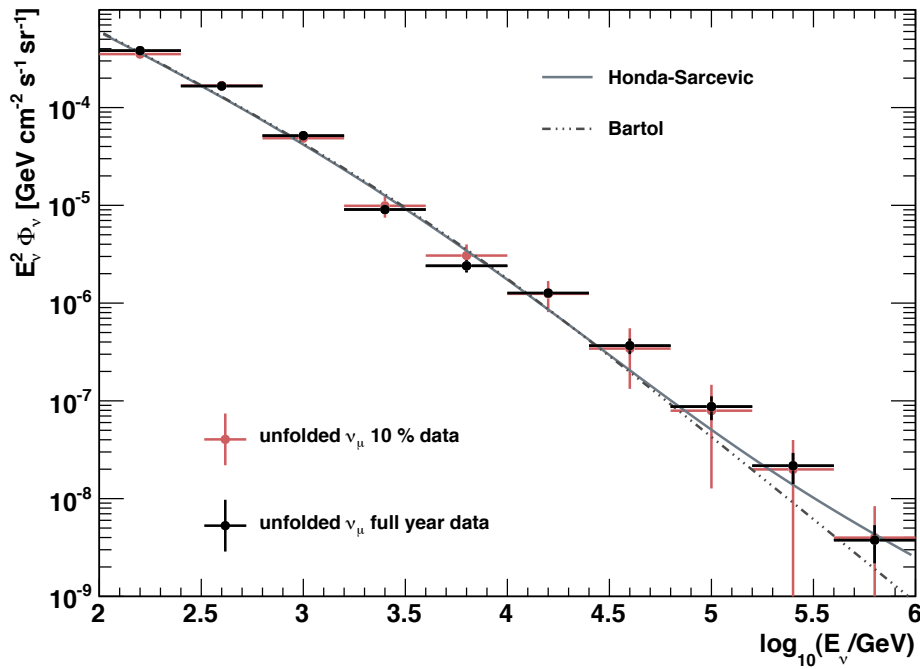
Figure 3.21: Unfolded atmospheric neutrino flux spectrum, averaged over the northern hemisphere. Shown is the result of the full year data taken with IC 59. Additionally the result of the 10 % of data is shown, obtained in the course of the "blind" analysis development (see Appendix. A). The flux is scaled with the square of energy. The presented uncertainties have been provided by the unfolding algorithm and therefore account only for statistical fluctuations. Two theoretical models are shown, that predict only the conventional neutrino flux (Bartol) and the combination of conventional and prompt flux (Honda-Sarcevic).

3.3.5 Verification of the result

The TRUEE intern verification tool is applied to check the unfolding result and the simulation of observables. As explained in Sec. 2.3.2 the MC simulated neutrino data set is weighted event-wise to describe the unfolded spline function. Thus, the distributions of observables can be compared between data and MC. Some examples are shown in the Fig. 3.22. The distributions of zenith angles show agreement between data and MC. The simulated $dEdX$ overestimates strongly the data and is clearly an improperly simulated variable, as the same extreme behavior is seen in the Fig. 3.13 before unfolding. The mismatch in the likelihood variables is not as strong as in $dEdX$. Its origin is discussed in the Sec. 3.34.
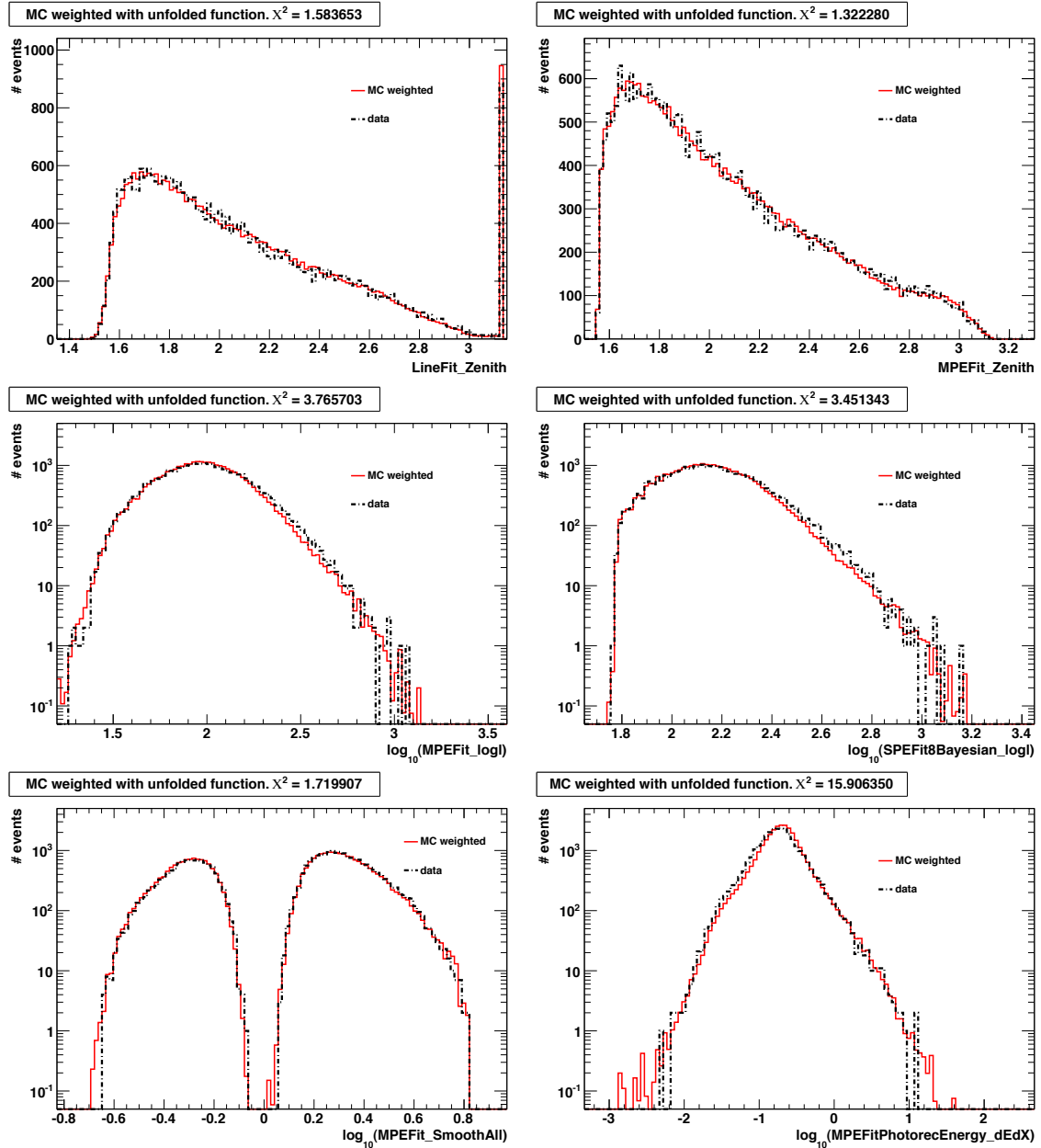
Figure 3.22: Comparison of observables distributions after weighting the MC events by the unfolded function. Shown are observables, that are not used for the unfolding. The agreement is tested with determination of the χ^2 value, printed in the histogram titles. A mismatch indicates an incorrect description of observables or unfolding variables by MC. Only in the case of $dEdX$ the strong overestimation by MC can be identified as due to wrong simulation. See also discussion in Sec. 3.34.

3.3.6 Zenith-dependent atmospheric neutrino spectrum

The atmospheric neutrino spectrum depends on the zenith angle. The flux of neutrinos, which enter the detector volume horizontally, is higher than the flux of vertically incoming neutrinos, which are e.g. up-going neutrinos from the direction of the Earth core. Moreover, at high energies the probability for neutrino absorption by the Earth is rising, and the number of detected up-going events decreases. This behavior is considered in the MC simulation, as can be seen in the effective area histogram in Fig. 3.20.

Unfolding of neutrino fluxes for two different zenith regions is made in the present analysis (Fig. 3.23). The zenith cut is set at $\theta = 124°$. The predicted fluxes, as averages over the considered zenith regions, respectively, are well described by the unfolded results. For the up-going events with $124° \leq \theta \leq 180°$ the statistics are low at high energies. A zenith-dependent unfolding with a finer zenith binning is expected to be performable after the optimization of the event selection and the reduction of the systematic uncertainties, which originate from the simulation (see Sec. 3.4).
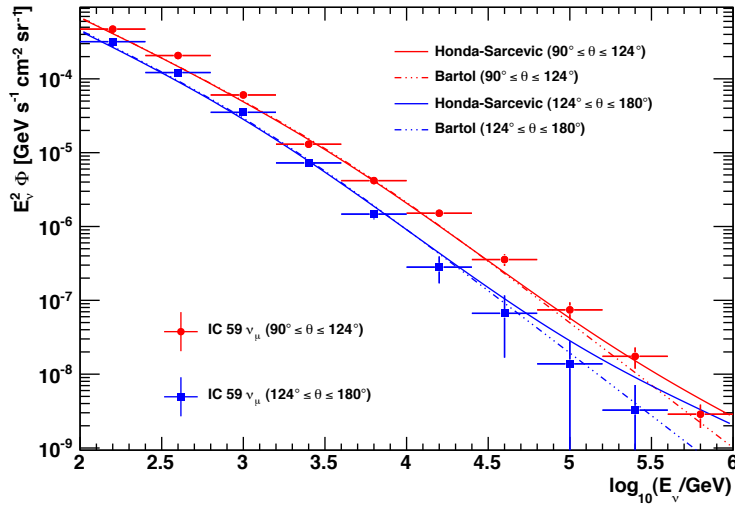
Figure 3.23: Unfolded atmospheric neutrino fluxes, averaged over two different zenith ranges. The theoretical models are shown as well. As expected, the vertical flux is lower than the horizontal flux, due to the higher probability for the π and K mesons to interact before decay. The error bars show only statistical uncertainties, provided by TRUEE.

The prompt neutrinos are expected to have isotropic flux without zenith angle dependency. Therefore, the zenith-dependent neutrino search under consideration of the seasonal variations of the atmospheric density can be used to probe the prompt neutrino flux [DG10].

3.4 Systematics studies

Additionally to the preparatory tests, performed with the MC sample, systematics studies with the data sample have to be carried out, to prove the reliability of the result and to estimate the confidence limits, by changing the initial conditions.

3.4.1 Theoretical uncertainties

First of all, the uncertainties from the theoretical calculations are considered. The theoretically predicted atmospheric neutrino flux model, which is used for comparisons, contains uncertainties that originate mainly from the hadronic interaction model and the primary cosmic ray spectrum and composition. The here used uncertainty prediction of around 15% is taken from Ref. [B+06]. A less optimistic uncertainty prediction of $+32/-22\%$ for the muon neutrino flux has recently been determined in Ref. [FBTD12]. The uncertainty of theoretical model is shown as a confidence band in the figures.

Furthermore, the assumptions made in simulation, concerning the physical effects, introduce uncertainties into the unfolding result via effective area. The cross section of neutrinos contribute with an uncertainty of 10%, as has been estimated in Ref. [A+10b]. Additionally, the simulated muon propagation induces the uncertainty of 5% [Kok99]. In Fig. 3.24 the unfolded atmospheric neutrino energy flux

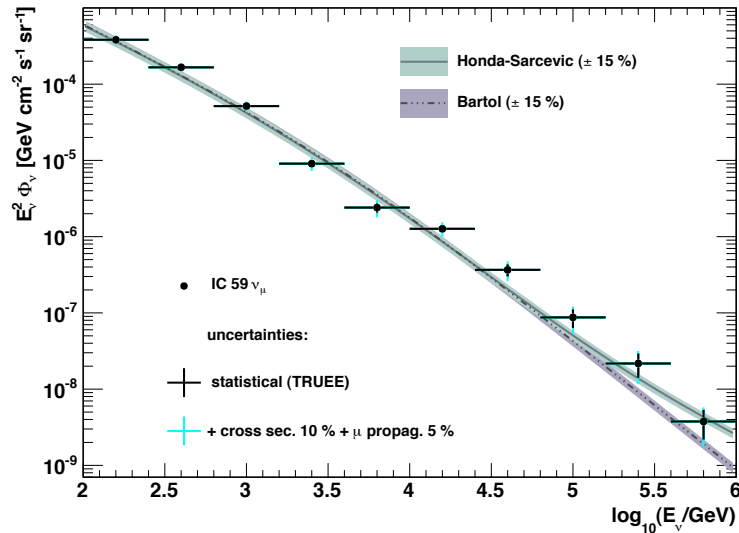Figure 3.24: Unfolded atmospheric neutrino flux spectrum, averaged over the Northern hemisphere. Shown is the result of the full year data taken with IC 59. The flux is scaled with the square of energy. The uncertainties from the error propagation in the unfolding and from the simulation are presented separately. The uncertainty of 15% in the absolute theoretical flux is indicated by shaded areas.

spectrum is shown after considering the uncertainties from calculations.

3.4.2 Stability of the result against purity variation

The cut on *signalness* of the Random Forest output is made at *signalness* $= 1.0$, that corresponds to an estimated purity of roughly 99.4% in the final neutrino sample, as explained in Sec. 3.2.2. In the following the stability of the unfolding result against the purity variations is tested. For this purpose a successive loosening of the *signalness* cut is made starting with the least possible steps of 0.002 and proceeding until the estimated purity level of 95%. At this level the influence of the background events on the final spectrum is expected to be negligible (see Appendix A).

Every sample with different purity is treated individually, i.e. the unfolding is performed separately by using corresponding response matrices and effective areas. The requirement for the reliability of the result is the absence of significant deviations between the determined fluxes with different purities.

The unfolded fluxes are shown in the Fig. 3.25. The purities for different *signalness* cuts are assigned in the legend and are also summarized in the Tab. 3.6. Since the zenith angle variable *MPEFit_Zenith* is included in the Random Forest event selection, the samples with the lower *signalness* cut contain a part of events coming from above the horizon. Therefore, a zenith cut at 90° is applied to allow the comparison of the fluxes, averaged over the region $90° \leq \theta \leq 180°$.

signalness cut	estimated purity [%]	number of events
1.0	99.4	29 890
0.998	98.8	38 694
0.996	97.8	43 632
0.994	97.6	47 056
0.992	97.1	49 687
0.990	96.7	51 904
0.980	95.0	60 291

Table 3.6: Variation of the *signalness* cuts and the corresponding purities estimated from the cross-validation checks within the Rapid Miner framework. Additionally the numbers of events of each sample are listed. These numbers have been determined after the zenith cut at 90°.

From the results in Fig. 3.25 the conclusion can be made, that the estimated neutrino flux does not depend on the purity variation up to the purity level of 95%. This is an important condition, since it ensures that the signal and background
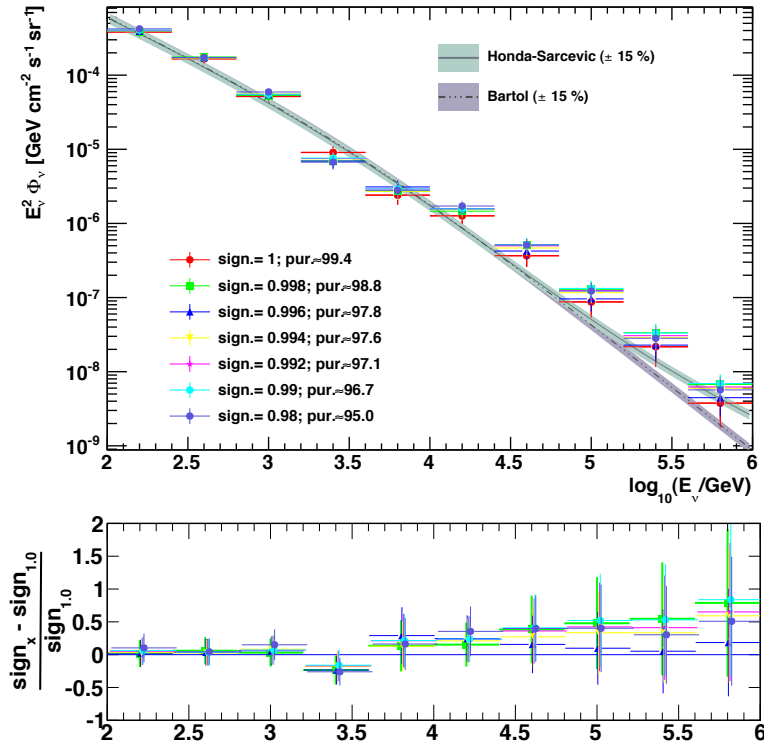
Figure 3.25: Unfolded atmospheric neutrino flux spectra determined from samples with different purities. Every sample has been treated independently with individual response matrix and effective area. The relative deviations of the samples with lower *signalness* from the sample with *signalness* = 1.0 are shown in the lower histogram. The deviations show an agreement between the samples, which proves the absence of purity-dependency of the spectrum within the considered *signalness* variation region.

event description by MC is made with an accurate approach and therefore, the final spectrum is not merely a result of a luckily placed *signalness* cut.

Due to the independency of the spectrum within the tested purity range, a mean *signalness* value (*signalness* = 0.99) can be used to make the cut. Thus, the obtained neutrino sample has more statistics without having any significant impact on the result. The following systematics tests are performed by using this sample with purity around 96.7 % and considering uncertainties from the purity variations. Those are calculated by determining the mean value $\overline{x}$ and the standard deviation s of the N different results x with varying purities. Thus, the uncertainty for every bin i is obtained according to the unbiased estimation of the standard deviation:

$$s^2 = \frac{1}{N-1} \sum_{i=1}^{N} (x_i - \overline{x_i})^2. \tag{3.6}$$

3.4.3 Depth-dependent unfolding

The following systematic tests are performed to study the measurement and simulation in the higher and lower ice regions, independently. For this purpose the detector is divided into two parts of different depth levels. With both parts unfolding of the neutrino flux spectrum is executed and the results are compared with each other and with the theoretical predictions.

Similarly to the previous analysis with IC 40 data, the variable $COGZ$ is used to split the detector. As explained in the Sec. 3.1.3 the $COGZ$ variable determines the center of an event in the vertical direction and thus can be considered as the mean depth of an event. Beforehand, the simulation of the variable $COGZ$ is tested by using nearly horizontal events, as those are measured in a limited depth of the detector. Therefore, the cut on the zenith distribution is applied at the $\theta < 95°$. The simulated $COGZ$ distribution of the horizontal events is compared to the measured data and can be inspected in Fig. 3.26.
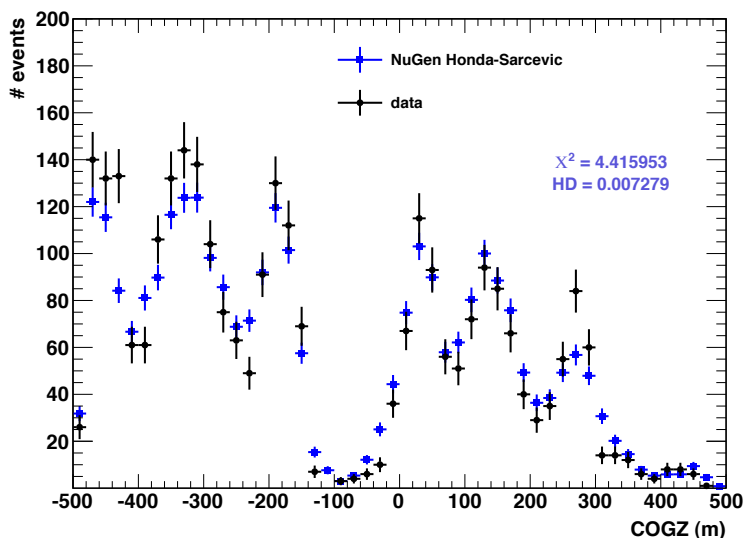

Figure 3.26: Comparison between the simulated (NuGen) and measured distributions of the $COGZ$ observable, which is used in the following for depth-dependent devision of the detector. Only the nearly horizontal events with zenith $\theta < 95°$ are taken to examine the $COGZ$ distribution.

A considerable improvement of the data description by MC can be observed, compared to the results of the IC 40 analysis, where a too smooth behavior of the simulated $COGZ$ could be registered.

Thus, the division of the detector can be made at the natural break point in the $COGZ$ distribution, which is indicated by the dust layer at the $COGZ = -100$ m. In the following, all events with $COGZ > -100$ m are considered as top events and events with $COGZ < -100$ m as bottom events.

The unfolding is performed with the top and bottom events separately by determining the individual response matrices and effective areas. The results are shown
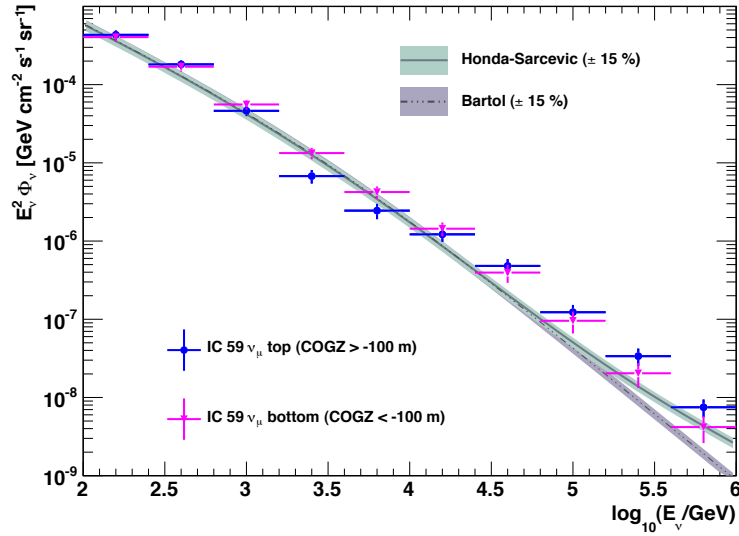
Figure 3.27: Estimated atmospheric neutrino flux spectrum, averaged over the Northern hemisphere. Shown are the result of the upper ($COGZ > -100\,\mathrm{m}$) and lower ($COGZ < -100\,\mathrm{m}$) part of the detector. The fluxes are scaled with the square of energy. The uncertainties include statistical deviations, calculated by TRUEE and systematic uncertainties from purity variation, cross-section and muon propagation.

in Fig. 3.27. A slight disagreement between the estimated fluxes and a larger deviation of the top result from the theoretical prediction can be observed. This is the main subjects of the discussion in Sec. 3.4.6. The systematic uncertainties due to the top-bottom divergence are determined as maximum deviations of top and bottom flux from the result, obtained with the full detector and are therefore asymmetric.

3.4.4 Ice model comparison

The ice model, which is used as standard in the simulation, is the SPICE model (see Sec. 3.1.4). To determine the influence of the ice model variation on the unfolding result, another set of neutrino simulation is used, to determine the response matrix in TRUEE. The new MC simulated neutrino event set employs the SPICE Mie model. The sample at the final neutrino level is obtained with the same event selection procedure, as applied on the measured data. In Fig. 3.28 the unfolded atmospheric neutrino flux spectrum is presented, obtained with the SPICE Mie response matrix. The unfolding, using the standard ice model, is shown as well. The systematic uncertainties, coming from the variation of the ice model are considered as deviations of unfolded flux with SPICE Mie from the flux determined with SPICE and are also asymmetric. A further discussion on the flux deviations can be found in Sec. 3.4.6.
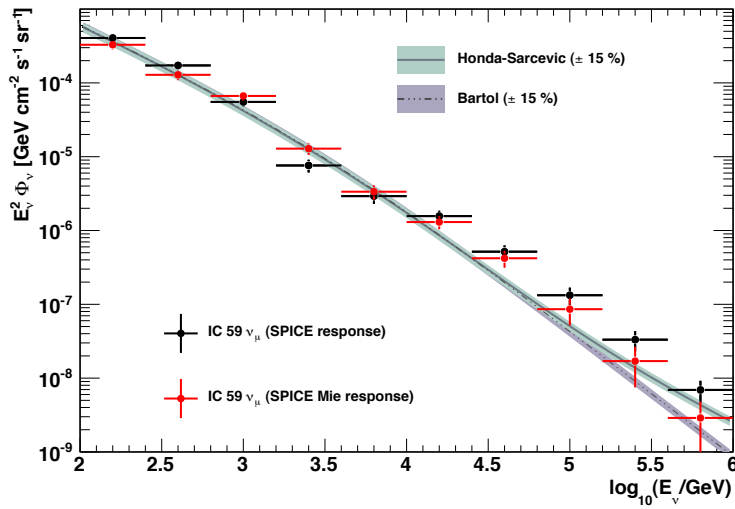
Figure 3.28: Estimated atmospheric neutrino flux spectrum, averaged over the Northern hemisphere. Shown are the result obtained with the response matrix determined for different ice models, SPICE, which is used as standard, and SPICE Mie. The fluxes are scaled with the square of energy. The uncertainties include statistical deviations, calculated by TRUEE and systematic uncertainties from purity variation, cross-section and muon propagation.

3.4.5 Final result with systematic uncertainties

The presentation of the final result of the unfolding analysis is made by taking into account all tested systematics. The uncertainties, determined above, are summed up as squares and the square-root of the sum is considered as the general systematic uncertainty in a bin, which then are added to the statistical uncertainties of the unfolding. In Fig. 3.29 the final result with all estimated uncertainties is shown. The influence of considered systematics can be examined in differently colored error bars. The largest systematics uncertainties in the high energy region come from top-bottom variation and the ice model test. Both systematics are related to the simulation of the ice properties, which deviate with the depth of the detector. The investigation and improvement of the simulation is expected to bring significant enhancement of the accuracy of the energy estimation. The parameters of the final result are summarized in the Tab. 3.7.
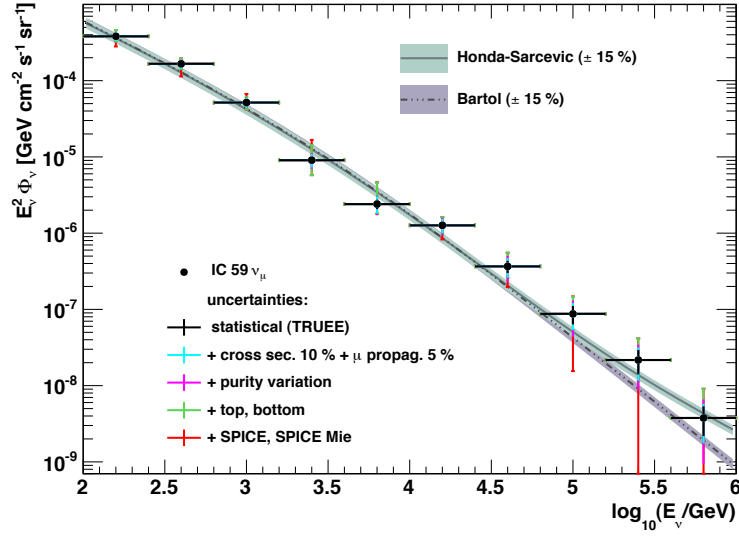
Figure 3.29: Unfolded atmospheric neutrino flux spectrum, averaged over the Northern hemisphere. Shown is the result of the full year data taken with IC 59. The flux is scaled with the square of energy. The uncertainties of different origins are presented separately in different colors.

$log_{10}(E_\nu/GeV)$	estimated flux	lower σ	upper σ
2.2	0.000381958	0.000101062	7.94575e-05
2.6	0.000166252	5.23471e-05	2.8863e-05
3	5.15716e-05	9.80483e-06	1.53309e-05
3.4	9.0624e-06	3.29522e-06	7.63437e-06
3.8	2.40598e-06	6.10846e-07	2.23868e-06
4.2	1.26662e-06	4.38154e-07	3.56084e-07
4.6	3.66726e-07	1.70061e-07	1.87318e-07
5	8.7327e-08	7.18153e-08	6.09239e-08
5.4	2.16872e-08	2.40366e-08	1.99349e-08
5.8	3.76463e-09	5.6363e-09	5.34366e-09

Table 3.7: Parameters of the final neutrino energy spectrum. Shown are the flux values in the common units of $GeV\,cm^{-2}s^{-1}sr^{-1}$ after multiplication by $(E_\nu)^2$, and the upper and lower flux uncertainties σ, since the error bars are not symmetric.

3.4.6 Depth-dependent correction of observables

The large systematic uncertainties of the final result motivate the investigation of the depth- and ice-dependent behavior of the unfolding variables. In Fig. 3.30 the comparison of unfolding variables between data and MC simulation with SPICE and SPICE Mie is shown for the top and bottom of the detector, separately.

In the upper part of the detector an overestimation of $QTot$ by the SPICE MC can be observed. While $NDirC$ and $LDirC$ are determined using only direct hits, the $QTot$ contains charge from all hits and is therefore dependent on the ice properties. Nevertheless, the total charge is very sensitive to the muon energy and is essential for the energy estimation.

A small correction of the MC simulated $QTot$ for all events with $COGZ > -100\,\mathrm{m}$ is tested to influence the final result and the behavior in top and bottom of the detector. The correction factor $f_{log_{10}(QTot)} = 0.974$ is obtained by minimization of the χ^2 value between data and MC. The distribution of the corrected $QTtot$ compared to true data can be found in Fig. 3.31.

After the correction of the simulated $QTot$, unfolding of the neutrino flux spectrum is performed for the top sample (Fig. 3.32) full and the detector (Fig. 3.33).

The unfolded full detector distribution shows a better agreement with the theoretical predictions. Furthermore, the agreement between the unfolding results of the upper and lower parts of the detector is improved due to the corrected $QTot$ simulation in top. Therefore, the correction improves the systematic uncertainties and the precision of the result. The better performance of the unfolding is confirmed by the verification plots in Fig. 3.34, that mainly show a better agreement, especially in the cases of likelihood variables, than the corresponding verification histograms in Fig. 3.22, obtained after the unfolding without correction of $QTot$.

As can be seen in the Fig. 3.30 the SPICE Mie model does not perfectly describe data as well, since disagreement can be observed for the observables with direct hits. A new description of the ice properties is needed to simulate the data accurately over the whole detector and therefore, reduce the systematic uncertainties. Alternatively, tests with the varying efficiency of the IceCube DOMs are encouraged for future analyses.
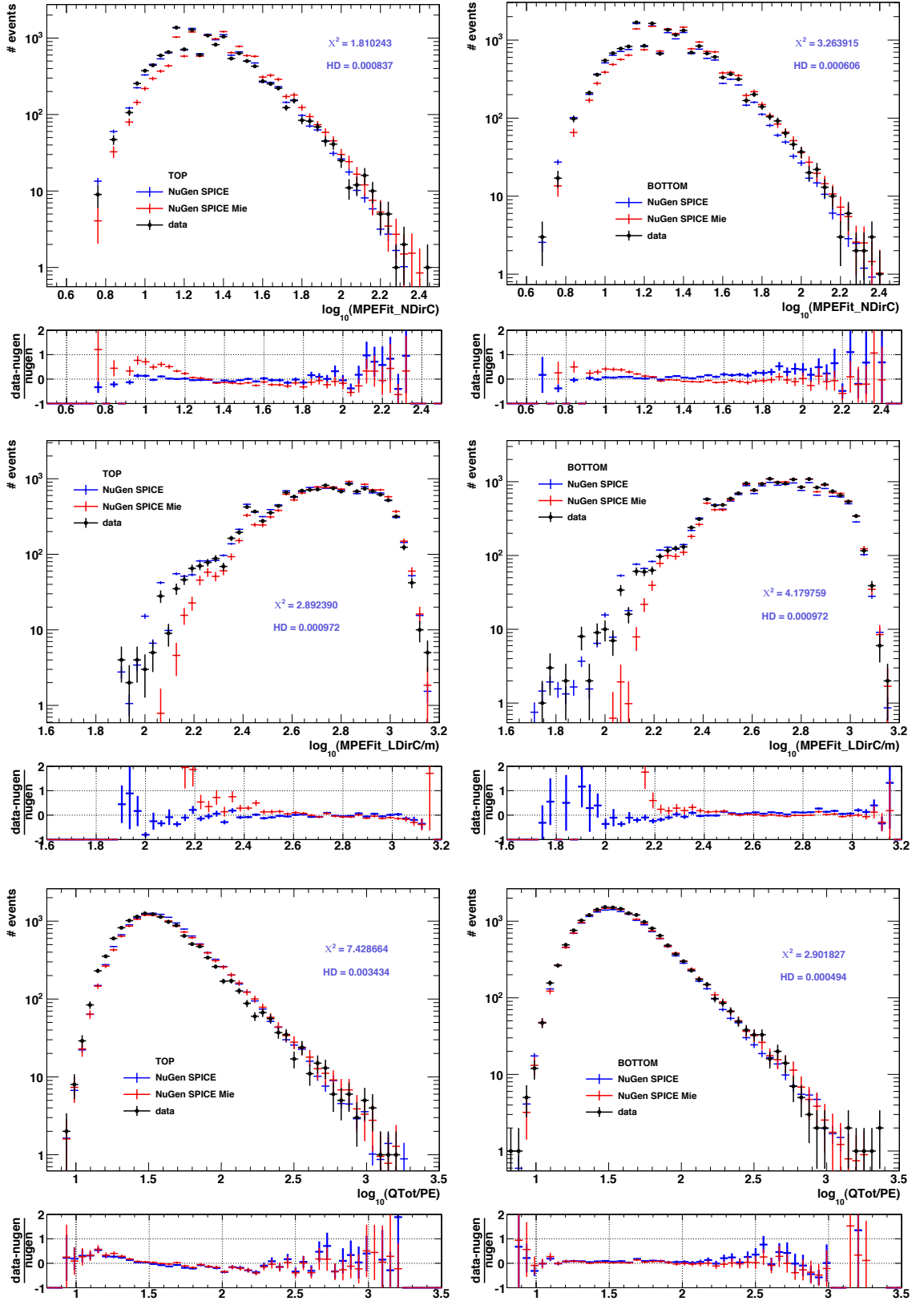
Figure 3.30: Data versus MC of unfolding observables for the top (left) and bottom (right) of the detector, separately. The χ^2 and Hellinger Distance is calculated between the SPICE model and data.
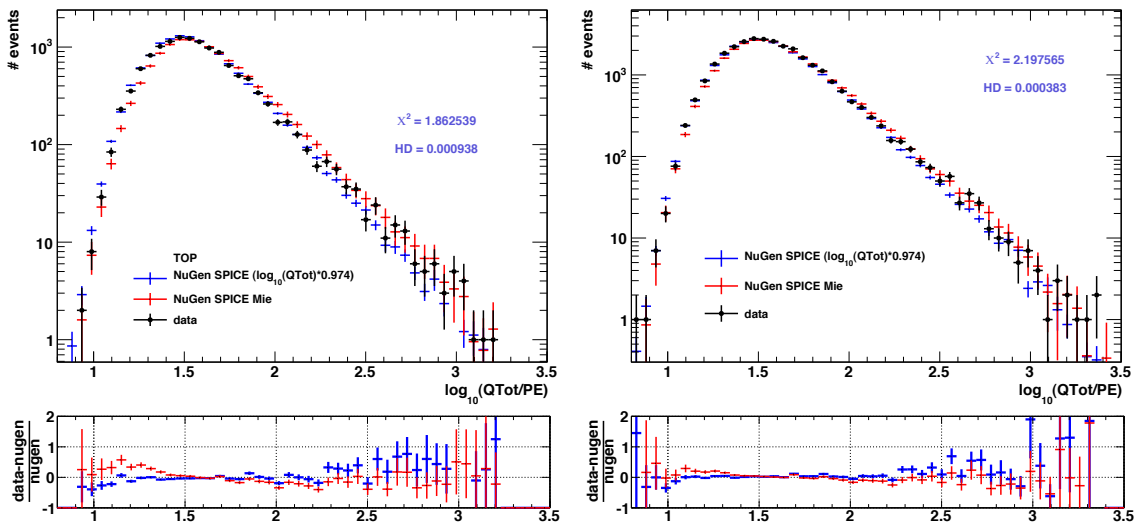
Figure 3.31: Unfolding variable *QTot* for the upper half of the detector (left) and the full detector (right) for measured data and modified MC simulation. The correction factor $f_{log_{10}(QTot)} = 0.974$, applied on the MC simulated event with $COGZ > -100\,\text{m}$, is determined by χ^2 comparisons. The MC weighting is made by the Honda-Sarcevic model. The χ^2 and Hellinger Distance are calculated for the SPICE model and data. The SPICE Mie model is identified to assume a very high light production in the whole detector, and therefore, provide too many direct hits per event, as can be seen in the comparison plots of *NDirC* and *LDirC*.
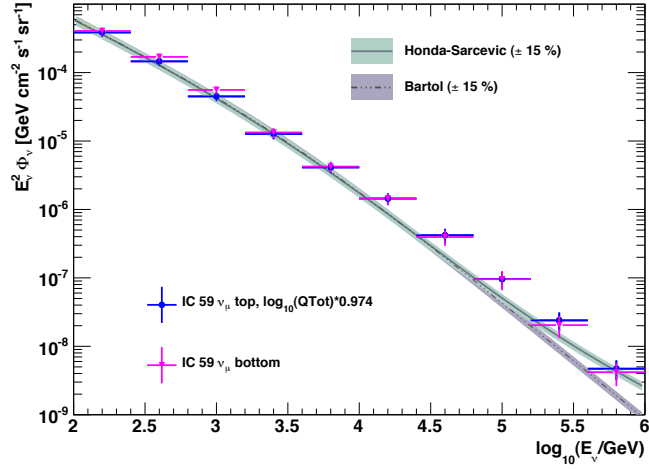
Figure 3.32: Unfolding of the neutrino flux spectrum of top events, by using corrected $QTot$ in the MC simulated events with $COGZ > -100\,\mathrm{m}$. The bottom result is shown as well. The agreement between the top and bottom results is improved dramatically, compared to Fig. 3.27. The result matches better the theoretical prediction. The unfolding is performed after *signalness* cut at 0.99. The considered uncertainties are only statistical and theoretical.
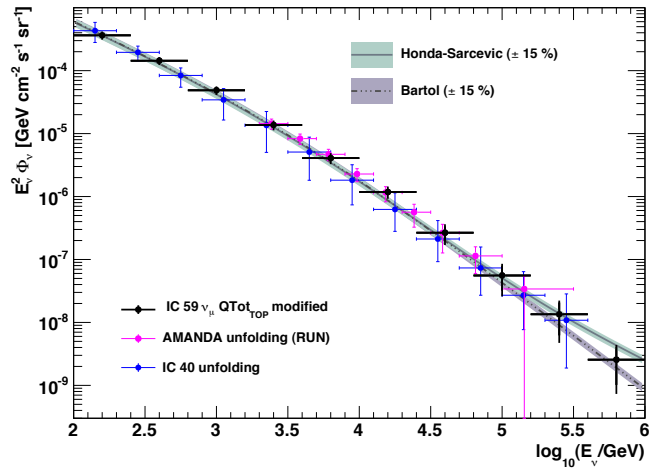
Figure 3.33: Unfolding of the neutrino flux spectrum for the full detector, by using corrected $QTot$ in the MC simulated events with $COGZ > -100\,\mathrm{m}$. The result matches better the theoretical prediction. The unfolding is performed at *signalness* = 1 to enable comparison to the original spectrum in Fig. 3.24. The considered uncertainties are only statistical and theoretical. For comparison the unfolding result of IC 40 analysis [A$^+$11d] and the AMANDA unfolding [A$^+$10b], which has been performed with the $\mathcal{RUN}$ algorithm, are shown.
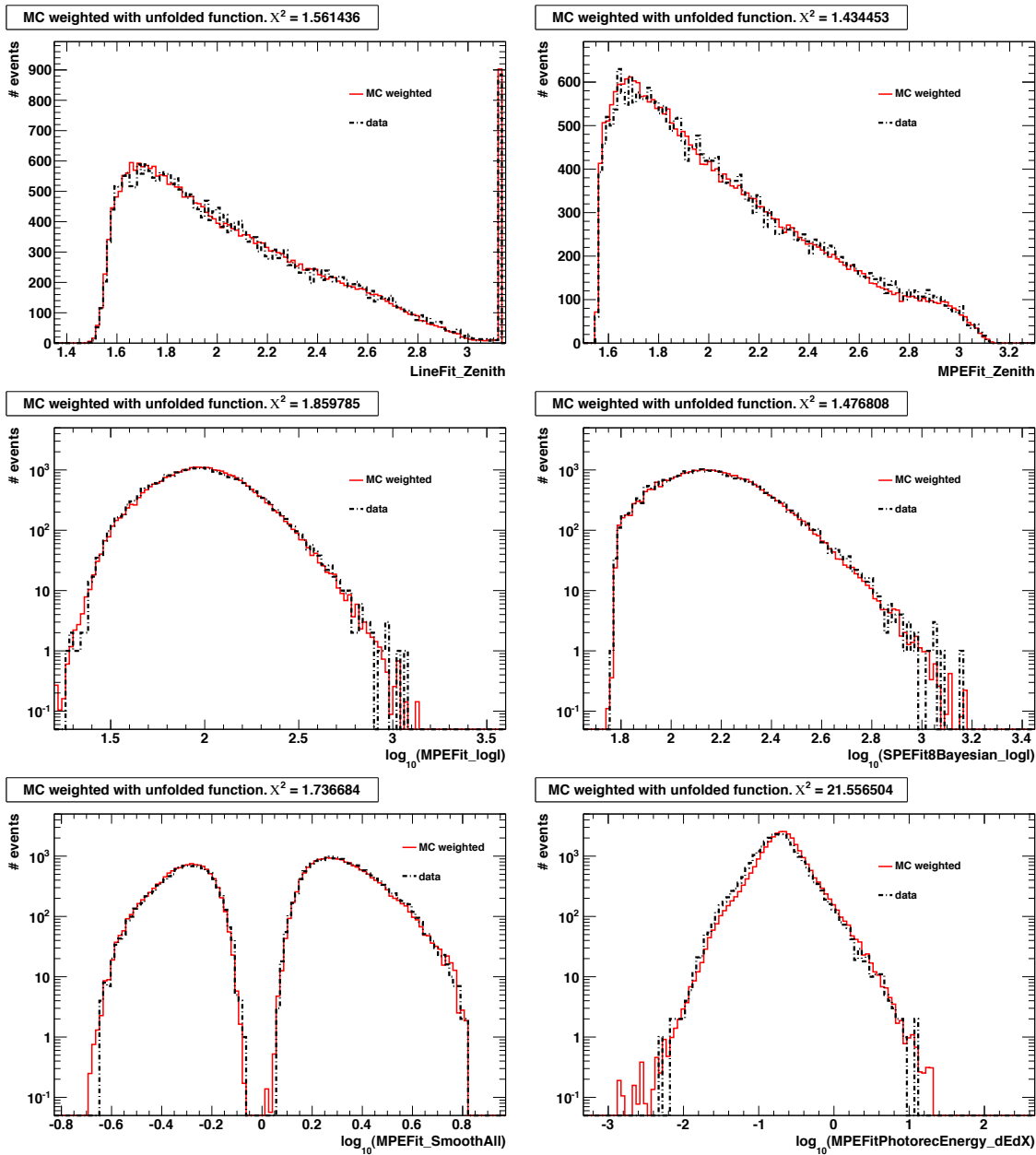
Figure 3.34: Comparison of the observable distributions after weighting the MC events by the unfolded function, which is obtained by using depth-dependently corrected *QTot* for unfolding. Shown are the same observables, as in Fig. 3.22. The agreement is tested with determination of the χ^2 value, printed in the histogram titles. A mismatch indicates an incorrect description of observables or unfolding variables by MC. Especially in the likelihood variables a clear improvement can be observed after the *QTot* correction. The *dEdX* has a worse agreement, due to its entirely increased overestimation by MC.

4 Summary and outlook

The present work consists of two main parts, the development of the TRUEE unfolding software in the C++ programming language and its application in the atmospheric neutrino analysis with the IceCube neutrino telescope.

The development of TRUEE has implied the understanding of the basic unfolding algorithm, $\mathcal{RUN}$, written in FORTRAN 77 and the knowledge of the requirements of an unfolding analysis. Thus, an efficient and functional software could be produced, which is easy to handle and extend. The included basis algorithm is well tested and has been successfully applied in particle and astroparticle physics.

In this thesis the advantages of the used algorithm, such as the event-wise input and the usage of B-splines, have been pointed out. The algorithm is able to estimate a very steep distribution covering several orders of magnitude and is therefore suitable for applications in astroparticle physics. The assumption for the sought variable distribution, which is made in the MC simulation to determine the response function, has a low influence on the result. Thus, a moderate deviation between the true and simulated distributions is acceptable, as long as the sought variable range is covered with sufficient statistics in the MC simulation.

It has been demonstrated that the new features and extensions of the algorithm bring a substantial facilitation into performance of an unfolding analysis. The preparative tests based on MC can be easily executed due to the new operation modes. The options for parameter selection enable a fast reduction of the parameter variety.

The installation of the software is straightforward on the Linux and MacOS machines thanks to the CMake system. The depiction of the outcome benefits from the manifold graphical tools obtained from the ROOT framework.

The $\mathcal{RUN}$ algorithm and its characteristics have been understood and further enhancements can be easily implemented in the future. The planned enhancement is for example an automatic second iteration of the unfolding procedure, with an intermediate approximation of the MC simulation to the unfolded distribution of the data. Thus, a potentially large slope deviation of the sought distribution between data and MC can be minimized. A long-term goal is the implementation of the time-dependency of the unfolded function, which is currently under development within the collaborative research center SFB 823. Furthermore, studies on the calculation of confidence bands, which are done by using bootstrapping methods, are performed in Dortmund in the scope of SFB 823.

The application of TRUEE in the atmospheric neutrino analysis with IceCube is one of the first demonstrations of its performance in the astroparticle physics. The atmospheric neutrino analysis is an important investigation for the search of the

origin of charged cosmic rays. An expected flattening of the neutrino spectrum at high energies would indicate a contribution of the extragalactic neutrinos, that are produced along with the charged cosmic rays. A minor enhancement in the slope could also show the influence of the prompt neutrinos coming from the charmed meson decays in the atmosphere. This would provide insight into the mechanism of charm meson production at very high energies, which cannot be gained with the designed particle accelerators on Earth.

For the analysis a neutrino sample is produced with negligible contribution of the background events caused by atmospheric muons. The employed event selection method has been developed in Dortmund and a further optimization is still carried out. Nevertheless, the performance of the implemented multivariate method, Random Forest, is already very promising at the current stage, as could be verified by the comparison plots between data and MC.

The unfolding procedure itself as well as the tests with MC demonstrate a reliability and stability of the unfolding software. The final outcome is the unfolded atmospheric neutrino flux spectrum for the energies $2.0 \leq log_{10}(E_\nu) \leq 6.0$. Therefore, the explored energy range of the preceding analysis of $log_{10}(E_\nu) \leq 5.5$ could be extended to higher energies. The result is compared to different theoretical models for atmospheric neutrinos. The predicted contribution of the prompt neutrinos from charmed meson decays could not be confirmed or excluded with the estimated spectrum due to the uncertainties. Therefore, no flattening of the spectrum can be claimed at this time. Enhancement of statistics and reduction of systematic uncertainties is expected in the course of the ongoing event selection optimization. Furthermore, the detector has been extended and is now operating in its final configuration. Therefore, the statistics at high energies is expected to be higher for the next analyses and the achievable energy scale can be enlarged.

Systematic tests revealed an imperfection of the event simulation in the upper half of the detector. The disagreement between data and MC affects one of the unfolding observables, $QTot$, which represents the whole measured charge in the detector. A slight correction of the simulated $QTot$ has a positive influence on the unfolding result for the whole detector and promotes convergent behavior between unfolded results for the upper and lower half of the detector. However, $QTot$ is very sensitive to the energy deposit of muons and is therefore an important observable for the energy estimation. As conclusion a detailed study of $QTot$ and its dependency on the ice model is encouraged for future analysis. The most likely explanation of the anomaly is the improper description of the ice properties in the upper part, as the ice is polluted by several dust layers. A possible solution could be a modification of the ice model only in the upper part of the detector. A study with varying DOM efficiencies should be performed as well.

Some general remarks on the unfolding analysis should be made at this point. Usually, the extensive tests with the MC simulation represent a good preparation for the unfolding of real data. TRUEE facilitates such tests by offering the two additional unfolding modes. The selection of optimal parameters and observables can be made and a statistical stability verification can be executed. Nevertheless,

the final settings have to be systematically tested by using real data. The result must be stable for small changes of the regularization influence and other variations in the measurement. Otherwise, further tests are needed with real data to track the source of instability. Usually, the replacement of one of the unfolding variables can bring improvement, since the MC model is just an approach and sometimes does not accurately describe all observables.

In summary, we presented the development of the new unfolding software, TRUEE, which is dedicated to solve general inverse problems and is especially suited for the unfolding analyses in astroparticle physics. We performed atmospheric neutrino analysis by using TRUEE and obtained promising results for the estimation of the atmospheric neutrino flux spectrum. Future atmospheric neutrino analyses with TRUEE and still partially constructed IceCube IC 79 detector are expected to give a hint for the production level of the charmed mesons, as the achievable energy scale is approaching the theoretically predicted region of dominance transition from conventional to prompt neutrinos. The measurement with the fully constructed IceCube detector is expected to prove or disprove the contribution of extragalactic neutrinos and shed light on the origin of the charged cosmic rays.

A Analysis development using 10 % of data

Before analyzing the full data sample, the complete analysis has been developed using only 10 % of the measured data, as a precedent "sanity check". This procedure ensures an untuned outcome, that is independent on expected results. The freely accessible fraction of data is scrambled over the full period of data taking and is called burn sample. The study has to be presented in form of the so-called unblinding proposal to the IceCube collaboration in order to get access to full data. Thus, the analysis in its final state can be reviewed and approved by the collaboration.

In the following some intermediate steps of the analysis development are presented, which are not described in the analysis section. This chapter can be used as a guide for mandatory tests for future unfolding analyses of atmospheric neutrinos. Furthermore, the analyst will be aware of possible problems.

A.1 Tests on the observed zenith anomaly

After obtaining the burn sample at the final neutrino level, the comparison of distributions between data and MC have to be carried out similarly to those shown in Sec. 3.2.3. In this process an anomalous dip in the zenith distribution has been observed, unpredicted by the MC simulation. The question on the origin of the dip lead to a series of tests. The possible explanations could be the improper ice model or event selection, an unpredicted physical effect or just a statistical fluctuation due to the lack of statistics.

The ice model influence could be excluded by using another MC neutrino sample with a different ice model (SPICE Mie) instead of data. No dip appeared in the SPICE Mie sample.

For the study of possible influence of attributes used in Random Forest, extensive tests have been made. For these so-called "n-1" tests the Random Forest event selection has been executed while eliminating one of the attributes successively. Since 27 attributes are used for the event selection, 27 tests have been made. No improvement could be observed in the zenith distribution.

A contingent energy-dependency of the dip, that could be a hint at unexpected physical effects, has been tested by plotting the zenith variable versus different energy estimators and comparing the two-dimensional data and MC distributions. Due to a lack of statistics no conclusion about energy-dependency of the dip could

be made. A potential energy unfolding of events within the zenith dip region also could not be accomplished due to the low statistics.

The dip as statistical fluctuation could be identified after examination of additional independent 10 % of the data. This is a very quick, simple and reliable test, that could exclude all other assumptions about the source of the dip. This should be kept in mind for future analyses, as the access to more data has to be approved by the collaboration and is therefore usually not the first choice.
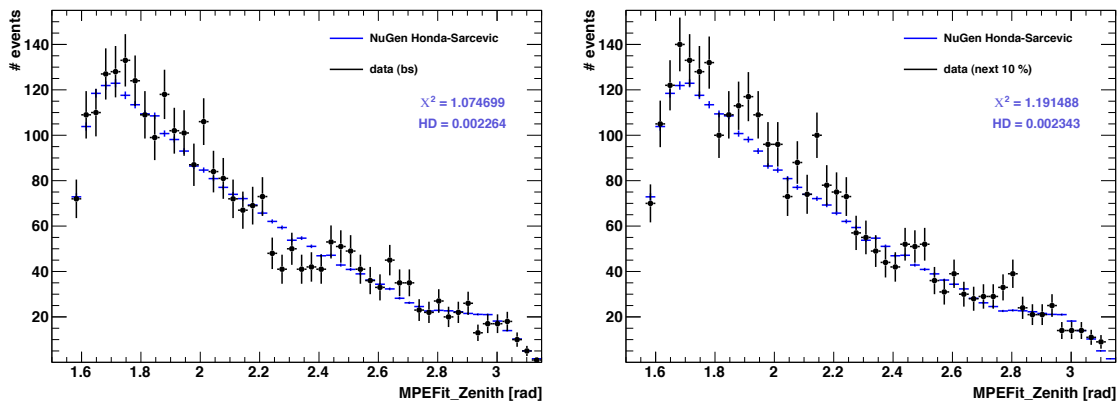

Figure A.1: Zenith distribution at the final neutrino level for burn sample (left) and for another independent 10 % of data. The dip in the data between 2.2 and 2.4 rad observed in the burn sample is not present in the other sample.

A.2 Background estimation with a new approach

First, a general remark should be made concerning MC simulation. The background estimation is an important step to ensure a reliable purity level in the data. Therefore, a high amount on CORSIKA events should be prepared for the analysis to make a solid prediction on the background events in the final data.

Furthermore, the question on the reliability of the background estimation, made by the cross-validation has been raised during the analysis review. A possible minor mismatch between MC and data could misalign the purity at the final level. Therefore, a test has been developed that allows a background estimation using only data and that confirms the background percentage predicted by cross-validations with MC. As preparation for the test the energy unfolding of CORSIKA events after different *signalness* cuts has been performed. The goal was to estimate the increasing background at the decreasing *signalness* levels and compare them to the MC.

Since the background events, which remain in the sample, are coincident muons, the reconstruction of the track is usually of bad quality and therefore the energy dependent variables are related to the lower energies. The unfolded energy distributions of the CORSIKA events in Fig. A.2 confirm the assumption showing contri-

butions mainly in the first three bins. All conditions including the response matrix for the unfolding have been kept the same, as for the data unfolding. Of course, the neutrino sample, used for the response matrix, has been cut at the same *signalness* value, as the sample, which has been used for unfolding. The CORSIKA sample has been recognized as signal sample by TRUEE and no background assumptions have been made within the unfolding software.

Based on this knowledge, the energy unfolding of the data sample has been carried out after different *signalness* cuts. The unfolded event distribution has to be examined, before the normalization to the flux. The results can be found in Fig. A.2. As expected, the significant enhancement could be observed in the first
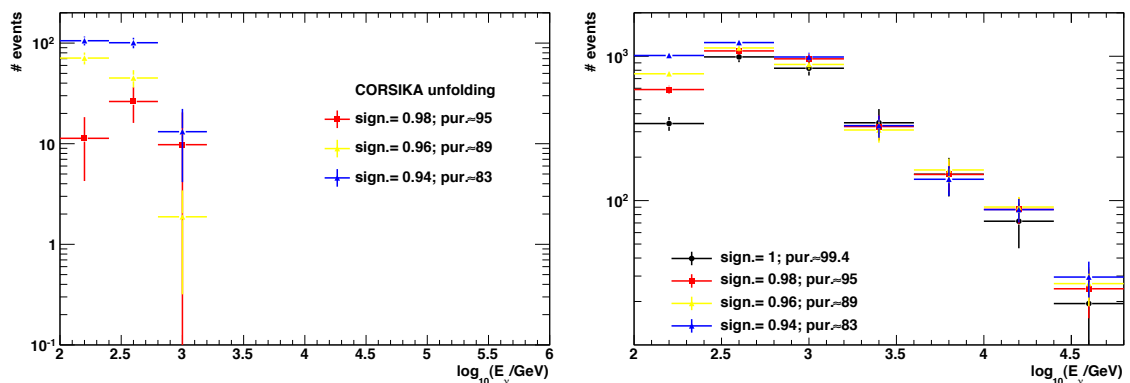

Figure A.2: Left: energy unfolding of simulated background events after different *signalness* cuts. As expected the coincident atmospheric muons are recognized as low energy events and cluster in the first three bins. Right: The unfolding of data after different *signalness* cuts. All results are scaled to the distribution with highest purity at high energies, since there the contribution of background is negligible. Shown is the zoom into lower energies, where the enhancement is visible due to the misreconstructed background events. From the excess the amount of background and thus the purity of the sample is determined after different *signalness* cuts and compared to the cross-validation results.

bins. The background contamination at highest *signalness* has been assumed to be negligible compared to the other levels. Therefore, all other distributions has been scaled to match the highest purity unfolding result at high energies. Subsequently, the enhancement in the low energy bins has been determined and the amount of background has been analyzed. The estimated purities, as comparison between the MC-based cross-validation and data-based approach, are summarized in Tab. A.1. The very good agreement between the two different estimation approaches proves the reliability of the results that have been obtained with MC.

signalness cut	estimated purity [%]	
	data-based	MC-based
0.98	95 ± 1	95 ± 1
0.96	90 ± 1	89 ± 0.8
0.94	85 ± 2.0	83 ± 0.7

Table A.1: Neutrino sample purity for different *signalness* cuts, estimated by using the new data-based method and the MC-based cross-validation.

A.3 Depth-dependent tests of unfolding variables

The originally chosen unfolding variables, *NCh*, *NString* and *LDirC*, showed very good performance in the *test mode* and good results in the burn sample, as has been shown in Ref. [MRR11]. After the division of the detector in the top and bottom part, a large disagreement of *NCh* and *NString* between the upper and lower part has been observed. An over-/underestimation of MC in the lower/upper part of the detector has led to strongly divergent results. To avoid this circumstance a new set of observables could be found, that showed minimal dependence of the burn sample result on the detector depths. The results can be seen in Fig. A.3. Therefore, this new set of observables is also used in the presented analysis.
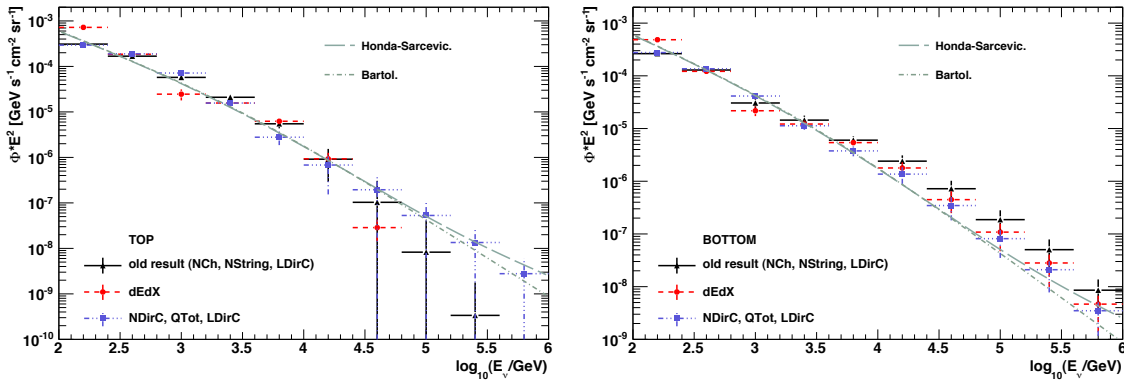

Figure A.3: Unfolding of neutrino flux measured in top (left) and bottom (right) of the detector, separately, using different sets of observables. While the results with the originally chosen combination of *NCh*, *NString* and *LDirC* show a divergent behavior in top versus bottom, the new set of *NDirC*, *LDirC* and *QTot* leads to stable results.

A.4 Resolution comparison of energy estimators

In the unfolding three observables are used at the same time, one of them directly measured. This aims a least bias by reconstruction algorithms and therefore an exact energy estimation. The new combination of the observables has been recognized by the IceCube collaboration as a new energy estimator, equivalent to the constructed energy estimator *dEdX*. Generally, every new energy estimator has to be proven to have a comparable performance, as the commonly used estimators. For demonstration of the performance a resolution test has been made for the new observable combination and compared to the *dEdX*. This test is based on the energy unfolding of simulated mono-energetic events. The results can be found in Fig. A.4. The resolution of the used observable combination is comparable to that of *dEdX*. Since the regularization in TRUEE assumes a smooth distribution, the obtained resolution can be considered as a pessimistic approach.
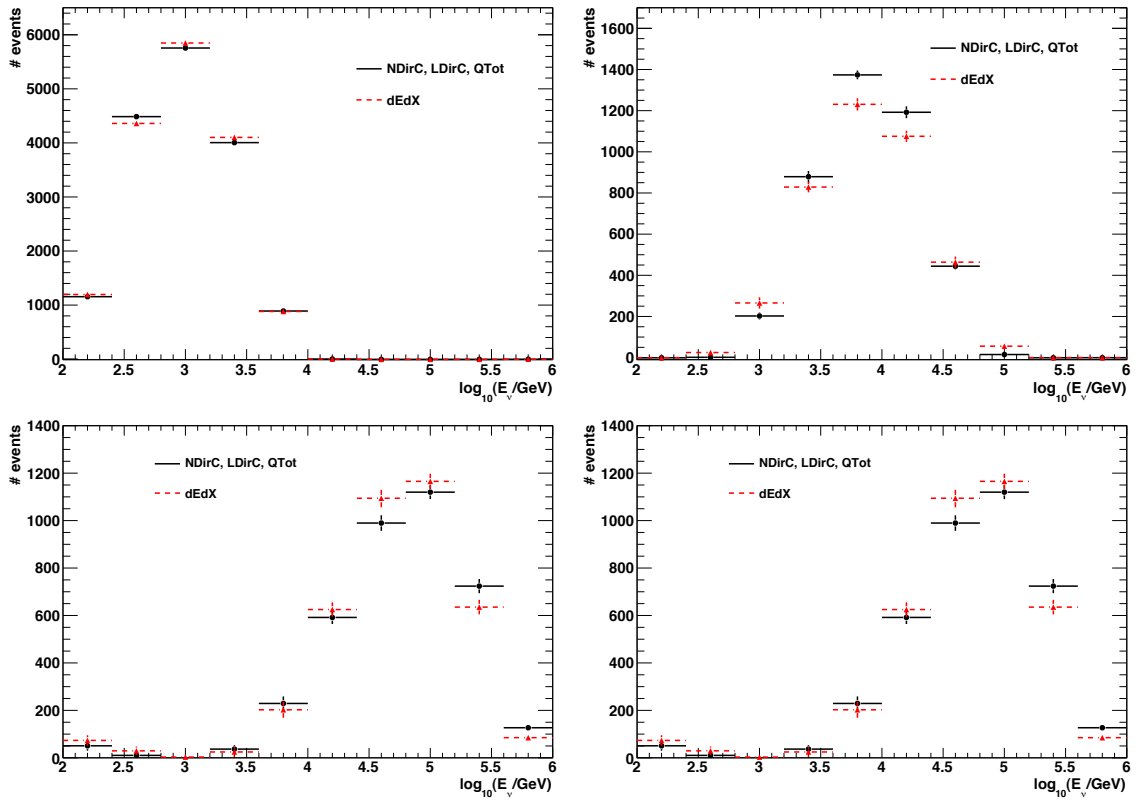
Figure A.4: Unfolded distributions of mono-energetic events, as tests of the resolution of the commonly used energy estimator *dEdX* and the new combination of observables *NDirC*, *LDirC* and *QTot*. Different MC sets with energies $log_{10}(E_\nu/GeV) = 3, 4, 5, 6$ have been simulated. The broadening of the unfolded peak is comparable for both energy estimators. The standard deviations of the Gaussian fit are summarized in Tab. A.2.

simulated energy $log_{10}(E_\nu/GeV)$	estimated mean and σ in $log_{10}(E_\nu/GeV)$	
	dEdX	NDirC, LDirC, QTot
3	2.98 ± 0.41	2.98 ± 0.41
4	3.88 ± 0.47	3.88 ± 0.43
5	4.78 ± 0.47	4.82 ± 0.49

Table A.2: Mean values and standard deviations of Gaussian fits to the unfolded mono-energetic distributions, obtained by using *dEdX* and the new set of observables as unfolding variables. The Gaussian fit could not be evaluated for the $log_{10}(E_\nu/GeV) = 6$.

It should be mentioned that a presentation of scatter plots and profile histograms (Sec. 2.3.3) has not been sufficient to compare the performance, since the plots treat the observables separately.

A.5 General remarks

When a new unfolding software is introduced it has to be demonstrated to which extend the MC distribution, used for the response matrix, influences the unfolded result. As has been explained in the Sec. 2.3.3 in the reality the dependency on the MC is unavoidable. The main concern has been about the possible fake of a spectrum flattening due to a flat MC. Therefore, unfolding with different neutrino flux models for the response matrix have been required, to ensure a possibly unbiased result. The different assumptions in the MC had no effect on the unfolded result. In fact an even stronger deviation between the slope of MC and unfolded data is acceptable TRUEE, as has been demonstrated in Sec. 2.3.3.

It has been requested to switch the axes of the scatter plots and profile histograms, for the demonstration of the energy dependency of an observable (Sec. 2.3.3).

Bibliography

[A+02]   J Ahrens et al. Observation of high-energy atmospheric neutrinos with the Antarctic Muon and Neutrino Detector Array. *Phys.Rev.*, D66:012005, 2002.

[A+04a]   J Ahrens et al. Muon track reconstruction and data selection techniques in AMANDA. *Nucl.Instrum.Meth.*, A524:169–194, 2004.

[A+04b]   J Ahrens et al. Sensitivity of the IceCube detector to astrophysical sources of high energy muon neutrinos. *Astropart.Phys.*, 20:507–532, 2004.

[A+05]   T Antoni et al. KASCADE measurements of energy spectra for elemental groups of cosmic rays: Results and open problems. *Astropart.Phys.*, 24:1–25, 2005.

[A+06]   M Ackermann et al. Optical properties of deep glacial ice at the South Pole. *Journal of Geophysical Research*, 111, 2006.

[A+07a]   J. Albert et al. Observations of mkn 421 with the magic telescope. *Astrophys.J.*, 663:125–138, 2007.

[A+07b]   J Albert et al. Unfolding of differential energy spectra in the MAGIC experiment. *Nucl.Instrum.Meth.*, A583:494–506, 2007.

[A+08a]   R U Abbasi et al. First observation of the Greisen-Zatsepin-Kuzmin suppression. *Phys.Rev.Lett.*, 100:101101, 2008.

[A+08b]   J Abraham et al. Observation of the suppression of the flux of cosmic rays above 4×10^{19}eV. *Phys.Rev.Lett.*, 101:061101, 2008.

[A+08c]   C Amsler et al. Review of Particle Physics. *Physics Letters B*, 667:277, 2008.

[A+09]   E-J Ahn et al. Cosmic ray interaction event generator SIBYLL 2.1. *Physical Review D*, 80, 2009.

[A+10a]   R Abbasi et al. Calibration and Characterization of the IceCube Photomultiplier Tube. *Nucl.Instrum.Meth.*, A618:139–152, 2010.

[A+10b]   R Abbasi et al. The Energy Spectrum of Atmospheric Neutrinos between 2 and 200 TeV with the AMANDA-II Detector. *Astropart.Phys.*, 34:48–58, 2010.

[A⁺11a] R Abbasi et al. A Search for a Diffuse Flux of Astrophysical Muon Neu-
         trinos with the IceCube 40-String Detector. *Phys.Rev.*, D84:082001, 2011.

[A⁺11b] R Abbasi et al. First search for atmospheric and extraterrestrial neutrino-
         induced cascades with the IceCube detector. *Phys.Rev.*, D84:072001, 2011.

[A⁺11c] R Abbasi et al. IceCube - Astrophysics and Astroparticle Physics at the
         South Pole. 2011.

[A⁺11d] R Abbasi et al. Measurement of the atmospheric neutrino energy spectrum
         from 100 GeV to 400 TeV with IceCube. *Phys.Rev.*, D83:012001, 2011.

[A⁺11e] R Abbasi et al. The IceCube Neutrino Observatory VI: Neutrino Oscilla-
         tions, Supernova Searches, Ice Properties. 2011.

[A⁺12a] R Abbasi et al. A Search for UHE Tau Neutrinos with IceCube. 2012.

[A⁺12b] R Abbasi et al. The Design and Performance of IceCube DeepCore. *As-
         tropart.Phys.*, 35:615–624, 2012.

[B⁺89]   E.V Bugaev et al. Prompt Leptons in Cosmic Rays. *Il Nuovo Cimento*,
         12 C(1), 1989.

[B⁺93]   D J Bird et al. Evidence for correlated changes in the spectrum and
         composition of cosmic rays at extremely high energies. *Phys. Rev. Lett.*,
         71:3401 – 3404, 1993.

[B⁺04]   G D Barr et al. A Three - dimensional calculation of atmospheric neutrinos.
         Phys.Rev., D70:023006, 2004.

[B⁺06]   G D Barr et al. Uncertainties in Atmospheric Neutrino Fluxes. *Phys.Rev.*,
         D74:094009, 2006.

[Bak11] M Baker. Time-Dependent Searches for Neutrino Point Sources with the
         IceCube Observatory. *Dissertation*, 2011.

[BCK02] J F Beacom, P Crotty, and E W Kolb. Enhanced signal of astrophysical
         tau neutrinos propagating through Earth. *Physical Review D*, 66:021302,
         2002.

[Bec08] J K Becker. High-energy neutrinos in the context of multimessenger
         physics. *Phys.Rept.*, 458:173–246, 2008.

[BL98]   V Blobel and E Lohrmann. *Statistische und numerische Methoden der
         Datenanalyse*. 1998.

[Blo84] V Blobel. Unfolding methods in high energy physics experiments. *DESY
         84-118*, 1984.

[Blo96]   V Blobel. The RUN manual: regularized unfolding for high-energy physics experiments. *OPAL Technical Note TN361*, May 1996.

[Blo10]   V Blobel. Unfolding - Linear Inverse Problems. *Notes for the Terrascale workshop at DESY*, 2010.

[BR97]   R Brun and F Rademakers. ROOT - An object oriented data analysis framework. *Nuclear Instruments and Methods in Physics Research Section A*, 389(1 - 2):81 – 86, 1997.

[Bre01]   L Breiman. Random Forests. *Machine Learning*, 45(1):5 – 32, 2001.

[BZ69]   V S Berezinsky and G T Zatsepin. Cosmic rays at ultrahigh energies (neutrino?). *Physics Letters B*, 28:423, 1969.

[CER93]   CERN. CERNLIB - Catalog of Program packages and entries. *Program Library Long Writeup, CERN*, 1993.

[Che34]   P A Cherenkov. Visible emission of clean liquids by action of gamma radiation. *Doklady Akademii Nauk SSSR*, 2:451, 1934.

[Chi09]   D Chirkin. Study of South Pole ice transparency with IceCube flashers. *IceCube Internal Report*, 2009.

[Chi11]   D Chirkin. Study of South Pole ice transparency with IceCube flashers. *in Proc. of 32nd ICRC (Beijing)*, 2011.

[CLR67]   I M Chakravarti, R G Laha, and J Roy. Handbook of methods of applied statistics. *Wiley*, 1, 1967.

[CR04]   D Chirkin and W Rhode. Muon Monte Carlo: A High-precision tool for muon propagation through matter. 2004.

[Cur08]   V Curtef. A new unfolding method for the MAGIC telescope. *Dissertation*, 2008.

[CY00]   L M Le Cam and G L Yang. Asymptotics in Statistics: Some Basic Concepts. *Springer*, 2000.

[dB01]   C de Boor. *A Practical Guide to Splines*. 2001.

[DC95]   H Drucker and C Cortes. Boosting Decision Trees. *NIPS*, pages 479 – 485, 1995.

[DG10]   P Desiati and T K Gaisser. Seasonal variation of atmospheric leptons as a probe of charm. *Phys.Rev.Lett.*, 105:121102, 2010.

[ERS08]   R Enberg, M H Reno, and I Sarcevic. Prompt neutrino fluxes from atmospheric charm. *Phys.Rev.*, D78:043005, 2008.

[F+02]   S Fischer et al. Yale: Yet Another Learning Environment. *Collaborative Research Center 531*, 2002.

[FBTD12]   A Fedynitch, J Becker Tjus, and P Desiati. Influence of hadronic interaction models and the cosmic ray spectrum on the high energy atmospheric muon and neutrino flux. 2012.

[Fer49]   E Fermi. On the origin of the cosmic radiation. *Phys. Rev.*, 75:1169–1174, Apr 1949.

[Fre03]   J Fredholm. Sur une classe d'équations fonctionnelles. *Acta Math.*, 27(365 - 390), 1903.

[FS09]   S J Fegan and D Sanchez. Fermi observations of TeV AGN. 2009.

[Gai03]   T K Gaisser. Atmospheric neutrino fluxes. *Nucl.Phys.Proc.Suppl.*, 118:109–117, 2003.

[Gai07]   Thomas K Gaisser. Atmospheric Neutrinos. *AIP Conf.Proc.*, 944:140–142, 2007.

[GBH08]   S Grullon, D Boersma, and G Hill. Photonics-based Log-Likelihood Reconstruction in IceCube. *IceCube Internal Report*, 200807001, 2008.

[GK04]   A Gazizov and M Kowalski. *ANIS: High Energy Neutrino Generator for Neutrino Telescopes.* 2004.

[Goz08]   S R Gozzini. Search for Prompt Neutrinos with AMANDA-II. *Dissertation*, 2008.

[Gre66]   K Greisen. End to the Cosmic-Ray Spectrum? *Phys. Rev. Lett.*, 16:748 – 750, 1966.

[H+98]   D Heck et al. *CORSIKA: A Monte Carlo code to simulate extensive air showers.* Jan 1998.

[H+07]   M Honda et al. Calculation of atmospheric neutrino flux using the interaction model calibrated with atmospheric muon data. *Phys.Rev.*, D75:043006, 2007.

[H+09]   M Hall et al. The WEKA Data Mining Software: An Update. *SIGKDD Explorations*, 11(1), 2009.

[Had02]   J Hadamard. Sur le problèmes aux dérivées partielles et leur signification physique. *Princeton University Bulletin*, pages 49 – 52, 1902.

[Hel11]   K Helbing. IceCube as a discovery observatory for physics beyond the standard model. 2011.

[Hil84]   A M Hillas. The origin of ultra-high-energy cosmic rays. *Ann. Rev. Astron. Astrophys.*, 22:425 – 444, 1984.

[HK10]   F Halzen and S R Klein. IceCube: An Instrument for Neutrino Astronomy. *Rev.Sci.Instrum.*, 81:081101, 2010.

[HL74]   R J Hanson and C L Lawson. *Solving Least Squares Problems.* 1974.

[Hoe03]   J R Hoerandel. On the knee in the energy spectrum of cosmic rays. *Astropart.Phys.*, 19:193–220, 2003.

[Ice12]   Website, 2012. http://www.icecube.wisc.edu.

[J$^+$81]   M Jonker et al. Experimental study of differential cross sections d/dy in neutral current neutrino and antineutrino interactions. *Physics Letters B*, 102:62–72, 1981.

[J$^+$83]   M Jonker et al. Experimental study of x-distributions in semileptonic neutral current neutrino interactions. *Physics Letters B*, 142:117–123, 1983.

[Joh11]   H Johansson. Searching for an Ultra High-Energy Diffuse Flux of Extraterrestrial Neutrinos with IceCube 40. *Universitetsservice AB, Stockholm*, 2011.

[K$^+$85]   D D Krasilnikov et al. EAS spectrum in the primary energy region above 10^{15} eV by the Akeno and the Yakutsk array data. *In NASA. Goddard Space Flight Center 19th Intern. Cosmic Ray Conf.*, pages 194 – 197, 1985.

[Kel08]   J L Kelley. Searching for Quantum Gravity with High-energy Atmospheric Neutrinos and AMANDA-II. *Dissertation*, 2008.

[Kis11]   F Kislat. Measurement of the all-particle cosmic ray energy spectrum with IceTop. *Astrophys. Space Sci. Trans.*, 7:175 – 178, 2011.

[Kle09]   S R Klein. IceCube: A Cubic Kilometer Radiation Detector. *IEEE Transactions on Nuclear Science*, 56(3):1141 – 1147, 2009.

[Kok99]   R P Kokoulin. Uncertainties in underground muon flux calculations. *Nuclear Physics B - Proceedings Supplements*, 70(1 -3):475 – 479, 1999.

[KR05]   J R Klein and A Roodman. Blind Analysis in Nuclear and Particle Physics. *Annual Review of Nuclear and Particle Science*, 55:141 – 163, 2005.

[L$^+$07]   J Lundberg et al. Light tracking for glaciers and oceans: Scattering and absorption in heterogeneous media with Photonics. *Nucl.Instrum.Meth.*, A581:619–631, 2007.

[Lin63]   J Linsley. Evidence for a primary cosmic-ray particle with energy 10^{20} eV. *Physical Review Letters*, 10(4):146 – 148, 1963.

[Lyo11]   L Lyons. Unfolding: Introduction. *presented at PHYSTAT 2011 (CERN, Geneva)*, 2011.

[M⁺06]   S Mizobuchi et al. Reconstruction methods of energy spectra for high redshift sources with the MAGIC Telescope. *in Proc. of 29th ICRC (Pune)*, 2006.

[M⁺12]   N Milke et al. Solving time-dependent inverse problems with TRUEE: Examples in astroparticle physics. *Nuclear Instruments and Methods in Physics Research Section A*, submitted 2012.

[Mac05]   C Mackenzie. Introduction to the Data Movement and Archival System for IceCube. 2005.

[MH03]   K Martin and W Hoffman. The CMake Build Manager - Cross platform and open source. *Dr. Dobbs*, 2003.

[MRR11] N Milke, W Rhode, and T Ruhe. Studies on the unfolding of the atmospheric neutrino spectrum with IceCube 59 using the TRUEE algorithm. *in Proc. of 32nd ICRC (Beijing)*, 2011.

[Neu06]   T Neunhoffer. Estimating the angular resolution of tracks in neutrino telescopes based on a likelihood analysis. *Astropart.Phys.*, 25:220–225, 2006.

[O⁺12]   A Olivas et al. IceCube simulation documentation. Website, 2012. http://wiki.icecube.wisc.edu/index.php/Simulation_Documentation_Wiki.

[Phi62]   D L Phillips. A Technique for the Numerical Solution of Certain Integral Equations of the First Kind. *J. ACM*, 9:84 – 97, 1962.

[Pun05]   M Punch. Results from observations of AGNs with the H.E.S.S. Telescope system and future plans. 2005.

[RM11]   T Ruhe and K Morik. Data Mining IceCube. *Proceedings of the ADASS XXI meeting*, 2011.

[RMS11] T Ruhe, K Morik, and B Schowe. Data mining on ice. *Proceedings of the GREAT conference on Astrostatistics and Data Mining*, 2011.

[S⁺02]   S P Swordy et al. The Composition of cosmic rays at the knee. *Astropart.Phys.*, 18:129–150, 2002.

[Smi58]   F Smithies. *Integral Equations*. 1958.

[Ste90]   V J Stenger. Track Fitting For Dumand II Octagon Array. *Esternal Report HDC-1-90*, 1990.

[The08]   The IceCube Collaboration. The IceCube Data Acquisition System: Signal Capture, Digitization, and Timestamping. *ArXiv e-prints*, oct 2008.

[Tik63]   A N Tikhonov. On the solution of improperly posed problems and the method of regularization. *Sov. Math.*, 5, 1963.

[Tru12]   Website, 2012. http://app.tu-dortmund.de/TRUEE/.

[Two63]   S Twomey. On the Numerical Solution of Fredholm Integral Equations of the First Kind by the Inverstion of the Linear System Produced by Quadrature. *J. ACM*, 10(1):97 – 101, 1963.

[Wor11]   M Wornowizki. Variablenselektion über Filterverfahren auf Daten des Neutrinodetektors IceCube. *Diploma thesis*, 2011.

[WZ91]   G M Wing and J D Zahrt. *A primer on integral equations of the first kind.* 1991.

[ZK66]   G T Zatsepin and V A Kuzmin. Upper Limit of the Spectrum of Cosmic Rays. *Pisma Zh. Eksp. Teor. Fiz.*, 4:114 – 117, 1966.

Acknowledgment

At this point I would like to acknowledge all persons who contributed to the success of this work.

First of all I want to thank my supervisor, Prof. Dr. Dr. Wolfgang Rhode, who gave me the opportunity to perform study in this interesting field. His support and his inspiring interest for astroparticle physics have always kept me motivated. I have learned a lot during my PhD time and could gather relevant personal and professional experience.

Further, I would like to thank the Jun.-Prof. Dr. Julia K. Becker Tjus for her help and competent assistance during the whole work.

The IceCube collaboration members are acknowledged for reviewing my analysis and for the many advises I have received. Especially in the working group for atmospheric and diffuse analyses I have experienced a nice atmosphere and very informative discussions.

I thank Prof. Dr. Volker Blobel for his assistance in understanding the $\mathcal{RUN}$ algorithm and his attempt to make TRUEE known by a high number of potential users.

I thank my colleagues at the TU Dortmund and RUB for productive discussions and interesting time I could spend with them. Special thanks go to the colleagues, who have been the first TRUEE users and helped me to consistently make progress by offering constructive critics and useful suggestions.

The members of the Statistics tools group of the Helmholtz alliance are acknowledged for fruitful discussions and exchange of ideas.

Not least, I want to thank my family and my boyfriend for making my time as beautiful as possible.